STRUCTURAL, BIOASSAY AND THERMAL STUDIES OF METAL COMPLEXES WITH NOVEL SCHIFF BASES

BY

MUHAMMAD IKRAM

DOCTOR OF PHILOSOPHY
IN
CHEMISTRY

INSTITUTE OF CHEMICAL SCIENCES
UNIVERSITY OF PESHAWAR
PAKISTAN
2012

STRUCTURAL, BIOASSAY AND THERMAL STUDIES OF METAL COMPLEXES WITH NOVEL SCHIFF BASES

By

MUHAMMAD IKRAM

DISSERTATION

SUBMITTED TO THE UNIVERSITY OF PESHAWAR IN PARTIAL FULFILEMENT OF THE REQUIREMENTS FOR THE DEGREE OF DOCTOR OF PHILOSPHY IN CHEMISTRY

INSTITUTE OF CHEMICAL SCIENCES
UNIVERSITY OF PESHAWAR
PAKISTAN
2012

APPROVAL SHEET

It is recommended that the dissertation prepared by Muhammad Ikram, entitled

"Structural, Bioassay and Thermal studies of Metal Complexes with Novel Schiff Bases" be

accepted as fulfilling the partial requirement for the degree of

DOCTOR OF PHILOSOPHY
IN
CHEMISTRY

_____
Supervisor
Prof. Dr. Saeed ur Rehman
Institute of Chemical Sciences
University of Peshawar

_____
Examiner

_____
Director
Prof. Dr. Imdad Ullah Mohammadzai
Institute of Chemical Sciences
University of Peshawar

INSTITUTE OF CHEMICAL SCIENCES
UNIVERSITY OF PESHAWAR
PAKISTAN
2012

DEDICATION

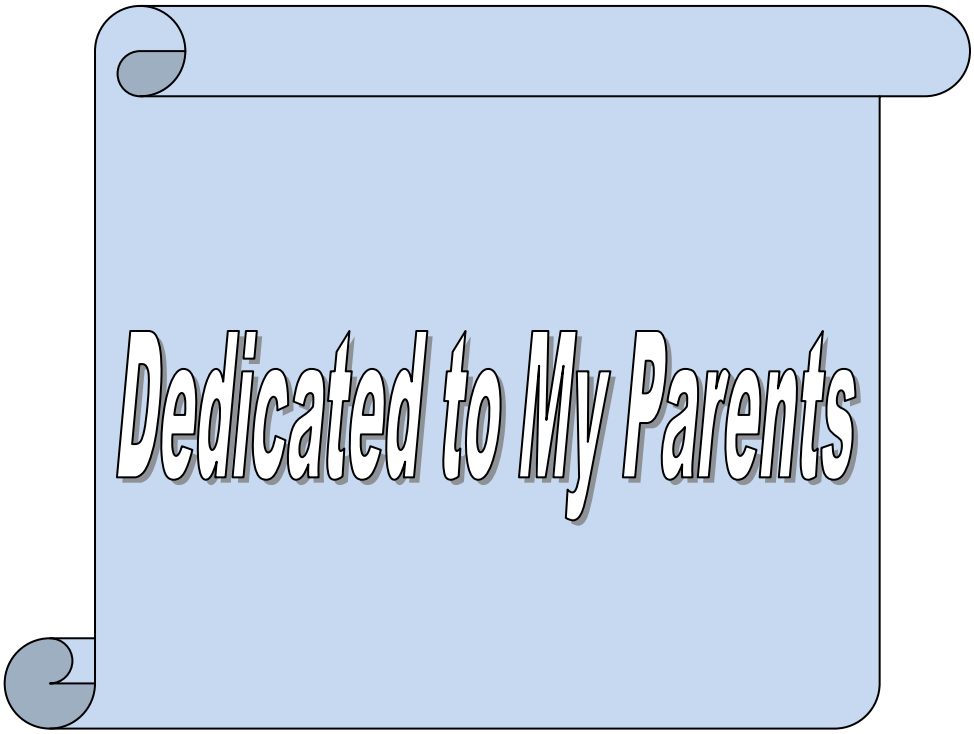

CONTENTS

List of Schemes

LIST OF TABLES

LIST OF FIGURES

IUPAC NAME INDEX

S.No	IUPAC Name	Identification code
1.	2-[(*E*)-(quinolin-3-ylimino)methyl]phenol	**H-QMP**
2.	Bis(2-[(*E*)-(quinolin-3-ylimino)methyl]phenolato)nickel(II)	**1**
3.	Bis(2-[(*E*)-(quinolin-3-ylimino)methyl]phenolato)cobalt(II)	**2**
4.	Bis(2-[(*E*)-(quinolin-3-ylimino)methyl]phenolato)copper(II)	**3**
5.	Bis(2-[(*E*)-(quinolin-3-ylimino)methyl]phenolato)zinc(II)	**4**
6.	2-{(*E*)-[(4-chlorophenyl)imino]methyl}phenol (CIMP)	
7.	Bis(2-{(*E*)-[(4-chlorophenyl)imino]methyl}phenolate)nickel(II)	**5**
8.	Bis(2-{(*E*)-[(4-chlorophenyl)imino]methyl}phenolate)cobalt(II)	**6**
9.	Bis(2-{(*E*)-[(4-chlorophenyl)imino]methyl}phenolate)copper(II)	**7**
10.	Bis(2-{(*E*)-[(4-chlorophenyl)imino]methyl}phenolate)zinc(II)	**8**
11.	2-{(*E*)-[(4-bromophenyl)imino]methyl}phenol	**BIMP**
12.	Bis(2-{(*E*)-[(4-bromophenyl)imino]methyl}phenolate)nickel(II)	**9**
13.	Bis(2-{(*E*)-[(4-bromophenyl)imino]methyl}phenolate)cobalt(II)	**10**
14.	Bis(2-{(*E*)-[(4-bromophenyl)imino]methyl}phenolate)copper(II)	**11**
15.	Bis(2-{(*E*)-[(4-bromophenyl)imino]methyl}phenolate)zinc(II)	**12**
16.	[1-({[(*Z*)-(2-hydroxynaphthalen-1-yl)methylidene]amino}methyl)cyclohexyl]acetic acid	**H-HMAC**
17.	[1-({[(*Z*)-(2-hydroxynaphthalen-1-yl)methylidene]amino}methyl)cyclohexyl]aceticacid]nickel(II)	**13**
18.	[1-({[(*Z*)-(2-hydroxynaphthalen-1-yl)methylidene]amino}methyl)cyclohexyl]aceticacid]cobalt(II)	**14**
19.	[1-({[(*Z*)-(2-hydroxynaphthalen-1-yl)methylidene]amino}methyl)cyclohexyl]aceticacid]copper(II)	**15**
20.	[1-({[(*Z*)-(2-hydroxynaphthalen-1-yl)methylidene]amino}methyl)cyclohexyl]aceticacid]zinc(II)	**16**
21.	methyl 2-{[(*E*)-(2-hydroxyphenyl)methylidene]amino}benzoate ()	**H-HAB**
22.	Bis(methyl 2-{[(*E*)-(2-	**17**

	hydroxyphenyl)methylidene]amino}benzoate)nickel(II)	
23.	Bis(methyl 2-{[(*E*)-(2-hydroxyphenyl)methylidene]amino}benzoate)cobalt(II)	**18**
24.	Bis(methyl 2-{[(*E*)-(2-hydroxyphenyl)methylidene]amino}benzoate)copper(II)	**19**
25.	Bis(methyl 2-{[(*E*)-(2-hydroxyphenyl)methylidene]amino}benzoate)zinc(II)	**20**
26.	2-(2-hydroxyphenyl)-3-{[(*E*)-(2-hydroxyphenyl)methylidene]amino}-2,3-dihydroquinazolin-4(1*H*)-one	**H-HHAQ**
27.	Bis(2-(2-hydroxyphenyl)-3-{[(*E*)-(2-hydroxyphenyl)methylidene]amino}-2,3-dihydroquinazolin-4(1*H*)-one)nickel(II)	**21**
28.	Bis(2-(2-hydroxyphenyl)-3-{[(*E*)-(2-hydroxyphenyl)methylidene]amino}-2,3-dihydroquinazolin-4(1*H*)-one)cobalt(II)	**22**
29.	Bis(2-(2-hydroxyphenyl)-3-{[(*E*)-(2-hydroxyphenyl)methylidene]amino}-2,3-dihydroquinazolin-4(1*H*)-one)copper(II)	**23**
30.	Bis(2-(2-hydroxyphenyl)-3-{[(*E*)-(2-hydroxyphenyl)methylidene]amino}-2,3-dihydroquinazolin-4(1*H*)-one)zinc(II)	**24**
31	Bis(4,4,5,5,6,6,7,7,8,8,9,9,9-tridecafluorononanoic acid)zinc(II)	**25**
32	Di(diethylether) (3,3,4,4,5,5,6,6,7,7,8,8,8-tridecafluorooctan-1-olate) zinc(II)	**26**

List of abbreviations and constants

TG	Thermogravimetry
DTA	Differential thermogravimetry

Constants

R	Molar gas constant in J/molK
k_B	Boltzmann constant
h	plank's constant

Symbols

E*	activation energy in $KJmol^{-1}$
Ts	temperature in kelvin for maximum mass loss
Td	temperature of decomposition
ΔS*	change in entropy of activation in $Jmol^{-1}K^{-1}$
A	Arrhenius pre-exponential factor in 1/s
ΔH*	change in enthalpy of activation in $KJmol^{-1}$
ΔG*	change in Gibb's free energy of activation in $KJmol^{-1}$
n	order of decomposition
∧m	molar conductance
μ_{eff}	magnetic susceptibility
UV	ultraviolet
IR	infrared

ACKNOWLEDGEMENTS

First of all I thank to **Almighty Allah**, the most Beneficent, and the most Merciful, Who enabled me to complete this work.

I am thankful to Higher Education Commission Pakistan for their financial support in the form Indigenous and IRSIP (six months research stay at Trinity College Dublin, Ireland) scholarships.

I wish to express my sincere gratitude, heartiest obligation and appreciation to my worthy, learned and experienced supervisor, Dr. Saeed-Ur-Rehman, professor Inorganic Chemistry at Institute of Chemical Sciences, University of Peshawar, for his continued guidance, help and kind attitude throughout my research work.

I am also very thankful to Prof. Dr. Imdadullah, Director of Institute of Chemical Sciences, University of Pehawar, Dr. Khurshid Ali, Dr. Nauman Ali, Dr. Waseem Hassan, and Dr. Faiz ur Rehman for their motivation and inspiration. I am also thankful to my other worthy professors and teachers at the Institute of Chemical Sciences for their help and cooperation.

I wish to pay my sincere thanks to my lab fellows Sadia Rehman, Gul Akhtar, Hanif ur Rehman, Waqas Ahmed, Ihsan Ali, Nasir Ullah, Adnan, Khan Maluk and Dr. Faridoon for their valuable assistance, guidance and fruitful suggestions. I am thankful to Mr. Rahim Khan (lab.supervisor) and his colleagues for their help.

I ardently extend my thanks to Dr. Robert James Baker, Dr. Carola Schulzke, Dr. Fenney Martin, Dr. Ruther Manual, School of Chemistry, Dr. Ken Mok, Dr. Soyoung Ming School of Biochemistry and immunology, Trinity College University of Dublin Dublin-2 Ireland, for their help, support and encouragement. I am also thankful to Mr. Muhammad Zubair, Mr. Ashta Chandra Ghosh, Ms. Aurora Ann Walshe and Ms. Emi Hashem, PhD scholars in School of Chemistry, Trinity College University of Dublin, Dublin Ireland and Mr. Tariq Zaman, PhD scholar at NUST University Islamabad for their help and cooperation.

Finally, I express my heartiest thanks to my great parents, sisters, and brothers for their cooperation and encouragement to achieve this target.

Muhammad Ikram

ABSTRACT

PART I

Schiff base chemistry was elaborately studied using the anionic ligands obtained by reacting, various primary aryl amines with medicinally important salicyldehyde. Different ligands, ranging from simple non rigid bidentate/tridentate anionic Schiff base ligands to sterically free twisting ligands have been prepared. All these ligands were complexed with transition metals like cobalt, nickel, copper and zinc. The coordination complexes of square planar and distorted tetrahedral geometry were obtained for bidentate anionic Schiff base ligands and octahedral for tridentate Schiff base ligands. Characterization of all the Schiff base ligands were done using various spectroscopic and analytical methods including ^{1}H, $^{13}C\{^{1}H\}$-NMR, infrared spectroscopic method, ES^{+}-MS, elemental analyses and conductance studies. Apart from it Schiff base ligands like 2-[(*E*)-(quinolin-3-ylimino)methyl]phenol (H-QMP), [1-({[(*Z*)-(2-hydroxynaphthalen-1-yl)methylidene]amino}methyl)cyclohexyl]acetic acid (H-HHMAC) and 2-(2-hydroxyphenyl)-3-{[(*E*)-(2-hydroxyphenyl)methylidene]amino}-2,3-dihydroquinazolin-4(1*H*)-one (H-HHAQ) were recrystallized from concentrated THF solution in *Pc*, *P1* and $C222_1$ space groups respectively. All the synthesized transition metal complexes of the representative Schiff base ligands were also characterized by elemental analyses, ES^{+}-MS, IR and UV Visible spectroscopic studies, magnetic susceptibilities and molar conductance studies. The metal complexes like **1** and **2** were recrystallized by slow diffusion of diethyl ether into the concentrated solution of metal complexes in CH_2Cl_2 in $P2_1/c$ space group having trans square planar arrangement of ligand around the metal centers.

Based upon the medicinal importance of the salicyldehyde unit the Schiff base ligands and its metal complexes were studied for their In Vitro enzyme inhibitory activities against urease, α-

chymotrypsin, acetylcholinesterase and butyrylcholinesterase in order to study their effectiveness to treat peptic ulcer and Alzheimer disease. Ligand like H-HHMAC was found active against urease α-chymotrypsin and acetylcholinesterase whereas the Schiff base ligands like CIMP and BIMP were found good inhibitors for α-chymotrypsin. It was found that metal based inhibitors for urease can be designed which include metal complexes like **7**, **11**, **18** and **22** respectively, similarly for α-chymotrypsin the metal based inhibitors include **18** and **19**, for acetylcholinesterase are **19**, **20**, **23** and **24** metal complexes and for butyrylcholinesterase the inhibitors are **2**, **3**, **14**, **18**, **19**, **20**, **22** and **23**. In all these compounds interesting results were obtained for **3** metal complex which is acting as selective inhibitor of butyrylcholinesterase and **7** and **11** which are acting as selective inhibitors for urease. Apart from it all the synthesized compounds were studied for their antimicrobial activities against pathogenic microbes including Gram positive bacteria *Bacillus atrophaeus*, *Bacillus subtilis*, *Staphylococcus aureus*, Gram negative bacteria *Klebsiella pneumoniae*, *Salmonella typhus*, *Pseudomonas aeruginosa*, *Escherichia coli*, *Agrobacterium tumefaciens*, *Erwinia carotovora*, fungal Strain *Candida albican*. These results suggest that metal complexes and Schiff base ligands are moderately active against these microbes.

All the compounds were studied for their thermal degradation studies using TG-DTA analysis in the temperature range 30-1000 ^{o}C under static air at 10 ^{o}C rise/minute. The thermogravimetry (TG) and Differential thermal analysis (DTA) curves were obtained and used for kinetic and thermodynamic calculations. The activation energies and order of pyrolysis were calculated using Horowitz–Metzger method. The TG results and calculated activation energies were subsequently used for the calculations of thermodynamic parameters including change in entropy of activation, change in enthalpy of activation and change in Gibb's free energy of activation.

Increasing activation energy order and also the order for stability was assigned to each studied series.

Part II

The synthesis of highly fluorinated zinc carboxylates [{$CF_3(CF_2)_5CH_2CH_2CO_2$}$_2$Zn], and alkoxides [{$CF_3(CF_2)_5CH_2CH_2O$}$_2$Zn(OEt_2)$_2$] and their use as catalysts for the ring opening polymerisation of ε-caprolactone are described. Quenching the polymerisation reaction with fluorous acids or alcohols regenerates the catalyst, which can be recovered by fluorous solvent extractions, and the catalytic activity is retained for three cycles. The superior recyclability of the alkoxide to the carboxylate zinc compound is due to the greater partition coefficient between fluorous and organic solvents. The well-defined aryloxide compound [$(ArO)_2Zn(THF)_2$] were also investigated, which yields very well controlled polymerisation, but cannot be recycled by quenching with a fluorous alcohol.

CHAPTER 1

1. INTRODUCTION

1.1 Schiff base ligands

Hugo Schiff reported the first Schiff base in 1864 by condensing carbonyl compound with amine resulting in the elimination of water molecules [1]. Different alkyl and aryl substituted Schiff bases can be produced containing the common skeleton RHC=N-R' where HC=N represent the the azomethine group, and R and R' are alkyl, aryl groups or even in the form of cyclo alkyl or heterocyclic groups. Dehydrating agents like calcium chloride, silica etc favours the formation of Schiff bases. Though the Schiff bases are stable compounds, care should be taken in the purification steps as it may undergo degradation viz; purification of Schiff bases on silica gel is not recommended as they undergo hydrolysis and splits into its parent constituent. The nitrogen in Schiff bases are sp^2 hybridized bear donatible lone pair which is of considerable chemical importance and the excellent chelating ability is imparted when there is some hetero chelating atom present close to the azomethine group. Examples of such ligands which bear both azomethine and other donating groups are shown in fig.1.1

That is why such ligands are getting particular attention due to flexibility in varying the chemical environment about the C=N group and such interesting ligands are actively involved in coordination chemistry. Aldehydes when condensed with amine produces important class of Schiff base. Some of the examples are shown figure 1.2.

Synthetic design of Schiff bases is influenced by stereogenic centers or chiral atoms, which can be achieved by introducing some coordinating hetero atoms like N, O, S, Se, As etc shown in Fig. 1.2.

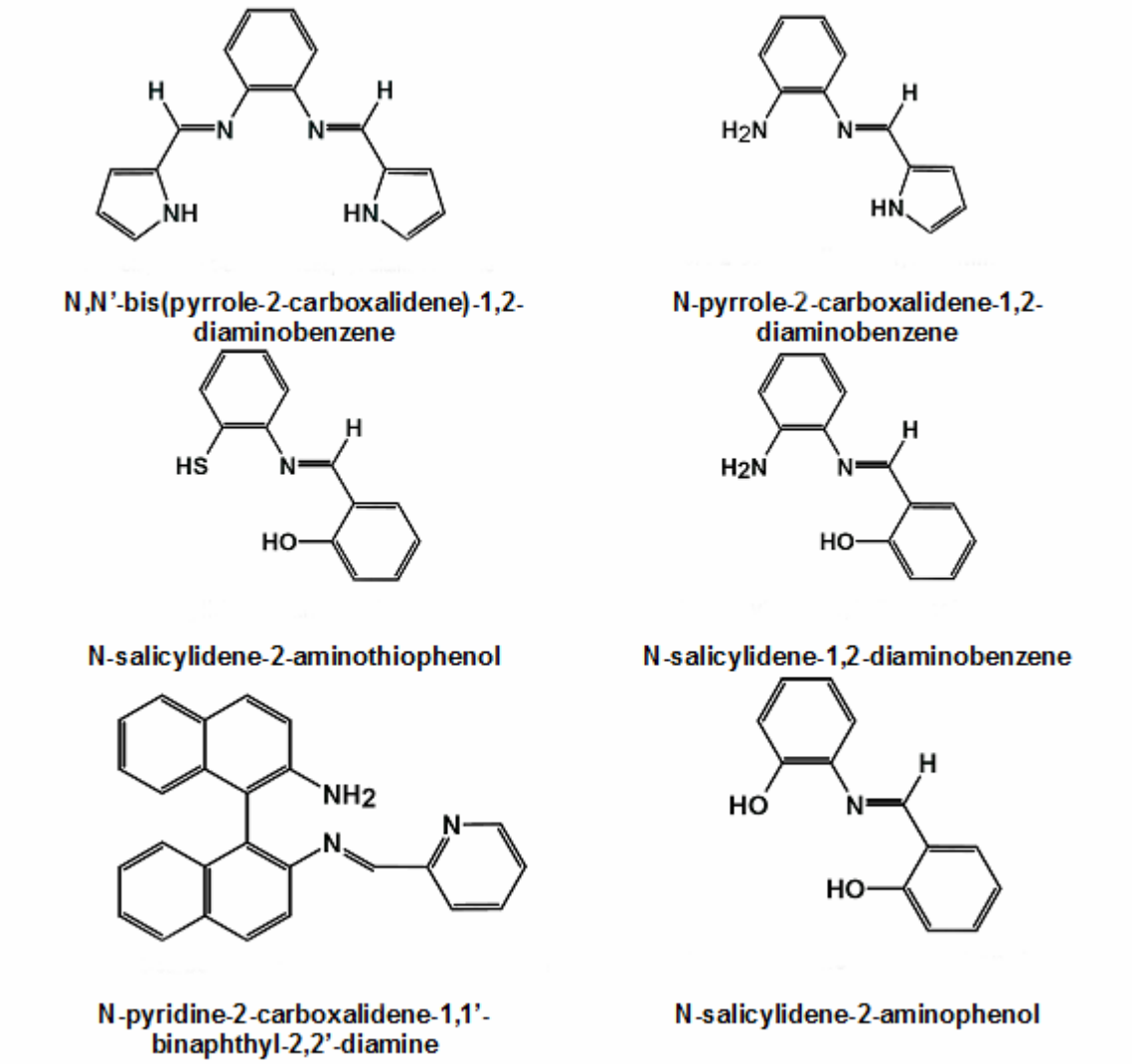

Figure 1.1 Examples of Schiff bases

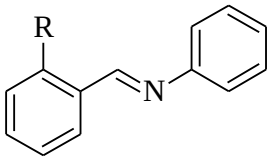

Where R = OH, SH, SeH, NH_2, PH_2, AsH_2 etc

Figure 1.2 Examples of Schiff bases with coordinating heteroatoms

1.2 Coordination compounds

Metal ions when surrounded by atoms or group of atoms or ions (ligands) produce coordination compound through coordinate covalent or the combination of both coordinate covalent and covalent interactions. The formation of coordination compounds is favoured by the presence of empty d-orbitals in central metal atoms which accommodate the incoming electrons from the donor atoms. The formation of coordinate covalent bond, in complexes, involves the donation of lone pair of electrons from ligands to the central metal atom/ion. The ligands may be neutral species like oxygen, sulphur, nitrogen, phosphorous, arsenic etc or it may be negatively charged (anion) such as halides, thiocynate, sulphide, nitrites, thiosulphate, azide etc as shown in figure 1.2 [2]. Coordination sphere in coordination compound is comprised of the central metal atom or ion, and the surrounding ligand. The number of ligands coordinated to the central metal atom or ion represent the coordination number. Simply it can be said that the coordination compounds are produced as a result of simple interaction of Lewis base and Lewis acid. Thus the interaction of the Lewis acid, central metal, with the Lewis base, ammonia, to form a complex $NiCl_2$ according to chemical equation:

$$NiCl_2 + 6NH_3 \rightarrow [Ni(NH_3)_6]Cl_2$$

Above coordination compound is produced by the donation of lone pair of electrons from ammonia to Ni(II) ion through coordinate covalent bond. The charges on the central metal ion and on the ligand, within the coordination sphere, are summed up and the complexes may be categorized as cationic, anionic, or neutral depending upon charge on the coordination sphere. The ligands which can cage the central metal atom or ion through more than one donor site are called chelating ligands. Chelating agent may be bidentate, tridentate or polydentate having two,

three or more donor sites respectively. The ligand like $N(CH_2CH_2NH_2)_3$, is said to be polydentate because there are four sites of attachment [3].

1.2.1 History of coordination compounds

History of coordination compound is as old as human beings and plants, both containing the complexes of iron and magnesium respectively. Therefore it can be said that coordination chemistry started when human being came into existence. German chemist and physician Andreas Libavius in 1597 was the pioneer of reporting the first known complex. His observations were based on the production of blue color when the brass is treated with ammonium salt (NH_4Cl) containing lime water. There are variety of coordination compounds and they have been used for variety of purposes since centuries. Alizarin dye is a calcium aluminum chelate complex of hydroxyanthraquinone and is bright red in color, was used extensively in India, Persia and Egypt. Artist use a pigment called Prussian blue, was known to man since 18^{th} century or ago than that period. Prussian blue is the complex of iron with molecular composition like $K_3[Fe(CN)_6]$. Hexachloroplatinate (IV) $K_2[PtCl_6]$ reported in 1760 was one of the ancient examples of coordination compound. It had been successfully employed to refine the elemental platinum.

There are various theories which were put forward when the coordination chemistry grown extensively. Most of the research on the properties of metal complexes and their use was the source of research in 19^{th} century and onward. But the past decade reveal the majority of work in this field. Various theories in coordination chemistry include the so called chain theory which was put forward by Swedish chemist Christian Wilhelm Blomstrand and was extended further by Danish chemist S.M. Jorgensen. This theory explained the nature of bonding on a wrong assumption. Werner was following Jorgenson's theory and put forward his theory in 1893. This

theory was actually based on the nature of different kind of attachments, primary and secondary. These theories were not sufficient to explain the complex nature of the bonding in coordination compounds. Therefore theories like Valence bond theory, crystal field theory, ligand fied theory and molecular orbital theory were developed subsequently with the passage of time. Linus pauling was the pioneer to propose VBT [4], similarly crystal filed theory (CFT) [5,6] was proposed by Van Vleck and the molecular orbital theory was put forward by Hund and Mulliken [7]. A separate distinct theory was given for ligand interaction with metal ions called as ligand field theory [6]. These theories not only explain the bonding situation in coordination compounds, properties like fluorescence, phosphorescence etc can also be explained to a greater extent making the coordination compounds useful in medicinal chemistry.

1.2.2 Synthetic routes followed for metal complexes of Schiff base ligand

Metal complexes can be synthesized by following many routes as shown in fig. 1.3.

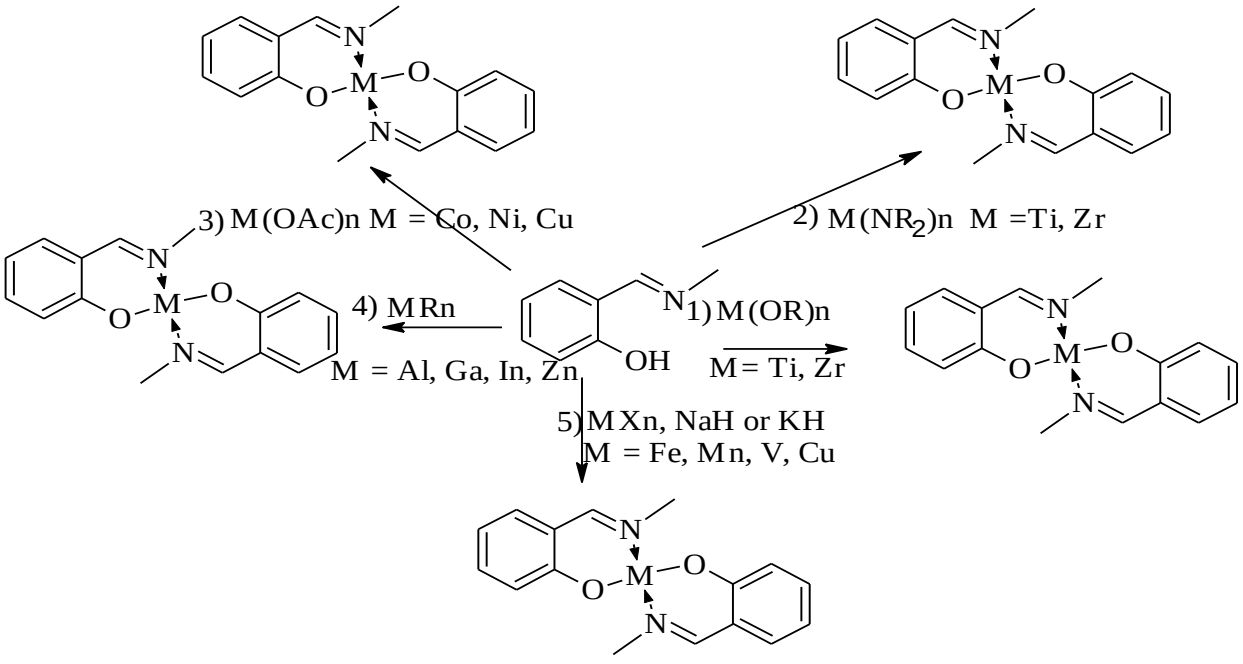

Figure 1.3 Different routes for the synthesis of coordination compounds

Route 1: Metal alkoxides [M(OR)n] of early transition metals (M = Ti, Zr), are used in this type of synthesis. This route is determined by equilibrium between metal salt and the Schiff base ligand, therefore different species are generated during the reaction. In order to avoid side products, Schiff base complexes with bulky ligands are used. Disproportionation reaction occur between Schiff base and the metal alkoxides and the stability is dominated by equilibrium constants for such type of complexes.

Route 2: Early transition metals like Ti and Zr can be complexed with Schiff base ligands using the metal amide route. This route follows the elimination of the phenolic proton by the amide which is converted to volatile $NHMe_2$.

Route 3: Metal complexation of the Schiff base ligand can also be performed by using metal acetate salts. Metals are usually present in the oxidation states Co(II), Co(III), Ni(II) and Cu(II). This type of metal complexation is carried out by reflux process.

Route 4: This route is the most efficient and clean route for metal complexes and organometallic compounds preparation. In this route alkyl derivatives of metals like aluminium, gallium and indium, in air and moisture free environment are used. Apart from it Fe, Mn, V, and Cu can also be complexed with Schiff base ligands by using their corresponding mesithyl derivatives. Metal halides are produced by following Grignard routes using alkyl halides.

Route 5: Early transition metal complexes with Ti and Zr metals can also be prepared by deprotonating the phenolic group using NaH or KH in coordinating solvents like THF and then reacting the corresponding Na or K salt of the Schiff bases with the metal salts. Metal salts are usually chlorides or bromides which are eliminated as ionic salts, being insoluble in THF. Therefore these salts can easily be separated by filteration process.

1.3 Applications of Schiff base transition metal complexes

The Schiff base complexes have a number of applications which will be discussed briefly:

1.3.1 As an electroluminescent materials

Since Tang and Van Styke first reported high-performance organic electroluminescent (EL) devices which were found useful in novel-type flat-panel displays [8]. The EL device is basically comprised of two parts like an emitting layer and a carrier transport layer, both of which are suitable organic materials. Along with organic dyes, chelate metal complexes and polymers are other major categories of materials used in the fabrication of organic EL devices. The chelate metal complexes because of their high emitting nature were employed as materials for RGB (red, green, and blue) emission.

Zn(II) Schiff base metal complexes are used as electroluminescent materials now a days [9,10]. The chelation was performed using the Schiff base, N,N'-bis(2- hydroxy-1-naphthylidene)-3,6-dioxa-1,8-diaminooctane. The zinc complex was found emitting blue light with an emission peak at 455 nm having maximum brightness of 650 cd m^{-2}, and hence was used as the emitting layer in an electroluminescence device. Fabrication of EL devices employing this kind of zinc complexes as blue electroluminescent material was carried out by thermal vacuum-deposition. Wei et al. prepared blue luminescent zinc and beryllium complexes of the Schiff bases derived from calixarene [11]. The Schiff bases derived from salisylaldehyde and its complexes have good solubility in normal solvents and can easily form thin films. One of the Schiff base is salicylidene(4-dimethylamino)aniline, Xie et al. reported the crystal structure, thermal stability and optoelectronical properties of bis[salicylidene(4-dimethylamino)aniline]zinc(II) [12], which exhibits very good light emission and charge transporting performance in organic light emitting

diodes (OLEDs). All such transition metal complexes with Schiff bases points to the possible use in full colour flat-panel displays as an emitting material.

1.3.2 In non-linear optical devices

Spin cross over effect is an effect in which low spin state is converted to high spin state by applying varying magnetic field. Nonlinear optics (NLO) deals with the interactions of electromagnetic field applied and electromagnetic field generated which vary in frequency, phase, or any other physical properties. This effect is observed when metal complexes show spin cross over effect. Therefore such complexes can manipulate photonic signals efficiently and are of importance in optical communication, optical computing, and dynamic image processing [13-23]. Metal and organic interactions, which cause various excited states, make these compounds unique [18-23]. Metal complexes are thermally stable as compared to the neat organic ligands and also they offer variation in structures, magnetic and electrochemical properties therefore they can be used for tunable NLO materials [24-26].

1.3.3 In electrochemical sensors

Schiff base complexes have been found to be effectively acting as sensors for either cations or anions [27-37]. Examples include the Schiff base complexes of Ru(III) were used for the selective determination of chloride ions in serum samples over a wide range of concentrations[38]. Apart from it some salicyldehyde derived Schiff base ligands were used for direct determination of aluminium in biological systems [39]. Similar Schiff base ligands were also employed for fabrication of sensors which selectively determines the Mn^{2+} ions [40].

1.3.4 Schiff base transition metal complexes in catalysis

Schiff base metal complexes were found very useful in both homogeneous and heterogeneous catalysis. The catalytic activity of a particular Schiff base metal complexes varies with the type

of ligand. A variety of catalytic activities for both homogeneous and heterogeneous catalysis have been seen over the few decades. Few of these catalytic activities are mentioned below:

1.3.4.1 Polymerization Reaction

1.3.4.1.1 Chain polymerization

Schiff base ligands complexed with aluminum as shown in scheme 1.1, are actively used for the polymerization of ethylene.

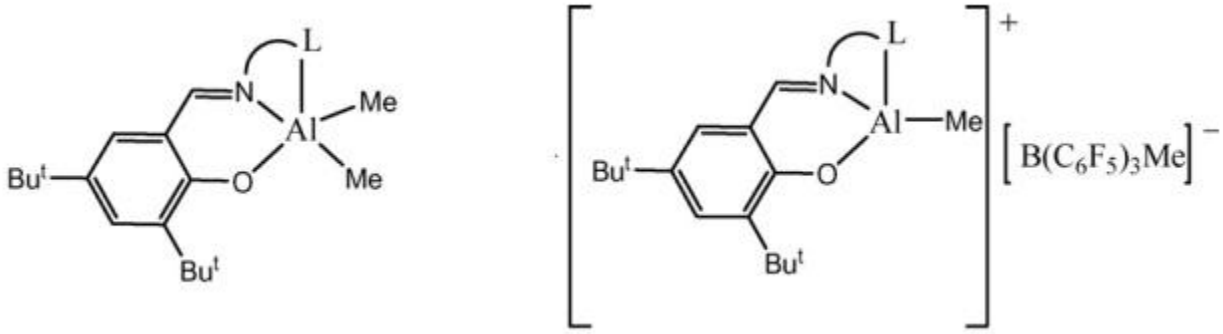

Scheme 1.1 Aluminium complex of tridentate saline type ligand

Schiff base like pyridyl bis(imido) when complexed with cobalt center or iron as shown in scheme 1.2, also catalyzes polymerization of ethylene.

The zirconium, titanium and vanadium complexes of phenoxy-imine were also used successfully in the polymerization of ethylene [41-49].

1.3.4.1.2 Ring opening polymerization

Ring opening of epoxides (shown in scheme 1.3), caprolactone or lactides (scheme 1.4) produces long chain polymers of particular interest promoting the green chemistry. Schiff base metal complexes of ruthenium and aluminium were depicted to be particularly useful in catalyzing the process.

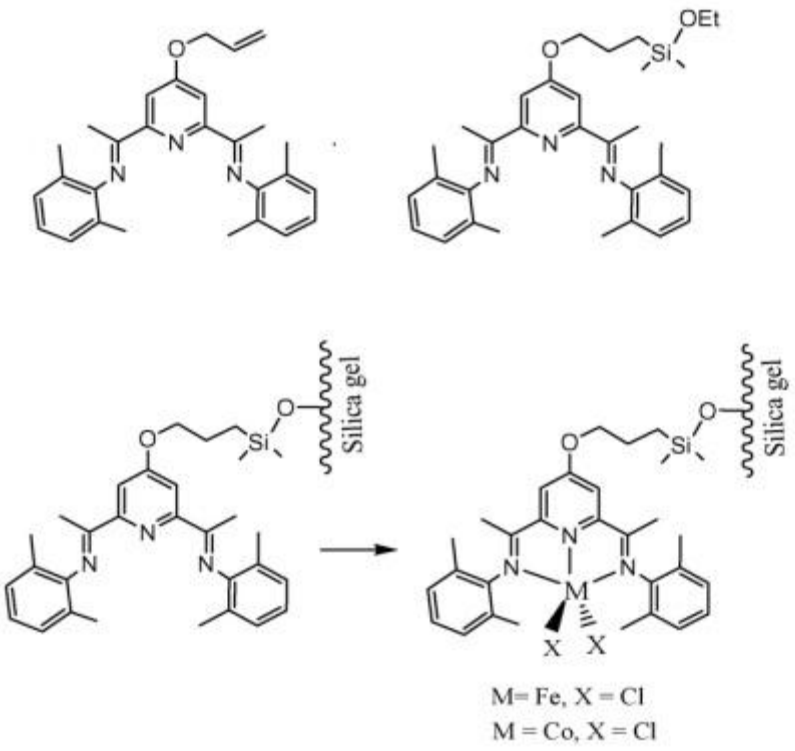

Scheme 1.2: Tridentate Schiff base complexes of cobalt and iron supported on silica

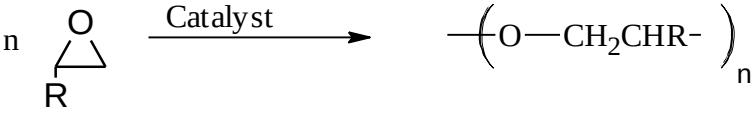

R= H, CH_3, CH_2Cl, $CH_2OCH_2CH{=}CH_2$

Scheme 1.3: Ring opening polymerization of Epoxides

1.3.4.2 Oxidation Reaction

Schiff base complexes of various metals like chromium(III), manganese(II), iron(II), cobalt(II), nickel(II) and copper(II) were tested for their activity in the oxidation reactions. Transition metals encapsulated in zeolite were seen very useful and effective in the oxidation catalysis of cyclohexane to cyclohexanol and cyclohexanone [50]. This type of catalysis was found more successful with Schiff base complexes of manganese(II) ions. Baer-Villager oxidation reaction

was also shown by cationic cobalt(III). 3-phenylcyclobutanone is oxidized to lactone in the presence of H_2O_2 by the cobalt (III) and Zr(III) Schiff base metal complex [51].

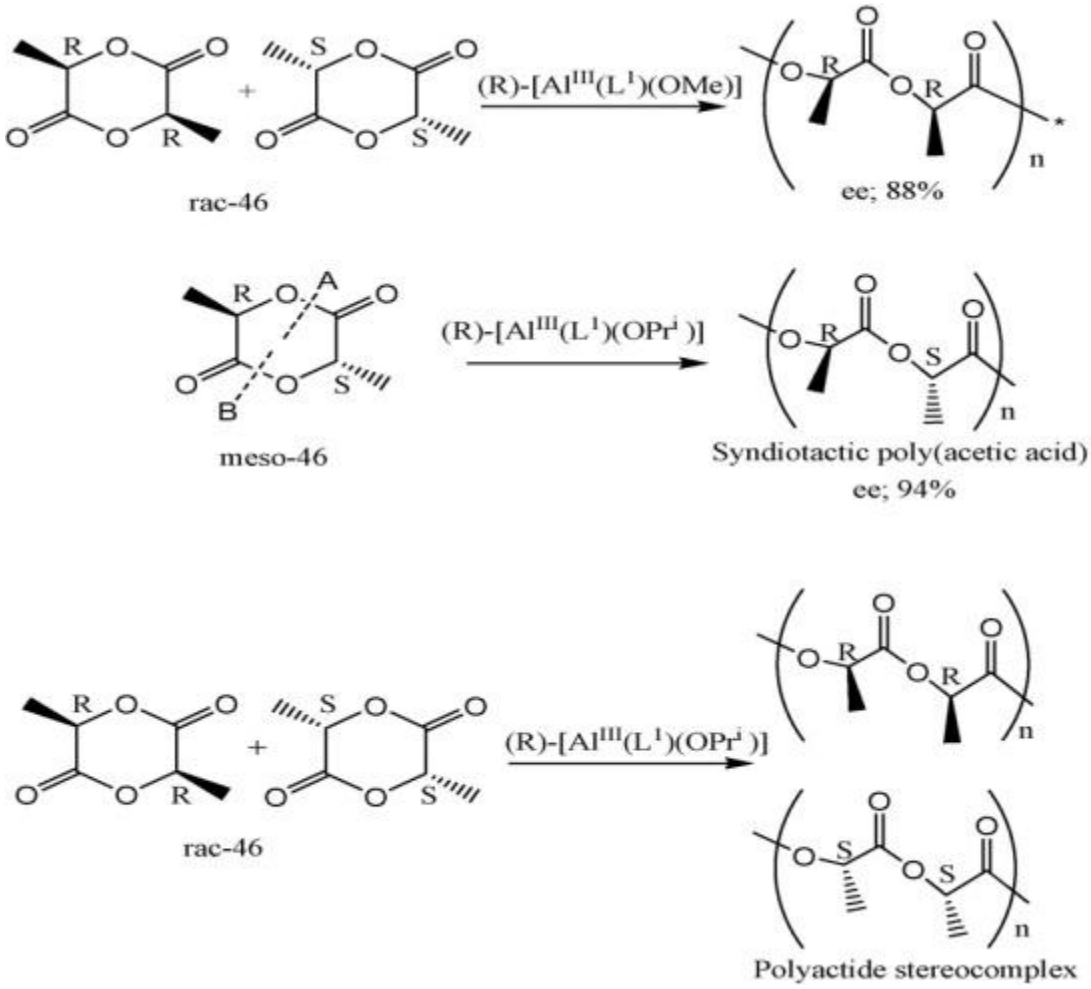

Scheme 1.4: Ring opening polymerization of lactide

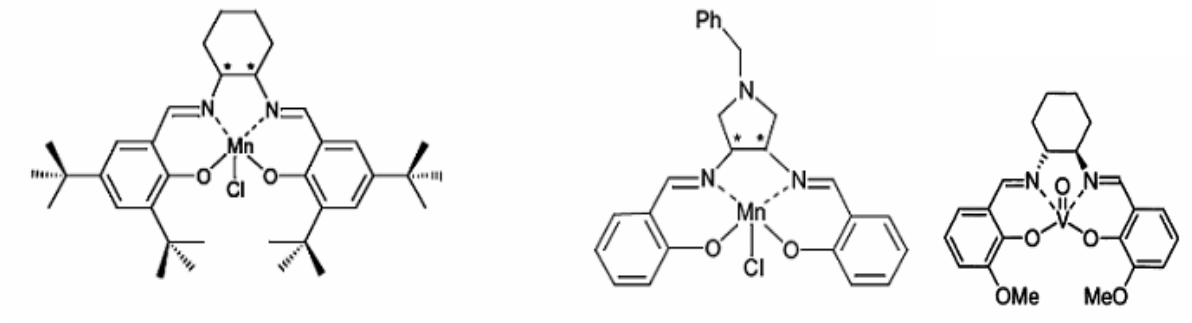

1 **2** **3**

Figure 1.4 Manganese and vanadium complexes of ONNO type Schiff base ligands

Manganese complexes of the types as shown in figure 1.4 were found to be involved actively in catalyzing oxidation of a range of silyl enolethers to α-hydroxyketones [52]. Apart from it, complex of the type **1** have been used in the asymmetric oxidation of silyl ketene acetals in high enantioselectivity [53].

Enantioselective sulfide oxidations to the corresponding sulfoxides can be achieved by using tetradentate Schiff base oxovanadium complex of type 3 with 42% ee selectivity.

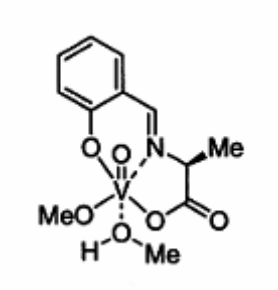

4

Figure 1.5 Oxovanadium complex of tridentate Schiff base ligand

The oxovanadium(V) complex **4**, which is produced by the condensation of amino acid derive Schiff base ligand, was found to catalyse the asymmetric oxidation of sulphoxide [54].

Schiff base ligands with donor sithe –O-N-O- when complexed with transition metals like Titanium(IV), vanadium(IV), copper(II) or zinc(II) have been found useful in asymmetric chemical transformation of benzaldehyde to cyanohydrin in the presence of trimethylsilylcyanide (TMSCN) (scheme 1.5) [55,56].

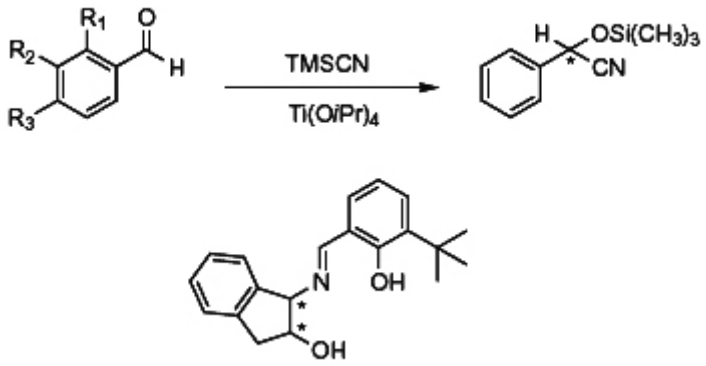

Scheme 1.5. Cyanohydrin formation by titanium Schiff base complex

Co(salen) and its various analogues, shown below in figure 1.6, have been successfully used for the oxidation catalysis of phenols and alcohols with dioxygen [57]. The mechanism of the catalysis is simple, Co(Salen) is providing the axial position available for the dioxygen to bind with in the presence of base like pyridine and use the dioxygen for oxidation reactions (Figure 1.6).

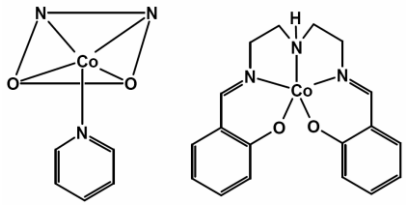

Figure 1.6 Cobalt salen Schiff base complexes

1.3.4.3 Epoxidation reactions

Chromium and manganese complexes of the chiral Schiff base ligand were found effective in the asymmetric epoxidation of the alkene [58].

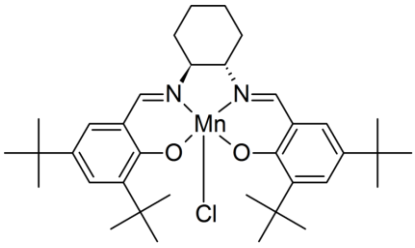

Figure 1.7 Manganese chiral Schiff base complex

Manganese Schiff base complexes of the O,N,N,O type known as Jacobsen's catalyst as shown in figure 1.7, have demonstrated to be very effective for the enantioselective epoxidation of unfunctionalised olefins [59,60]. Apart from it some Ruthenium complexes like trans-$[RuCl_2(bpydip)]$ and trans-$[Ru(OH)_2(bpydip)](PF_6)_2$ with tetradentate Schiff base ligand N,N'-bis(7-methyl-2-pyridylmethylene)-1,3-diiminopropane (bipydip) have been used successfully as catalysts in the epoxidation of cyclohexene and conjugated olefins [61, 62].

1.3.4.4 Hydrogenation reactions

Schiff base metal complexes of ruthenium have been found active in the asymmetric reduction of dialkyl ketones. The catalytic reaction regulated by $[RuX(PPh_3)(LL')]$ where X = Cl^- or Br^-, and LL' = [ONNO] donor of the heterocyclic Schiff base ligands is carried out in the presence of isopropanol and KOH [63-66]. Following Schiff base ligands can be used for the asymmetric reduction (fig. 1.8),

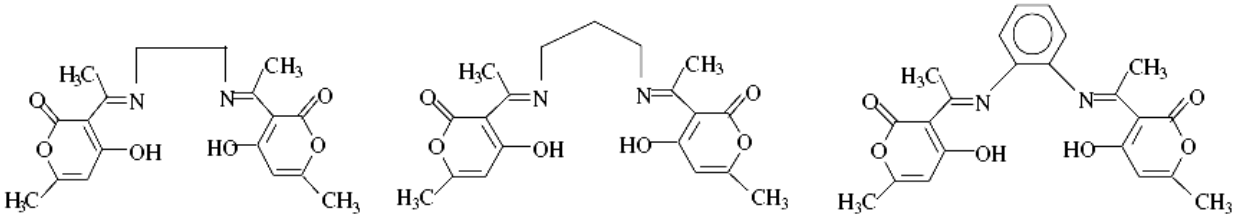

Figure 1.8 ONNO types of Schiff base ligands

Palladium complexes as shown below in figure 1.9, contain anionic linkage like chloride and acetate, have been employed for the reduction of alkenes and alkynes [67]. Two representative examples of these Schiff base complexes are given below (fig1.9).

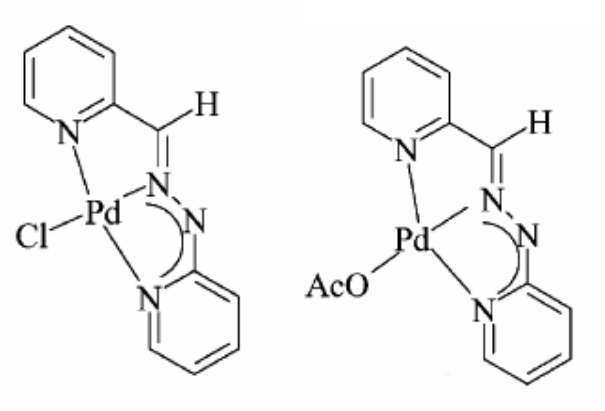

Figure 1.9 Palladium complexes of tridentate Schiff base ligands

Chiral P,N,O ferrocene based dimeric complexes of the Schiff bases have been used for the reduction reactions. Such types of chiral Schiff base ligand of ferrocene are represented in fig 1.10.

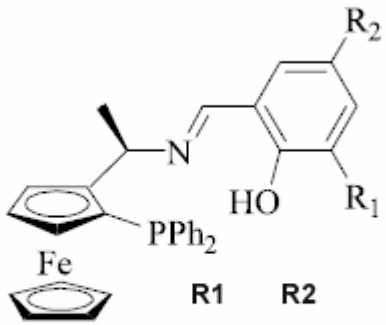

Figure 1.10 Schiff base anionic ligand of ferrocene

1.3.5. In medicinal chemistry

Many medically important compounds are known with Schiff base linkages [68-70]. It has been seen that metal complexation effects the biological activities of the Schiff base ligands to a great extent [71-73]. Depending upon the metal center, the coordination compounds of the metals like Cobalt(II), nickel(II) and copper(II) were found very useful in antimicrobial, antiviral and antifungal activities. For example Schiff bases derived from 3-substituted-4-amino-5-mercapto-1,2,4-triazole and 8-formyl-7-hydroxy-4-methylcoumarin illustrated enhanced antibacterial activities against *Escherichia coli*, *Staphylococcus aureus*, *Streptococcus pyogenes*, *Pseudomonas aeruginosa* and *Salmonella typhi* antifungal (*Aspergillus niger*, *Aspergillus flavus* and *Cladosporium* [74] and the Cr(III), Fe(III) and Co(III) complexes 1,4-bis[3-(2-hydroxy-1-naphthaldimine)propyl]piperazine and 1,8-bis[3-(2-hydroxy-1-naphthaldimine)-*p*-menthane, show moderate antimicrobial activity than parent ligand [75]. Metal complexation of Schiff base ligand derived from vanillin and DL-α-aminobutyric acid with metal ions like Co(II), Ni(II), Cu(II) and Zn(II) complexes were also found to exhibit higher antibacterial activity as compared to the free Schiff bases [76]. Apart from it binuclear complexes have been found very active against pathogenic bacterial and fungal strains, as an example presented by mono and binuclear transition metal complexes of the Schiff base derived from phenylaminoacetohydrazide and dibenzoylmethane, which have been found more active against pathogenic bacteria and fungi than the neat ligand [77].

Many scientists had reported the antimalarial activities of the Schiff base metal complexes. According to them metal complexes act as chloroquine that target hemozoin either by covalent or non-covalent interactions [78-80]. When metal complexes interact covalently with the hemozoin, the labile part made available by the transition metal complex is replaced by any nitrogenous

base of DNA or RNA. Similarly, there are some non-covalent DNA or RNA interactions which include intercalative, electrostatic and groove binding of cationic metal complexes along the periphery of DNA helix, or along the major or minor groove. Intercalation refers to the partial insertion of aromatic heterocyclic rings between the DNA base pairs.

Investigations on the DNA binding studies of transition metal complexes lead routes for the rational drug design, as well as provide the full mechanistic approach to DNA repair or rupture during drug interactions [81-93]. Ruthenium, platinium, rhodium, silver, gold, iron, chromium, cobalt and vanadium centered metal complexes of the Schiff base ligands were used significantly for the DNA binding, rupture of DNA strings, or mutation in DNA. For example Ru(II)–PPh_3/$AsPh_3$ complexes of the hydrazone oxime ligands have been found active against selected bacterial species and they were tested for their capabilities to bind to Herring sperm DNA in mixed modes [92].

Tridentate –NNO- Schiff base ligand, derived from the condensation reaction of 2,6-dibenzoyl-4-methylphenol with diamines produced Ni(II), Cu(II) and Zn(II) complexes which had been tested for their native calf thymus DNA binding studies [94-99]. Quinolone, a medically very important compound had been condensed with salicyldehyde to produce Schiff base salicylaldehyde-2-phenylquinoline-4-Carboylhydrazone, complexed with Co(II) and Cr(III) and have been tested for DNA binding studies via groove binding mode of interaction [100,101].

Research on the DNA binding studies was extended to the binuclear metal complexes as well, for example copper(II) complexes of the Schiff base ligand, N,N'-bis(3,5-tert-butylsalicylidene-2-hydroxy)-1,3-propanediamine, have been found effective in the cleavage of plasmid DNA without the addition of any external agents and in the presence of hydrogen peroxide at pH = 7.2 almost at body temperature. Mostly the DNA cleavage is followed when the complexes have the

capabilities to oxidise the substrate [102]. Apart from it other DNA binding mechanisms like electrostatic interactions can also be proposed for the metal complexes. Such type of metal complexes which interact electrostatically with DNA have also been synthesized by the condensation of the salen ligand with Fe(III) [103]. Other interactions through which metal complexes interact with DNA, through coordination or chemical nucleases to promote its degradation [104].

1.3.6. Coordination chemistry of Co, Ni, Cu and Zn (II) metal ions

A number of proteins and enzymes containing coordination compounds of copper have been isolated from both plants and animals. For example Ascorbic acid oxidase, cytochrome oxidase, tyrosinases, hemocyanin etc. All of them are of particular importance inside the body for example (I)Ascorbic acid oxidase is involved in catalytic oxidation of ascorbic acid to ehydroascorbic acid in the presence of O_2, which act as electron-acceptor in the process. (II) Cytochrome oxidase is involved in four electron reduction of oxygen to water, in which cytochrome C act as elctron donor and copper is essential part of it. (III) Tryrosinases and catechol oxidases, act as a catalyst for the melanin pigment formation. Both of these enzymes contain binuclear copper which coordinate oxygen during the charge transfer from ligand to copper. (IV) Hemocyanin works in a similar manner like tyrosinases and oxidases in lower animals, like snails and crabs and it is evidenced that it can bind and carry oxygen for the respiration process [8]. All these proteins are copper based mononuclear or binuclear enzymes.

Zn^{2+} is an essential constitutent of the body of all animals. Several disorders have been found to be due to the zinc deficiency. 2 to 3 grams of zinc is present in human baody in the form of more than eighty enzymes e.g RNA and DNA polymerases, transphorylases, alcohol dehydrogenases, carbonic anhydrases etc [9].

Another important coordination compound of cobalt, Vitamin B_{12}, is present in plants, animals and microorganisms. It metabolises the nucleic acids and plays a vital role in protein synthesis. Its deficiency causes pernicious anemia in humans [10].

Chelate therapy is widely used for the treatment of metals, present in amounts toxic to the organism's body. Excess of copper and iron are removed by chelating D-penicillamine and desferrioxime B with these metals. Some coordination compounds of platinum have been effectiently employed in inhibiting the growth of tumours.

1.3.7. Aim of work

We have focused upon the synthesis of Co(II), Ni(II), Cu(II) and Zn(II) metal complexes of some already known and some novel Schiff base ligands, their complete analytical and spectroscopic characterization. These metal complexes have been studied biologically for their inhibitory activities against *acetyl cholinesterase, butyrylcholinesterase, urease, α-chymotrypsin,* and antimicrobial activities. This work will lead to the development in the work related to metal based drugs, a new emerging field of study. Individually each of the studied enzyme inhibitory activities are discussed as follows:

1.3.7.1. AChE and BChE inhibition

Alzheimer's disease (AD) is a degenerative brain disease, which destroys the neurons and the connections to the cerebral cortex and causes dementia which progresses from short term memory loss to complete immobility [105]. Dementous neurofibillary tangles are probably caused by the oxidative effects of lipids [106-108]. Amyloid beta (Aβ or Abeta) is a peptide linkage of 36 to 43 amino acids and appears to be the main constituent of amyloid plaques found in the brains of patients with Alzheimer's disease. Aβ is involved in oxidative stress of the lipids found in the cell membranes of the tissues which ultimately lead to dementia. The hydrolysis

reaction as shown in scheme 1.6 below takes place at the catalytic site, of which the residue serine 200 (Ser-200) is an integral part.

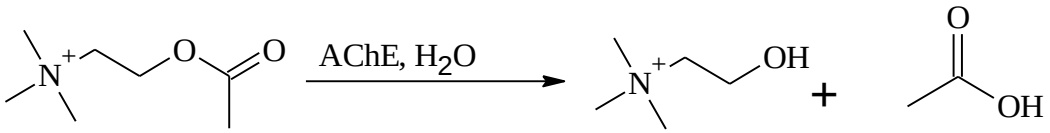

Scheme 1.6. Hydrolysis of ACh by AChE

Inhibition of acetylcholinesterase is considered as a promising approach for the treatment of Alzheimer's disease (AD) and which can lead to the possible therapeutic treatment of Parkinson's disease, ageing, and myasthenia gravis [109,110]. Meanwhile, inhibition of butyrylcholinesterase (BChE) has been found to be directly associated with the side effects of the acetylcholineesterase (AChE) inhibitors. The selective or the combination of both the inhibitors will lead to drugs discovery for the treatment of Alzheimer Disease (AD) [111]. BChE has been found in significantly higher quantities in AD plaques than in the plaques of age related non-demented brains, therefore it becomes apparent that drugs involved in the inhibition of BChE inhibition only may also act as possible therapeutic agent for the treatment of AD. Therefore the side effects profile of AChE selective inhibitors may not only restricted to AChE only but it can effect BChE as well [112]. To overcome AD, drugs have been developed which prevent the hydrolysis of the acetylcholine by blocking the acetylcholinesterse (AChE). Acetylcholinesterase inhibitors (AChEIs) prevent the acylation of the hydroxyl group of Ser200. Reported AChEIs are (-)-Huprine, Tacrine, and Hup A Dimers (fig.1.11) [113-124].

Furthermore, it was found that the brain requires high metal ion [Cu(II), Zn(II) and Fe(III)] concentrations for numerous essential functions. In Alzheimer's patients the metal ion homeostasis is severely deregulated. The metals are not aggregates but only part of these i.e. they accumulate in the form of Aβ aggregates in dementia and hence stressful oxidative processes are

triggered. Therapies, which are currently used for overcoming the oxidative stress, include i) ameliorating or inhibiting Aβ aggregation and induced ROS (Reactive Oxygen Species) generation, ii) use of antioxidants and iii) use of metal chelators. Clioquinol metal complexes are found to be the most promising drugs in AD treatment. Despite the human trials for clioquinol drugs already taking place, the mode of action is still not clear [125]. Our interest in investigating AChE and BChE inhibition came from the study carried out by Budimir et al. of the metal based drugs of this important class of ligands. According to them, ligands of such class can take part in metal exchange reactions which will ultimately lead to decrease in Aβ plaques [125].

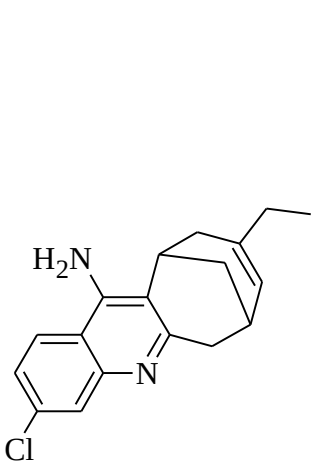

(-)-Huprine

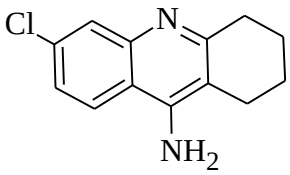

Tacrine

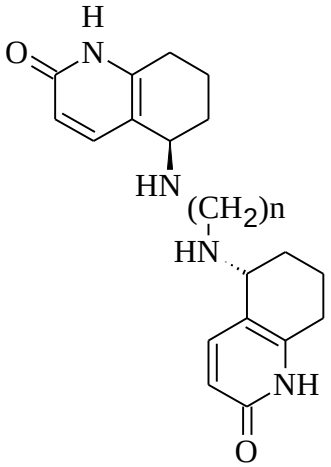

Hup A Dimers where n = 10 & 12

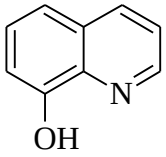

Cliquinol

Figure 1.11 Drugs used for treating Alzheimer Disease

It was also found that metal chelators of the N, O -type with an aromatic environment can easily cross the blood brain barrier and can cause the formation of metalated rings including aromatic properties with Aβ plaques. The ab-initio DFT of various aromatic ligands toward copper complexation studies carried out by Sodupe et.al. shows that increasing the sigma donating property of the ligand might affect the therapeutic activity of the complexes [125]. In the synthesized Schiff base ligands the various alkyl and aryl groups attached to nitrogen are increasing the electron density of the ring and hence the covalency toward transition metal ions. It was also found to offer opportunities for inducing substrate chirality and reorientations in geometry around the metal center, thereby tuning the metal's electronic structure. Metal complexes of Ni(II), Co(II), Cu(II) and Zn(II) were synthesized by condensing with Schiff base as ligand precursor. The metals are not aggregates but only part of these i.e. they accumulate in the form of Aβ aggregates in dementia, therefore these metal complexes are supposed to be active in overcoming the oxidative stress of metal ion accumulation in Aβ aggregation. The brain of Alzheimer patients show that metal ions present inside the body accumulate in plaques which consequently produce hydrogen peroxide causing damage to the brain. Previously it was reported that metal complexes containing copper aggregate the senile plaque more efficiently than any other metal complex [126]. Here we extended the research in this field to certain other metal ions such as cobalt (II) and nickel(II). These metal complexes will potentially lead to increased metal ion concentration through exchange processes and decreased senile plaques. This study should be of great importance in the exploration of metal based drugs for neurological disorders.

1.3.7.2. Urease and chymotrypsin inhibition

The coordination compounds are of considerable interest because metal ions are found in the active sites of a large number of metalloproteins as discussed in section 1.3.5 [127–129].

Enzymes and proteins like hemocyanine, tyrosinases, oxidases, etc are involved in various biological processes such as biological electron-transfer reaction, oxygen atom insertion into substrates, dioxygen reduction to hydrogen peroxide or water and hydrolytic reactions. Urease (urea amidohydrolase EC 3.5.15) is a nickel containing metalloenzyme which catalyzes the hydrolysis of urea to ammonia and carbon dioxide. Urease uses urea and release ammonia which is acting as rich nitrogen source [130-133]. This enzymatic behavior can be seen in various organisms like algae, fungi, bacteria and even human beings which causes an abrupt elevation in the blood pH with side effects like cell death, kidney failure, severe ulcer, urolithiasis, pyelnephritis, and hepatic encephalopathy, hepatic coma and urinary catheter encrustation including cancer as well [130, 134]. Systemic nitrogen transport pathways in plants are defended by urease [135]. Due to the diverse functions of this enzyme, there are several reports for the inhibition of this enzyme by potent and specific compounds which may provide an invaluable addition for treatment of infections related to pus formation, peptic ulcer etc.

α-Chymotrypsin (EC 3.4.21.1) is a protease enzyme secreted by pancreas inside the body. It was found that it is involved in catalyses of the breakdown of polypeptide chains and proteins. Chymotrypsinogens is the precursor of chymotrypsin which was found in the cleavage of the active enzyme before the target side, consequently digesting the tissues inside the body such as in cases of pancreatitis [136]. α-Chymotrypsin has been found to be involved in clearance of ulcer by digesting damaged tissue and debris in the infected site [136-138]. Selective urease inhibitors which are also not involved in inhibiting α-chymotrypsin, may enhance the rate of healing the peptic ulcer. Due to this unique feature of action in treating peptic ulcers both urease and α-chymotrypsin were selected for their inhibitory activities of the synthesized compounds.

1.3.7.3. Antimicrobial and antioxidant activities

Different pathogenic microbes bear resistance to the antibiotic drugs. Therefore effective drugs must be developed which can kill the bacterial or fungal strain and become candid drug for the disease being treated. It is actually medical obligation to develop a drug of novel and more efficient mechanistic approach. Schiff bases have been pointed to as promising antibacterial agents. For example, N-(salicylidene)-2-hydroxyaniline is effective against Mycobacterium tuberculosis H37Rv, exhibiting an MIC value of 8 lg/mL [139]. There is an increasing interest in the synthesis, characterization and biological studies of the Schiff base chemistry in medicinal applications. Variety of Schiff bases have been reported from time to time which were derived from aldehyde and various amines. In 2005, Panneerselvam et al. [140] described the synthesis and in vitro antibacterial activity of some morpholine-derived Schiff bases. These compounds have been tested for antimicrobial activities against different pathogenic bacteria and were found active against S. aureus and Micrococcus luteus. It was found that these bacterial were most sensitive to the morpholine-derived Schiff base (MIC= 20 and 32 lg/mL, respectively). Similarly Streptococcus epidermidis was more sensitive to this morpholine-derived Schiff base ligand (MIC =17 lg/mL) and Bacillus cereus and E. coli with MIC= 21 and 16 lg/mL, respectively. Free radicals inside human body play a pathogenic role in most of the chronic degenerative diseases which include cancer, autoimmune, inflammatory, cardiovascular and neurodegenerative diseases, and aging [141,142]. Free radicals can be classified into two types i.e. endogenous and exogenous, former arise from metabolic processes inside cell whereas the latter come from various daily useable things like smoking, drugs, food additives, charcoal cooking, overheated food, burnt food, exposure to UV rays etc. Free radicals coming from endogenous processes are majorly dominating the other sources. This type of free radicals are

coming from the oxidative breakdown of fats and protiens to fatty acids and amino acids respectively. Fats are converted to fatty acids in the peroxisome of the cell along with involvement of P450 enzyme. Likely wise proteins which are comprised of very extensive covalent bonds also produce thousands of free radicals daily [143,144].

Oxygen free radicals are extensively found inside human body which cause damage to the cells and results in type 2 diabetes. In this kind of diabetes the free radicals were found to be involved in oxidation process of numerous lipids of the cell membrane. This whole process lead to the interference in the activity of islet cells to release or make insulin or otherwise absorb components to make insulin. Like wisely, atherosclerosis, another very fatal disease is also caused by the oxidation process in lipid cholesterol which is contained inside the Low-density lipoprotein (LDL) molecule-Ox-LDL. Some other degenerative diseases also have roots in oxidized lipids [145,146].

Thereby, drugs which scavenge the free radicals in order to decrease the oxidation processes inside body, must be developed [147,148]. Owing to the fact increased attention in biological research attracted the researchers to develop such drugs. Gabapentin and many other Schiff base ligands are already being used for various diseases, therefore, a novel Schiff bases obtained after reacting amine with 2-hydroxy aldehydes.

Schiff base ligands were presumed to be potential models of protiens active sites, therefore study of metal complexes for their reactivity toward dioxygen or free radicals and antimicrobial activities will reveal the interaction mode inside body [149]. Here we are reporting the metal complexes of novel Schiff base ligands with divalent metal ions like Co, Ni, Cu and Zn and their effectiveness toward various Gram positive, Gram negative and fungal strains. Transition metal

complexes with such bidentate ligands can also be studied for their enhanced reactivity toward dioxygen [150,151].

1.3.7.4. Thermal studies

Thermogravimetry is a process in which a substance is decomposed in the presence of heat, bonds inside the molecules are broken, new free radicals and neutral molecules are produced etc. [151, 152]. Differential scanning calorimetric (DSC) method have been widely used to determine non-isothermal transformation kinetics. Differential thermal analysis (DTA) and differential scanning calorimetry (DSC) were found to be important in obtaining the specific heat and enthalpies of the compounds. Both the techniques can be used to determine the amount of heat, taken up from or emitted to the surroundings, per unit time during isothermal changes. Heat capacities, Gibb's free energy, transition temperatures, melt enthalpies, entropy etc., can be measured and also phase transitions, crystallization processes, thermal conductivities etc. can be calculated from those curves. The thermodynamic parameters are of valuable importance for the study of heat transport mechanism in different compounds in solid state. Thermal decomposition behavior depends on the nature of metal complex; therefore it may occur in one or more steps. Decomposition mostly ends with the formation of the metal oxides. It is also found that thermal behavior of the metal complexes is related to the decomposition of the ligand molecule. The thermal stability of the complexes, in solid state, was verified by comparing the initial temperatures of decomposition of the complexes. Kinetic and thermodynamic parameters like activation energy, enthalpy, entropy, Gibb's free energy and heat capacity of thermal decomposition are calculated by differential thermal analysis and other thermo analytical methods. The practically important Schiff base compounds have been the focous of attention for their thermal behavior [153-155].

The present work reports the thermal degradation of the Schiff base metal complexes of divalent Ni, Co, Cu and Zn metal ions.

1.4 References

[1] H. Schiff, *Ann. Suppl.,* **1864**, 3, 343.

[2] Dwyer and Meller, *Chelating Agent and Metal Chelates,* Academic Press, New York **1964**, 283-329.

[3] J. E. Huheey, E. A. Keiter and R. L. Keiter, *Inorganic Chemistry,*4th edition., HarperCollins, New York, **1993**, appendix A3.

[4] W.K. Musker and M.S. Hussain *Inorg. Chem*., **1966,** 5, 1416.

[5] G. Schwarzenbach and H. A. Hella, *Chem Acts*., **1949,** 32, 1682.

[6] S.R Bullock and J. L. Berwartch, *J. Org. Chem.*, **1949,** 14, 355.

[7] Carlopetic and G. Tisi, *Aust. J. Chem.,* **1980,** 33 Importances and applications of Coordination compounds.tutor vista.com

[8] a. F.A Cotton And G.Willikinson, Advanced Inorganic Chemistry, Interscience publishers 3rd edition **1936**.

b. P.A. Vigato, S. Tamburini. *Coord. Chem. Rev.,* **2004**, 248, 1717.

c. N.E. Borisova, M.D. Reshetova, Y.A. Ustynyuk. *Chem. Rev.*, **2007,** 107, 46.

d. P.G Cozzi. *Chem. Soc. Rev.,* **2004,** 33, 410.

e. M. Kojima, H. Taguchi, M. Tsuchimoto, K. Nakajima. *Coord. Chem. Rev.,* **2003,** 237, 183.

f. J. Costamagna, J. Vargas, R. Latorre, A. Alvarado, G. Mena. *Coord. Chem. Rev.,* **1992**, 119, 67.

g. A. Syamal, M.R. Maurya. *Coord. Chem. Rev.,* **1989**, 95, 183.

h. C.W. Tang, S.A. VanSlyke. *Appl. Phys. Lett.,* **1987,** 51, 913.

[9] T. Yu, W. Su, W. Li, Z. Hong, R. Hua, B. Li. *Thin solid Films,* **2007**, 515, 4080.

[10] Y. Yi, X. Q. Wei, M.G. Xie, Z.Y. Lu. *Chin. Chem. Lett.,* **2004**, 15, 525.

[11] X. Q. Wei, Z.Y. Lu, P. Zou, M.G. Xie. *Chin. Chem. Lett.*, **2003**, 14, 263.

[12] J. Xie, J. Qiao, L. Wang, J. Xie , Y. Qiu. *Inorg. Chem. Acta*, **2005,** 358, 4451.

[13] D.R. Kanis, M.A. Ratner, T.J. Marks. *Chem. Rev.*, **1994**, 94, 195.

[14] L.R. Dalton, A.W. Harper, R. Ghosn, W.H. Steier, M. Ziari, H. Fetterman, Y. Shi, R.V. Mustacich, A.K.Y. Jen, K.J. Shea. *Chem. Mater.*, **1995**, 7, 1060.

[15] R.G. Benning. *J. Mater. Chem.*, **1995**, 5, 365.

[16] S.R. Marder, D.N. Beratan, L.T. Cheng. *Science*. **1991,** 252, 103.

[17] T. Verbiest, S. Houbrechts, M. Kauranen, K. Clays, A. Persoons. *J. Mater. Chem.*, **1997**,7, 2175.

[18] N.J. Long. *Angew. Chem. Intl. Ed.*, **1995**, 34, 21.

[19] M. Bourgault, C. Mountassir, H. Le Bozec, I. Ledoux, G. Pucetti, J. Zyss. *J. Chem. Soc., Chem. Comm.*, **1993**, 1623.

[20] S. Di Bella, I. Fragata, I. Ledoux, M.A. Draz-Garcia, P.G. Lacroix, T.J. Marks. *Chem. Mater.*, **1994**, 6,881.

[21] W.M. Laidlaw, R.G. Denning, T. Verbiest, E. Chauchard, A. Persoons. *Nature*. **1994,** 363, 58.

[22] B.J. Coe, J.D. Foulon, T.A. Hamor, C.J. Jones, J.A. McCleverty, D. Bloor, G.H. Cross, T.L. Axon. *J. Chem. Soc. Dalton Trans.*, **1994**, 3427.

[23] H.S. Nalwa. *Appl. Organomet. Chem.*, **1991**, 5, 349.

[24] G.L. Geoffroy, M.S. Wrighton. *Organometallic Photochemistry; Academic Press: New York*, **1979**.

[25] J.P. Collman, L.S. Hegedus. *Principles and Applications of Organotransition Metal Chemistry; University Science Books: Mill Valley*, CA, **1987**.

[26] O. Kahn. *Molecular Magnetism; VCH Publishers: New York*, **1993**.

[27] S. Di Bella. *Chem. Soc. Rev.*, **2001**, 30, 355.

[28] T. Shamspur, I. Sheikhshoaie, M.H. Mashhadizadeh. *J. Anal. At. Spectro.*, **2005,** 20, 476.

[29] S. Sadeghi, M. Eslahi, M.A. Naseri, H. Naeimi, H. Sharghi, A. Shameli. *Electroanalysis*, **2003**, 15, 1327.

[30] M. H. Mashhadizadeh, I. Sheikhshoaei, S. Saeid-Nia. *Sens. Actuators B chem.*, **2003,** 94, 241.

[31] R.K. Mahajan, I. Kaur, M. Kumar. *Sens. Actuators B chem.*, **2003,** 91, 26.

[32] M.H. Mashhadizadeh, I. Sheikhshoaei. *Anal. Bioanal. Chem.*, **2003,** 375, 51.

[33] L. P. Singh, J. M. Bhatnagar. *Talanta,* **2004**, 64, 313.

[34] A.R. Fakhari, T.A. Raji, H. Naeimi. *Sens. Actuators B chem.*, **2005**, 104, 317.

[35] T. Jeong, H.K. Lee, D.C. Jeong, S. Jeon. *Talanta*, **2005,** 65, 543.

[36] M. Shamsipur, M. Yousefi, M. Hosseini, M.R. Ganjali, H. Sharghi, H. Naeimi. *Anal. Chem.*, **2001,** 73, 2869.

[37] M.R. Ganjali, T. Poursaberi, M. Hosseini, M. Salavati-Niasari, M. Yousefi, M. Shamsipur. *Anal. Sci.*, **2002**, 18, 289.

[38] M.R. Ganjali, M.R. Pourjavid, M. Rezapour, T. Poursaberi, A. Daftari, M. Salavati-Niasari. *Electroanalysis.*, **2004,** 16, 922.

[39] V.K. Gupta, R.N. Goyal, A.K. Jain, R.A. Sharma. *Electrochim. Acta*, **2009**, 54, 3218-3224.

[40] V.K. Gupta, A.K. Jain, G. Maheshwari. *Talanta*., **2007**, 72, 49.

[41] R.G. Cavell, K. Aparna, R.P. Kamalesh Babu, Q.Wang, *J. Mol. Catal. A. Chem*., **2002,** 189, 137.

[42] P.A. Cameron, V.C. Gibson, C. Redshaw, J.A. Segal, M.D. Bruce, A.J.P. White, D.J. Williams, *Chem. Commun.,* **1999,** 1883.

[43] S.D. Ittel, L.K. Johnson, Brookhart, *Chem. Rev*., **2000,** 100, 1169.

[44] V.C. Gibson, E.L. Marshall, *Compr. Coord. Chem*., II**, 2004,** 9, 1.

[45] G.J.P. Britovsek, V.C. Gibson, B.S. Kimberly, P.J. Maddox, S.J. McTavish, G.A. Solan, A.J.P. White, D.J. Williams, *Chem. Commun*., **1998**, 849.

[46] G.J.P. Britovsek, V.C. Gibson, D.F. Wass, *Angew. Chem. Int. Ed*., **1999**, 38, 428.

[47] Kim, Byeong H. Han, C. Sik Ha, Jae Kon Kim, Hongsuk Suh, *Communications to the Editor* **2003,** 36, 18.

[48] S. Matsui, T. Fujita, *Catal. Today*., **2001,** 66, 63.

[49] Y. Nakayama, H. Bando, Y. Sonobe, T. Fujita, *J. Mol. Catal. A. Chem*., **2004,** 141.

[50] Y. Kou, J Tian, D. Li, W. Gu, X. Liu, S. Yan, D. Liao, P. Cheng, *J. Chem. Soc. Dalton Trans,.* **2009,** 2374.

[51] T. Uchida, T. Katsuki, *Tetrahedron Lett.,* **2001**, 42, 6911.

[52] D.R. Reddy, E.R. Thornton, *J. Chem. Soc. Chem. Comm.*, **1992**,172.

[53] A. Waldemar, T.F. Rainer, R.S. Veit, R.S.-M. Chantu, *J. Am. Chem. Soc.*, **1998**, 120, 708.

[54] K. Nakjima, M. Kojima, K. Toriumi, K. Saito, J. Fujita, *Bull. Chem. Soc. Jpn.*, **1989,** 62, 760.

[55] Z. Flores-Lopez, M. Parra-Hake, R. Somanathan, P.J.Walsh, *Organometallics*, **2000,** 19, 2153.

[56] A. Gama, L.Z. Flores-Lopez, G. Aguirre, M. Parra-Hake, R. Somanathan, P.J. Walsh, *Tetrahedron: Asymmetry*, **2002,** 13, 149.

[57] J. Bozell, B. Hames, D. Dimmel, *J. Org. Chem.*, **1995,** 60, 2398.

[58] E.M. McGarrigle, D.G. Gilheany, *Chem. Rev.*, **2005,** 105, 1563.

[59] N. Finnley, P.J. Pospil, S. Chang, M. Palucki , R. Konsler, K. Hansen, E. Jacobsen, *Angew. Chem. Intl. Ed. In English*, **1997,** 36, 1720.

[60] E.N. Jacobsen. *Comprehensive Organometallic Chemistr*y II, Eds. E. W. Abel, F. G. A. Stone and E. Willinson, Pergamon, New York, **1995,** 12, 1097.

[61] V.R. de Souza, G.S. Nunes, R.C. Rocha, H.E. Toma, *Inorg. Chim. Acta*, **2003,** 56, 348.

[62] K. Nakata, T. Takeda, J. Mihara, T. Hamada, R. Irie, T. Katsuki, *Chem. Eur. J.* **2001,** 7, 3776.

[63] Y. Nishibayashi, I. Takei, S.Vemara, M. Hidai, *Organometallics*, 18 (1999) 2291.

[64] T. Langer, G. Helmchen, *Tetrahedron Lett.*, **1996,** 37, 1381.

[65] J.W. Faller, A.R. Lavoie, *Organometallics*, **2001,** 20, 5245.

[66] D.J. Cross, J.A. Kenny, I. Houson, L. Campbell, T. Walsgrove, M. Wells, *Tetrahedron: Asymmetry*, **2001,** 12, 1801.

[67] M. Costa, P. Pelagatti, C. Pelizzi, D. Rogolino. *J. Mol. Catal. A: Chem.*, **2002,** 178, 21.

[68] J. Patole, D. Shingnapurkar, S. Padhye, C Ratledge. *Bioorg. Med. Chem. Lett.*, **2006,** 16, 1514.

[69] V.T Dao, M.K Dowd, M.T Martin, C. Gaspard, M. Mayer, R.J. Michelot, *Eur. J. Med. Chem.*, **2004,** 39, 619.

[70] Khan A, Sarkar S, Sarkar D, *International Journal of Antimicrobial Agents*, **2008,** 32, 40.

[71] M.S. Iqbal, A.H. Khan, B.A. Loothar, I.H. Bukhari, *Med. Chem. Res.*, **2009,** 18, 31.

[72] P.G. Kulkarni, G.B. Avaji, Bagihalli, S.A Patil, P.S. Badami, *J. Coord. Chem.*, **2009**, 62, 481.

[73] G. Puthilibai, S. Vasudevan, S.K. Rani, G. Rajagopal, *Spectrochim. Acta - Part A*: *Mol. Biomol. Spec.,* **2009,** 72, 796.

[74] G.B. Bagihalli, P.G. Avaji, S.A. Patil, P.S. Badami, *Eur. J. Med. Chem.*, **2008,** 43, 2639.

[75] E. Keskioglu, A.B. Gunduzalp, S. Cete, F. Hamurcu, B. Erk, *Spectrochim. Acta - Part A***, 2008,** 70, 634.

[76] M.S. Nair, R.S. Joseyphus, *Spectrochim. Acta - Part A*, **2008,** 70, 749.

[77] A.S. El-Tabl, F.A. El-Saied, W. Plass, A.N. Al-Hakimi, *Spectrochim. Acta - Part A*, **2008,** 71, 90.

[78] D.E. Goldberg, V. Sharma, A. Oskaman, I.Y. Gluzman, T.E. Wellems, D.J. Piwnica-Worms, *Bio. Chem.*, **1997,** 272, 6567.

[79] V. Sharma, A. Beatty, D.E. Goldberg, D. Piwnica-Worms, *Chem. Comm.*, **1997,** 223.

[80] V. Sharma, D. Piwnica-Worms, *Chem. Rev.*, **1999,** 99, 2545.

[81] K.E. Erkkila, D.T. Odom, J.K. Barton, *Chem. Rev.*, **1999,** 99, 2777.

[82] C. Liu, M. Wang, T. Zhang, H. Sun, *Coord. Chem. Rev.*, **2004,** 248, 147.

[83] D.S. Sigman, A. Mazumder, D.M. Perrin, *Chem. Rev.*, **1993,** 93, 2295.

[84] K.J. Humphreys, K.D. Karlin, S.E. Rokita, *J. Am. Chem. Soc.*, **2002,** 124, 8055.

[85] E.A. Kesicki, M.A. DeRosch, L.H. Freeman, C.L. Walton, D.F. Harvey, W.C. Trogler. *Inorg. Chem.*, **1993,** 32, 5851.

[86] S.A. Tysoe, R. Kopelman, D. Schelzig, *Inorg. Chem.*, **1999,** 38 (23), 5196.

[87] C. Liu, S. Yu, D. Li, Z. Liao, X. Sun, H. Xu, *Inorg. Chem.*, **2002,** 41 (4), 913.

[88] A.C. Lim, J.K. Barton, *Biochem.*, **1993,** 32 (41), 11029.

[89] S. Dhar, M. Nethaji, A.R. Chakravarty, *Inorg. Chem.*, **2006,** 45, 11043.

[90] M. Roy, S. Saha, A.K. Patra, M. Nethaji, A.R. Chakravarty, *Inorg. Chem.*, **2007,** 46, 4368.

[91] A.T. Chaviara, E.E. Kioseoglou, A.A. Pantazaki, A.C. Tsipis, P.A. Karipidis, D.A. Kyriakidis, C.A. Bolos, *J. Inorg. Biochem.*, **2008,** 102, 1749.

[92] N. Chitrapriya, V. Mahalingam, L.C. Channels, M. Zeller, F.R. Fronczek, K. Natarajan, *Inorg. Chim. Acta*, **2008,** 361, 2841.

[93] S.K. Gupta, D.D. Agarwal, D. Raina, *Indian J. Chem. A*, **1996,** 35A, 995.

[94] S.K. Gupta, D. Raina, *Trans. Met. Chem.*, **1997,** 22, 372.

[95] S.K. Gupta, D. Raina, *Trans. Met. Chem.*, **1997,** 22, 225.

[96] S.K. Gupta, K. Jain, Y.S. Kushwah, *Indian J. Chem. A*, **1999,** 38A, 506.

[97] S.K. Gupta, Y.S. Kushwah, *Polyhedron*, **2001,** 20, 2019.

[98] S.K. Gupta, P.B. Hitchcock, Y.S. Kushwah, *J. Coord. Chem.*, **2002,** 55, 1401-1407.

[99] S.K. Gupta, P.B. Hitchcock, Y.S. Kushwah, G.S. Argal. *Inorg. Chim. Acta*, **2007,** 360, 2145.

[100] Z-H. Xu, F-J. Chen, P-X. Xi, X-H Liu, Z-Z Zeng, *J. Photochem. Photobiol. A-Chem.*, **2008,** 196, 77.

[101] R. Vijayalakshmi, M. Kanthimathi, V. Subramanian, B.U Nair, *Biochim. Biophys. Acta*, **2000,** 1475, 157.

[102] Y. Kou, J Tian, D. Li, W. Gu, X. Liu, S. Yan, D. Liao, P. Cheng, *J. Chem.Soc. Dalton. Trans*., **2009,** 2374.

[103] A. Silvestri, G. Barone, G. Ruisi, M.T. Lo Giudice, S. Tumminello, *J. Inorg. Biochem.*, **2004,** 98, 589.

[104] E.V. Hackl, V.L. Galkin, Y.P. Blagoi, *Int. J. Biol. Macromol.*, **2004,** 34, 303.

[105] H. Sugimoto, H. Ogura, Y. Arai, Y. Iimura, Y. Yamanishi, *Japanese J. Pharmacol.*, **2002,** 89(1), 7.

[106] J. L. Sussman, M. Harel, F. Frolow, C. Oefner, A. Goldman, L. Toker, I. Silman, *Science.*, **1991,** 253(5022), 872.

[107] M. H. Parker, A. B. Reitz, *Chemtracts: Org. Chem.*, **2000,** 13 (1), 51.

[108] G. M. Shankar, S. Li, T. H. Mehta, A. Garcia-Munoz, N. E. Shepardson, I. Smith, F. M. Brett, M. A. Farrell, M. J. Rowan, C. A. Lemere, C. M. Regan, D. M. Walsh, B. L. Sabatini, D. J. Selkoe, *Nat. Med.*, **2008,** 14 (8), 837.

[109] S. Nochi, N. Asakawa, T. Sato, *Biol. Pharm*. *Bull.*, **1995,** 18, 1145.

[110] W. Tong, E.R. Collantes, Y. Chen, W.J. Welsh, *J. Med.* Chem., **1996,** 39, 380.

[111] Q. Yu, H. W. Holloway, T. Utsuki, A. Brossi, N. H. Greig, *J. Med. Chem*., **1999**, 42, 1855.

[112] (a) N.H. Greig, T. Utsuki, Q. Yu, X. Zhu, H.W. Holloway, T. Perry, B. Lee, D.K. Ingram and D.K. Lahiri. *Curr. Med.* Res. *Opin.*, **2001**, 17, 159. (b) M. Racchi, M. Mazzucchelli, E. Porrello, C. Lanni, S. Govoni, *Pharmacol.* Res., **2004,** 50(4), 441.

[113] P Camps, D Muñoz-Torrero, *Mini*-Rev. *Med. Chem*., **2002,** 2(1), 11.

[114] N. Tezer, *J. Mol. Struct. THEOCHEM.*, **2005,** 714(2–3),), 133.

[115] H. Haviv, D. M. Wong, I. Silman, J. L. Sussman, *Curr. Top. Med. Chem.*, **2007,** 7(4), 375.

[116] H. Dvir, D. M. Wong, M. Harel, X. Barril, M. Orozco, F. J. Luque, D. Munoz-Torrero, P. Camps, T. L. Rosenberry, I. Silman, J. L. Sussman, *Biochem.*, **2002,** 41(9), 2970.

[117] G. Evin, G. Lessene, S. Wilkins, *Recent Pat. CNS Drug Discov.*, **2011,** 6(2), 91.

[118] M. Harel, I. Schalk, L. Ehretsabatier, F. Bouet, M. Goeldner, C. Hirth, P. H. Axelsen, I. Silman, J. L. Sussman, *Proc. Nat. Acad. Sci. USA*, **(1993),** 90, 9031.

[119] G. Koellner, G. Kryger, C. B. Millard, I. Silman, J. L. Sussman, T. Steiner, *J. Mol. Biol.*, **2000,** 296(2), 713.

[120] S. Alcaro, L. Scipione, F. Ortuso, S. Posca, V. Rispoli, D. Rotiroti, *Bioorg. Medicinal Chem. Lett.,* **2002,** 12(20), 2899.

[121] M. M. Hurley, J. B. Wright, G. H. Lushington, W. E. White, *Theor. Chem. Acc.,* **2003,** 109(3), 160.

[122] Y. K. Zhang, J. Kua, J. A. McCammon, *J. Am. Chem. Soc.*, **2002,** 124(35), 10572.

[123] M. L. Bolognesi, M. Bartolini, A. Cavalli, V. Andrisano, M. Rosini, A. Minarini, C D.Melchiorre, Eur. *J. Med. Chem.*, **2004,** 47(24), 5945.

[124] A. A. N. de Paula, J. B. L. Martins, M. L. dos Santos, L. D. Nascente, L. A. S. Romeiro, T. Areas, K. S. T. Vieira, N. F. Gamboa, N. G. Castro, R. Gargano, *Eur. J. Med. Chem.,* **2009,** 44(9), 3754.

[125] (a). A. Budimir, N. Humbert, M. Elhabiri, I. Osinska, M. Biruš, A. M. Albrecht-Gary, *J. Inorg. Biochem.*, **2011,** 105(3), 490. (b). A. Rimola, J. Alí-Torres, C. Rodríguez-Rodríguez, J. Poater, E. Matito, M. Sol, and M. Sodupe, *J. Phys. Chem.* A. **2011**, 115 (45), 12659. (c). H. S. Ved, M. L. Koenig, J. R. Dave, B. P. Doctor, *Neuro Report*. **1997**, 8, 963.

[126] G.L. Ellman, *Arch. Biochem. Biophys.,* **1958,** 74, 443.

[127] H.L.T.Mobley, R.P.Hausinger, *Microbiol. Rev.,* **1989,** 53, 85.

[128] K.W.Leon, J. Jarvik (Eds.), *International Review of Cytology, Academic Press, San Diego,* **1993**.

[129] H.L.T.Mobley, M. D., Island, R.P., Hausinger, *Microbiol. Rev.* **1995,** 59, 451.

[130] P.E.Wilcox, *Chymotrypsinogens—chymotrypsins, Methods in Enzymology.,* **1970,** 19, 64.

[131] (a) F.A.Cotton, G.Wilkinson, C.A. Murillo, *Ad. Inorg. Chem., Wiley, NewYork,* **1999**

(b) M.E.Cuff, K.I.Miller, K.E.van Holde, W.A.Hendrickson, *J. Mol. Biol.* **1998,** 278, 855.

(c) E.I.Solomon, U.M.Sundaram, T.E.Machonkin *Chem. Rev.* **1996,** 96, 2563.

(d) N.Kitajima, Y.Moro-oka, *Chem. Rev.*, **1994,** 94, 737.

(e) K.A.Magnus, H.Ton-That, J.E.Carpenter, *Chem. Rev.,* **1994,** 94, 727.

[132] (a) R.H.Holm, P.Kennepohl, E.I.Solomon, *Chem. Rev.,* **1996,** 96, 2239.

(b) E.T.Adam, Copper protein structures. *Adv. Protein. Chem.*, **1991,** 42, 145.

(c) S.K.Chapman, Perspectives on Bioinorganic Chemistry, in: R.W.Hay, J.R.Dilworth, K.B. *Nolan (Eds.), JAI Press, London,* **1991**, p. 95.

[133] S.Schindler, *Eur. J. Inorg. Chem.,* **2000,** 2311.

[134] H.L.T.Mobley, M. D., Island, R.P., Hausinger, *Microbiol. Rev.*, **1995,** 59, 451.

[135] A.Coblentz, *J. Am. Geriatr. Soc*. **1968,** 16(9), 1039.

[136] M. Arfan, , M. Ali, H. Ahmad, I. Anis, A. Khan, M. I. Choudhary, M.R. Shah, *J. Enz. Inh. Med. Chem.* **2010,** 25, 296.

[137] R.J.P. Cannell, S.J. Kellam, A.M. Owsianka, J.M. Walker, *Planta Med.*, **1988,** 54, 10.

[138] L.Zhang, S.B.Mulrooney, A. F.K.Leung, Y.Zeng, B.C. K.Ben, R. P.Hausinger, H. Sun, *Bio. Metals,* **2006,** 19, 503.

[139] a.I. Cantuti-Castelvetri, B. Shukitt-Hale, J.A. Joseph, *Int. J. Dev. Neurosci.,* **2000,** 18, 367.

b. P. Panneerselvam, R.R. Nair, G. Vijayalakshmi, E.H. Subramanian, S.K.Sridhar, *Eur. J. Med. Chem.,* **2005**, 40(2), 225.

[140] a. Baquero F. Gram-positive resistance: challenge for the development of new antibiotics. *J Antimicrob Chemother.*, **1997,** 39(Suppl.A), 1.

b. Y.J. Surh, K.S. Chun, H.H. Cha, Y.S. Keum, K.K. Park, S.S. Lee, *Mutat Res.*, **2001,** 480, 243.

[141] J. Vaya, M. Aviram, *Curr. Med. Chem.,* **2001,** 1, 99.

[142] O.I. Aruoma *Mutat Res.,* **2003,** 523, 9.

[143] K. Beckman and B. Ames, *Physiology Rev.*, **1998,** 78: 548.

[144] B. Ames, et al, *Proc Natl. Acad. Sci. USA,* **1993,** 90, 7915.

[145] K.J. Williams,; Tabas, *Arteriosclerosis, thrombosis, and vascular biology,* **1995,** 15 (5), 551.

[146] C.P. Sparrow, J. Olszewski *J. Lipid Res.,* **1993,** 34 (7), 1219.

[147] O. Blokhina, E.Virolainen, K.V. Fagerstedt, *Ann. Bot.,* **2003,** 91, 179.

[148] P.C.H. Hollman, M.B. Katan. *Food Chem Toxicol.,* **1999,** 37, 937.

[149] Masataka Ohashi, Tomomi Koshiyama, Takafumi Ueno, Manabu Yanase, Hiroshi Fujii, and Yoshihito Watanabe, *Angew. Chem. Int. Ed.,* **2003**, 42, No. 9, 1005.

[150] (a) E.K. Beloglazkina, A.G. Majouga, R.B. Romashkina, N.V. Zyk, *Tetrahedron Lett.,* 47 (2006) 2957–2959; (b) D. Gao, Q. Gao, *Catal. Commun*., **2007,** 8, 681. (c) Y. Zhang, Z. Li, W. Sun, C. Xia, *Catal. Commum.,* **2008,** 10, 237.

[151] P. Datta, A. P. Mukhopadhyay, P. Manna, R.T Edward. Tiekink, P. C. Sil, C. Sinh, *J. Inorg. Biochem.,* **2011,** 105, 577.

[152] G. J. Kharadia, S. C. Panchania & K. D. Patel, Studies on Some Coordination Polymeric Chains of Metal Ions with QM1N, Int. J. Polymer. Mater., **2010**, 59(8), 577.

[153] F. Carrasco, The evaluation of kinetic parameters from thermogravimetric data: comparison between established methods and the general analytical equation, Thermochim. Acta, **1993,** 213,115.

[153] S. S. Konstantinoviae, B.C. Radovanoviæ, A. Krkljes, Thermal behaviour of Co(II), Ni(II), Cu(II), Zn(II), Hg(II) and Pd(II) complexes with isatin-aˆ-thiosemicarbazone, J. Therm. Anal. Calorim. **2007**, 90, 525.

[154] Y. H. Fan, Z. X. Gao, C. F. Bi, S. T. Xie, X. Zhang, Synthesis and thermal decomposition kinetics of La(III) complex with unsymmetrical Schiff base ligand, J. Therm. Anal. Calorim. **2008**, 91, 919.

[155] M. Lalia-Kantouri, L. Tzavellas, D. Paschalidis, Novel lanthanide complexes with di-2-pyridyl ketone-p-chlorobenzoylhydrazone: thermal investigation by simultaneous TG/DTG-DTA and IR spectroscopy, J. Therm. Anal. Calorim. **2008**, 91, 937.

CHAPTER 2

2. EXPERIMENTAL

2.1 Materials and methods

All chemicals, buffers and solvents used were of analytical grade. Metal(II) acetates and chlorides (where metal(II) = Co, Ni, Cu and Zn) were obtained from Riedel-de-Haen, and were partially dehydrated by drying the hydrated salts in a vacuum oven for several hours at 80 – 100^{o} C. 3-aminoquinoline, 2-hydroxynaphthaldehyde, 2-[1-(aminomethyl)cyclohexyl]acetic acid, and methylanthranilate were obtained from Sigma Aldrich whereas salicylaldehyde was obtained from Acros Organics, sodium hydroxide, 4-chloroaniline and 4-bromoaniline were obtained from Merck. Hydrazine monohydrate was obtained from PANREAC quimica SA. Solvents were obtained from local suppliers of Sigma Aldrich, Merck or Fluka and were distilled at least twice before use. Electric eel acetylcholineesterase, horse serum butrylcholinesterase, acetylthiocholine iodide, butrylthiocholine chloride, 5-5′-thiobis-2-nitrobenzoic acid (DTNB) and eserine were purchased from Sigma. Unless otherwise stated, all reactions were carried out under a dinitrogen atmosphere.

2.2 Instrumentation

Elemental analyses were carried out on Varian Elementar II. Melting points were recorded on a Gallenkamp apparatus. IR spectra were recorded using Shimadzo FTIR Spectrophotometer Prestige-21. ^{1}H-NMR were measured with Bruker DPX 400 MHz (400.23 MHz) whereas, ^{13}C{^{1}H}NMR were recorded on Bruker AV 400MHz (150.9 MHz) spectrometers in $CDCl_3$ at room temperature. Chemical shifts are reported in ppm and standardized by observing signals for residual protons. UV-Visible spectra were recorded on a BMS UV-1602. Metal complexes were studied, at room temperature, for their molar conductivity in the solution state using conductivity

meter HI-8333. Magnetic susceptibilities were measured on a Sherwood Gouy Balance at room temperature calibrated with $Hg[Co(SCN)_4]$. Mass spectra were recorded on a LCT Orthogonal Acceleration TOF Electrospray mass spectrometer. Single crystal analyses were carried out using Rigaku Saturn-724 diffractometer (graphite-monochromated Mo Kα radiation, λ = 0.71073 Å) at 108(2) K.

2.3 Crystal Structure Determinations

Suitable single crystals for X-ray structural analyses of the crystalline compounds were mounted on a glass fiber, and the respective data were collected on a Rigaku Saturn-724 diffractometer (graphite-monochromated Mo Kα radiation, λ = 0.71073 Å) at 108(2) K. The structures were solved by either direct methods (SHELXS-97) and refined against all data by full-matrix least-squares methods on F^2 (SHELXL-97) [1] or Olex-2 using Charge Flipping. All non-hydrogen-atoms were refined with anisotropic displacement parameters in case of SHELXS-97. The hydrogen atoms were refined isotropically on calculated positions using a riding model with their U_{iso} values constrained to 1.5 U_{eq} of their pivot atoms for terminal sp^3 carbon atoms and 1.2 times for all other carbon atoms. Whereas in case of solving the structure with Olex-2 the refinement was done with olex-2 refine using Gauss-Newton minimization [2-3].

2.4 AChE and BChE inhibition assay

AChE Inhibition was determined spectrophotometrically, with acetylthiocholine as substrate, by modifying the method reported by Ellman [4]. The reaction was carried out in 100 µM sodium phosphate buffer (pH 8.0) at 25^{o}C. In a typical assay, 140 µl of buffer, 20 µl of enzyme preparation (final concentration 0.037 U/ml in 0.1 M phosphate buffer solution), and 20 µl (0.05mM) of metal compound solution were mixed and incubated for 30 min. 10 µl (0.15mM) of 5,5′-dithio-bis-nitrobenzoic acid (DTNB) was added, and the reaction was initiated by adding

10 µl of acetylthiocholine. Butyrylthiocholine chloride was used as a substrate to assay BChE under similar conditions as above. The rates of hydrolysis of acetylthiocholine and butyrylthiocholine were determined by monitoring the formation of the yellow 2-nitro-5-sulfanylbenzoate anion (as a result of the reaction of DTNB with the thiocholine released by the enzymatic hydrolysis) at a wavelength of 412 nm. Methanol was used as negative control. Galanthamine dissolved in methanol was used as standard drug at 10 µg\ml concentrations. All the reactions were performed in triplicate in 96-well microplates in Spectrmax 340 (Molecular Devices, USA).

2.5 Determination of IC_{50} values

The concentrations of test compounds that inhibited the hydrolysis of both the tested substrates (acetylthiocholine and butyrylthiocholine) by 50% (IC_{50}) were determined by monitoring the effect of increasing concentrations of these compounds on the inhibition values. The IC_{50} values were then calculated using the EZ-Fit Enzyme Kinetics program (Perrella Scientific Inc., Amherst, USA).

2.6 Urease inhibition assay

Urease enzyme was obtained from jack bean source, 25 µL of the enzyme solution and 5 µL of test compounds (0.5 mM concentration) were mixed and incubated with 55 µL of buffers containing 100 mM urea for 15 min at 30 °C in each well of 96-well plate. Final volumes were maintained as 200 µL by adding 45 µL phenol reagent (1% w/v phenol and 0.005% w/v sodium nitroprussside), and 70 µL of alkali reagent (0.5% w/v NaOH and 0.1% active chloride NaOCl) to each well. During the process ammonia was produced which was consequently measured as a urease activity by indophenol method. Using a microplate reader (Molecular Devices, CA, USA), the change in absorbance was measured at 630 nm after 50 min at pH 6.8 [5-6].

2.7 α-Chymotrypsin inhibition assay

Cannell method was modified and used for the chymotrypsin activity [7]. This was performed in 50 mM Tris-HCl buffer pH 7.6 with 10 mM $CaCl_2$. α-Chymotrypsin (12 Units/mL prepared in buffer) with the various concentration of test compound (prepared in DMSO) was incubated at 30 °C for 25 min. The reaction was started by adding *N*-succinyl-L-phenylalanine-*p*-nitroanilide (prepared in buffer) at final concentration of 0.4 mM. The change in absorbance was continuously monitored at 410 nm.

2.8 Antimicrobial activity

About 2.8 g/L nutrient agar and nutrient broth were prepared in deionized water and kept in autoclave set at 1.5 Pounds pressure for about 15 min. Under inert atmosphere the nutrient agar media were poured aseptically into sterilized petri dishes in laminar flow. The petri dishes were kept for about 24 hr at 37 ^{o}C in inverted position. Bacterial cultures were adjusted to 0.5 McFarland turbidity standard and Candida albican was adjusted to 108 cfu/ml. Sterile filter paper of diameter 6mm was used for bacterial strains whereas its thickness ranged upto 13 mm for fungal strains. These filter papers were in the form of discs and were seeded with 0.5 McFarland and 106 cfu/ml cultures of bacteria and fungi respectively. Solutions (0.5 mM) of the synthesized compounds were applied to the prepared discs and incubated for 18 hr at 37 ^{o}C. Subsequent measurements of the zone of activity were carried out [8].

2.9 TG-DTA analysis

The TG-DTA analyses were carried out using TG/DTA Diamond model by Perkin Elmer at heating rate 10 ^{o}C/min in temperature range 30-1000 ^{o}C under static air. Specific mass of samples were contained in ceramic pans crucibles adjusted on platform support giving a proportional signal to recorder, observed by computer interface and the results were plotted in

the form of mass loss of sample vs. temperature for TG and microvolts vs. temperature for DTA. All the results were referenced to thermal decomposition of alumina. The activation energies of all the samples was calculated using Horowitz-Metzger method [9]. It was found that linear plots can be obtained while $LnLnWo-W_t^f/W-W_t^f$ {where Wo = initial mass taken, W = weight remaining at a given temperature, W_t^f = final weight} were plotted against Θ {where Θ = Tc-Ts}. The slope of the straight line was used to calculate the activation energy through the expression (1):

$$Slope = E^*/RTs^2 \qquad (1)$$

Order of decomposition was calculated from the relationship between reaction order and concentration at maximum slope [9]. Thermodynamic parameters of activation were evaluated by using the following expressions (2), (3) and (4), respectively [10]:

$$\Delta S^* = 2.303 Log[Ah/k_B Ts]R \qquad (2)$$

$$\Delta H^* = \Delta E^* - RT \qquad (3)$$

$$\Delta G^* = \Delta H^* - T\Delta S^* \qquad (4)$$

2.10 Synthesis of 2-[(*E*)-(quinolin-3-ylimino)methyl]phenol (H-QMP)

Salicyaldehyde (1.2 cm^3, 0.011 mol) was added to a solution of 3-aminoquinoline (1.6g, 0.011mol) in ethanol which was stirred for 3 hr. An orange solution was obtained and concentrated using rotary evaporator. The product was purified by washing with 10% copious n-hexane and methanol solution. The synthetic route is shown in scheme 2.1.

2.11 Synthesis of $[M(QMP)_2]$ where M= Co and Ni (II) acetates (1) and (2)

0.011 moles of metal (II) acetates were stirred in a minimum volume of dried methanol and 0.024 mol of H-QMP in a minimum volume of dried methanol was added to the metal solution.

The mixture was stirred for 2-3 hrs at room temperature. The metal complex was collected after filtration and copiously washed several times with 5% n-hexane containing methanol.

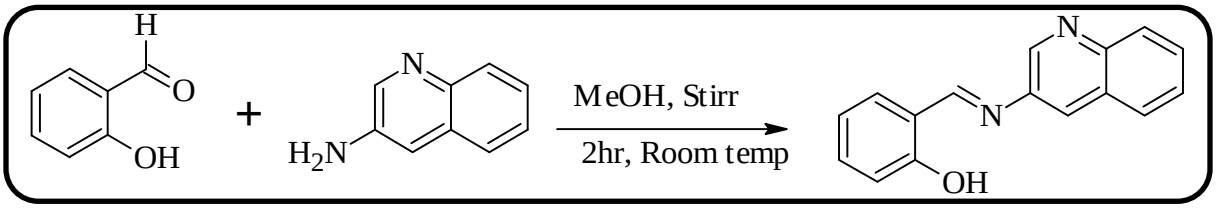

Scheme 2.1 Synthesis of 2-[(*E*)-(quinolin-3-ylimino)methyl]phenol (H-QMP) Schiff base ligand

2.11.1 bis(2-[(*E*)-(quinolin-3-ylimino)methyl]phenolato)cobalt(II) (1)

X-ray quality crystals were formed by slow diffusion of dichloromethane and diethyl ether. After three days dark brown single crystals were appeared.

2.11.2 bis(2-[(*E*)-(quinolin-3-ylimino)methyl]phenolato)nickel(II) (2)

X-ray quality crystals were formed by slow diffusion of dichloromethane and diethyl ether. After three days dark green diamond shaped single crystals appeared.

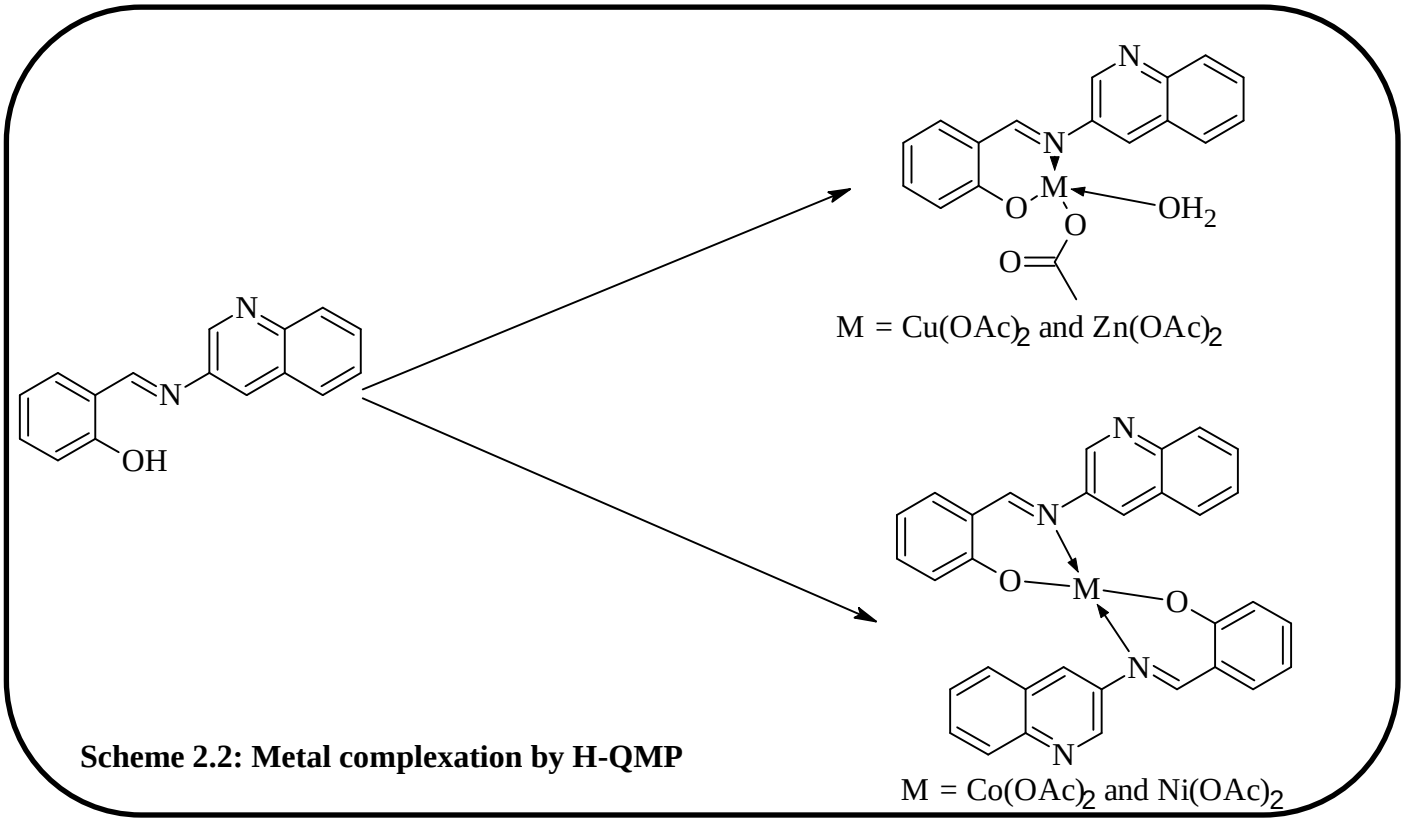

Scheme 2.2: Metal complexation by H-QMP

2.12 Synthesis of [M(QMP)(CH_3COO)]H_2O where M = Cu and Zn(II) acetates (3) and (4)

0.011 mol of metal (II) acetates was stirred in a minimum volume of dried methanol to which 0.011 mol of H-QMP in a minimum volume of dried methanol was added. The mixture was stirred for 2-3hrs at room temperature. In metal salts containing water of crystallization excess dimethoxy propane was added for dehydrating and the solution was stirred for 3 hr at room temperature under nitrogen before adding the ligand. The metal complex was collected after filtration and washed many times with n-hexane containing methanol.

2.13 Synthesis of 2-{(*E*)-[(4-chlorophenyl)imino]methyl}phenol (CIMP)

The ligands were prepared according to the reported procedure. 10 mmol of chloroaniline was taken and reacted at room temperature with 10mmol salicyldehyde in 10 cm^3 of ethanol. 2-3 drops of sulphuric acid was added as catalyst. The ligands quickly precipitated out as yellow solid which were filtered and washed with n-hexane three times. The product was recrystalised from methanol as yellow needles.

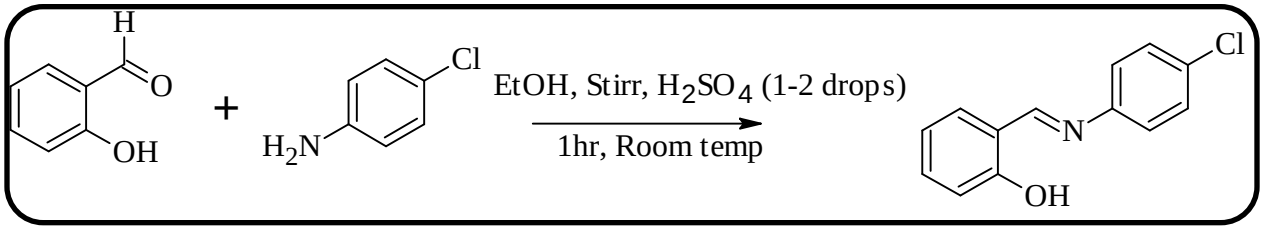

Scheme 2.3. Synthesis of 2-{(*E*)-[(4-chlorophenyl)imino]methyl}phenol(CIMP) Schiff base ligand

2.14 Synthesis of [$M(CIMP)_2$] where M = Co, Ni, Cu and Zn(II) acetates (5), (6), (7) and (8)

10 mmol of the Schiff base ligand in 10 cm^3 of dried methanolic solution was added to the dehydrated methanolic solution of 0.4mmol metal salts and stirred the mixture for 3-6 hrs. Partial dehydration of the metal salts was achieved by keeping the metal salts in oven at 105 ^oC for 3 hrs. These metal salts were dissolved in 10 cm^3 dried methanol and excess dimethoxy propane

was added to it to achieve the complete dehydration. On mixing the metal salt solution with ligand solutions, the complexes either precipitated instantaneously otherwise obtained by concentrating the solutions using rotary evaporator. The product was washed with 10% copious methanol containing n-hexane solution.

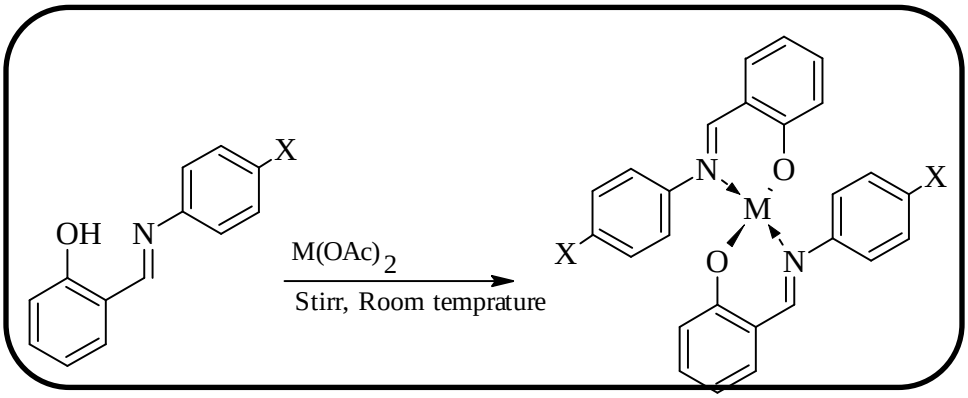

Where X = Cl-, Br- and M = Co, Ni, Cu and Zn

Scheme 2.4 Metal complexes of the Schiff bases CIMP and BIMP

2.15 Synthesis of 2-{(*E*)-[(4-bromophenyl)imino]methyl}phenol (BIMP)

The ligands were prepared according to the reported procedure. 10 mmol of chloroaniline was taken and reacted at room temperature with 10mmol salicyldehyde in 10 cm^3 of ethanol. 2-3 drops of sulphuric acid was added as catalyst. The ligands quickly precipitated out as yellow solid which were filtered and washed with n-hexane three times. The product was recrystalised from methanol as yellow needles.

2.16 Synthesis of [M(BIMP)$_2$] where M = Co, Ni, Cu and Zn(II) acetates (9), (10), (11) and (12)

10 mmol of the Schiff base ligand in 10 cm^3 of dried methanolic solution was added to the dehydrated methanolic solution of 0.4 mmol metal salts and stirred the mixture for 3-6 hrs. Partial dehydration of the metal salts was achieved by keeping the metal salts in oven at 105 ^oC

for 3 hrs. These metal salts were dissolved in 10 cm^3 dried methanol and excess dimethoxy propane was added to it to achieve the complete dehydration. On mixing the metal salt solution with ligand solutions, the complexes either precipitated instantaneously otherwise obtained by concentrating the solutions using rotary evaporator. The product was washed with 10% copious methanol containing n-hexane solution.

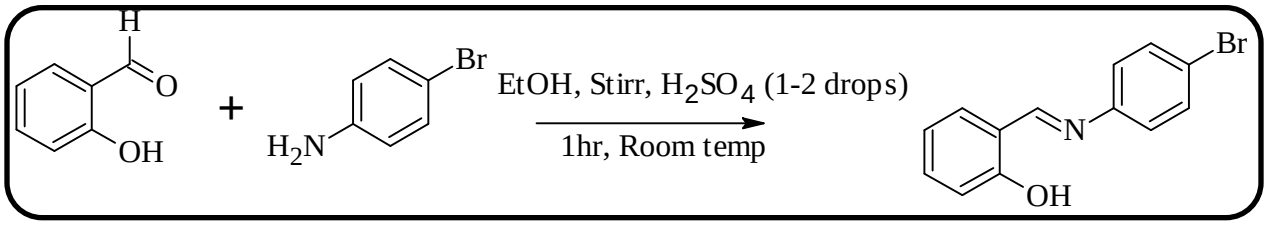

Scheme 2.5. Synthesis of 2-{(*E*)-[(4-chlorophenyl)imino]methyl}phenol(BIMP) Schiff base ligand

2.17 Synthesis of [1-({[(*Z*)-(2-hydroxynaphthalen-1-yl)methylidene]amino}methyl) cyclohexyl]acetic acid (H-HMAC)

The ligand of the amino acid was prepared by adding 10 mmol of methanolic solution of NaOH to 10 mmol methanolic solution of amino acid ([1-(aminomethyl)cyclohexyl]acetic acid). Both the solutions were prepared in minimum quantity of distilled methanol. The mixture was stirred for 2 hrs at room temperature in order to remove zwitterions from the solution completely. Then 12 mmol of 2-hydroxynaphthaldehyde was added to this stirred solution. Dark brown precipitate appeared instantly which was filtered after sometime and washed with 5% methanol containing distilled water. The precipitate was washed with distilled methanol and then with n-hexane. Single crystals of x-ray quality were grown in THF by keeping the solution at room temperature for several days.

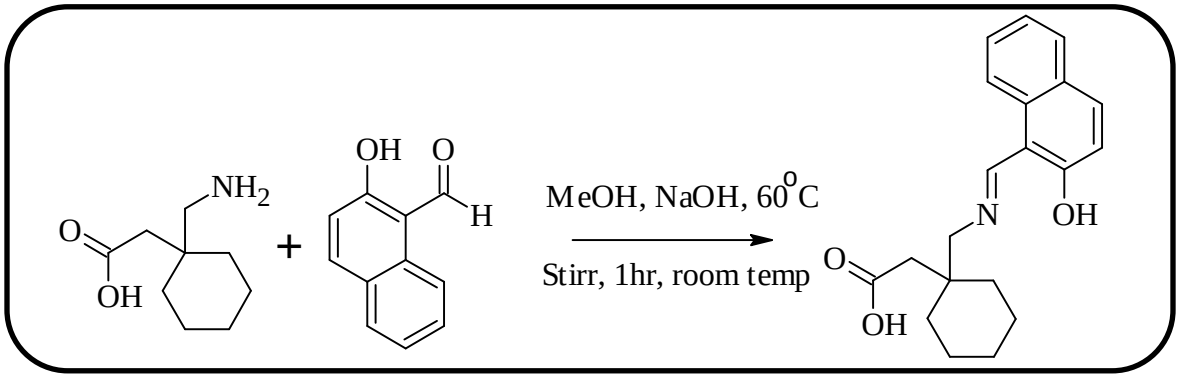

Scheme 2.6. Synthesis of[1-({[(*Z*)-(2-hydroxynaphthalen-1-yl)methylidene]amino}methyl) cyclohexyl]aceticacid(H-HMAC)

2.18 Synthesis of [M(HMAC)$_2$] where M= Co, Ni, Cu and Zn (II) acetates (13), (14), (15) and (16)

All the coordination complexes were synthesized by following the same method. Complexes were synthesized by reacting 10 mmol solution of HMAC prepared in 15 cm^3 distilled methanol with 10 mmol solution of metal chloride salt in 10 cm^3 methanol. An abrupt color change was observed which gave greenish precipitate after stirring the mixture for some time. The precipitates were filtered, washed with methanol and then with n-haxane.

2.19 Synthesis of methyl 2-{[(E)-(2-hydroxyphenyl)methylidene]amino}benzoate (H-HAB)

10 mmol of the methyl anthranilate was added to 10 cm^3 distilled methanol and stirred for 10 min. 12 mmol salicyldehyde was added to the methylanthranilate solution and the resulting mixture stirred for 2 hrs at 40 ^{o}C. On concentrating the solution orange product was isolated which was washed with 5% copious n-hexane and methanol solution.

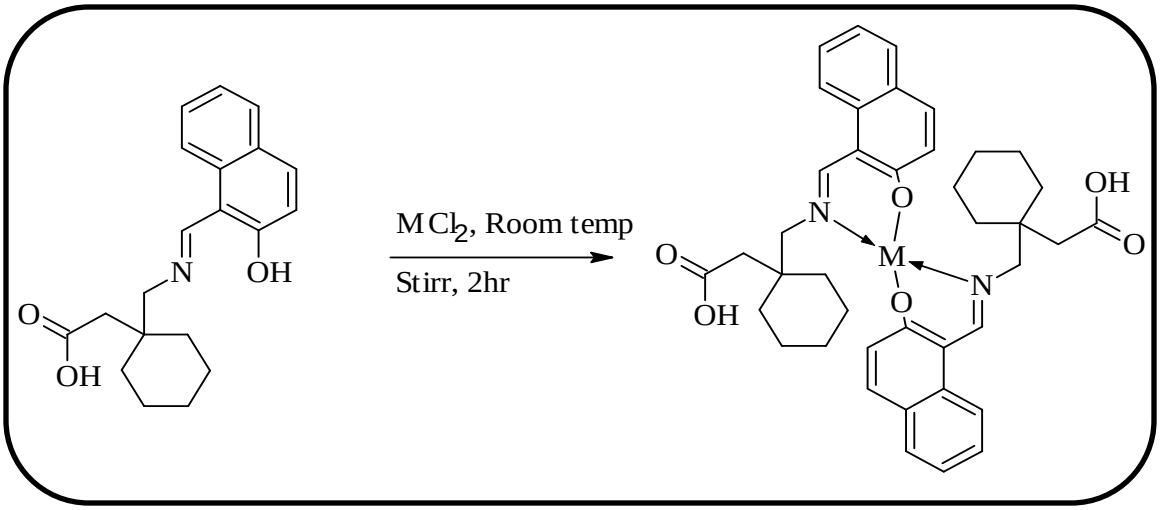

Where M = Co, Ni, Cu and Zn

Scheme 2.7 Metal complexes of the Schiff base HMAC

The product was recrystalised from distilled methanol by keeping for several days at room temperature.

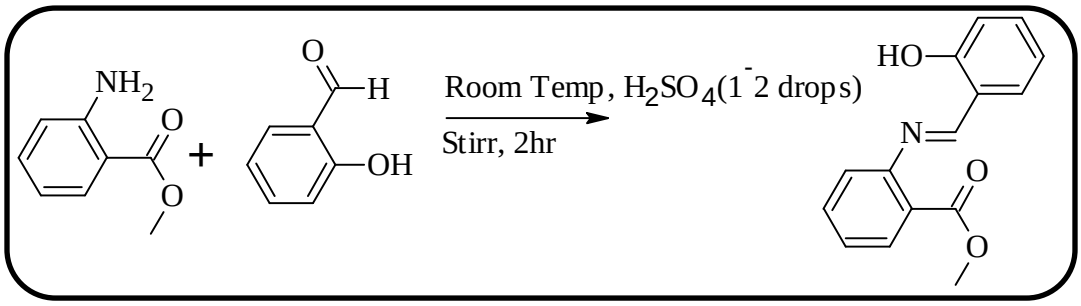

Scheme 2.8 Synthesis of methyl 2-{[(*E*)-(2-hydroxyphenyl)methylidene]amino}benzoate(H-HAB) Schiff base ligand

2.20 Synthesis of [M(HAB)$_2$] where M= Co, Ni, Cu and Zn (II) chlorides (17), (18), (19) and (20)

All the coordination complexes were synthesized by following the same method. Complexes were synthesized by reacting 10 mmol solution of HHAB prepared in 15 cm^3 distilled methanol with 10 mmol solution of metal acetate salt in 10 cm^3 methanol. An abrupt color change was

observed which gave greenish precipitate after stirring the mixture for some time. The precipitates were filtered, washed with methanol and then with n-haxane.

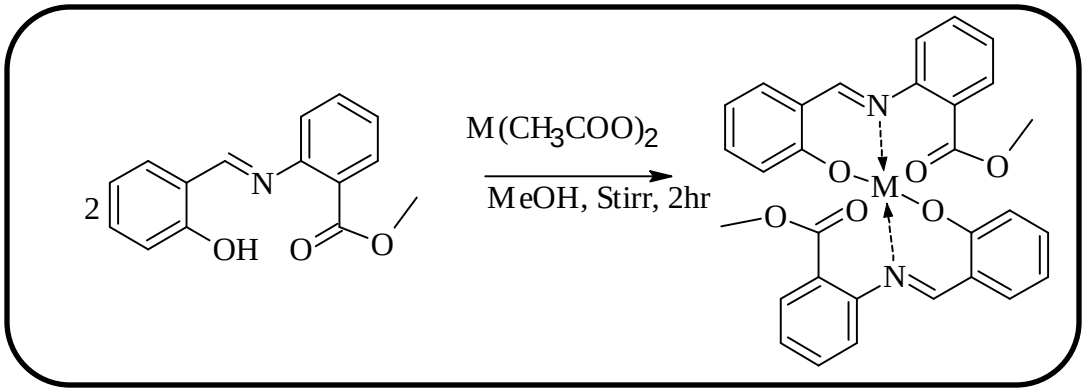

Scheme 2.9 Metal complexes of the Schiff base H-HAB

2.21 Synthesis of 2-(2-hydroxyphenyl)-3-{[(E)-(2-hydroxyphenyl)methylidene]amino}-2,3-dihydroquinazolin-4(1H)-one (H-HHAQ)

Benzohydrazide was prepared by condensing 25 mmol of hydrazine hydrate with 20 mmol of methyl anthranilate in 20 cm^3 of distilled methanol [9]. The resulting mixture was stirred and refluxed at 80 ^oC for 3 hrs and left the solution overnight. Beautiful glassy crystals were isolated after a day. 10 mmol of the benzohydrazide ligand was dissolved in 10 cm^3 of distilled methanol and added 20 mmol salicyldehyde to it. The mixture was stirred for 1hr at room temperature. It was concentrated on rotary evaporater, yellow Schiff base ligand was obtained which was washed with 5% copious n-hexane containing methanol and was recrystalised from THF.

2.22 Synthesis of [M(HHAQ)$_2$] where M= Co, Ni, Cu and Zn (II) chlorides (21), (22), (23) and (24)

0.011 mol of metal (II) chlorides were stirred in a minimum volume of dried methanol and 0.024 mol of H-HHAQ in a minimum volume of dried methanol was added to the metal solution. The mixture was stirred for 2-3 hrs at room temperature.

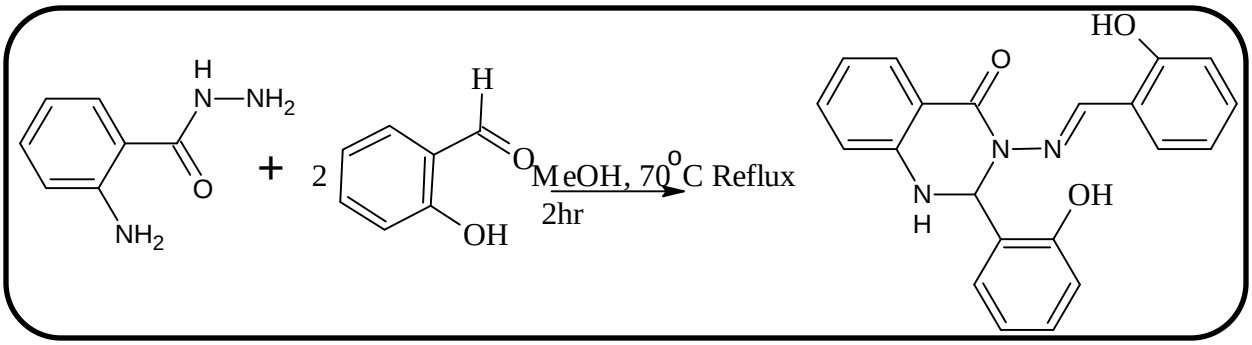

Scheme 2.10 Synthesis of 2-(2-hydroxyphenyl)-3-{[(*E*)-(2-hydroxyphenyl)methylidene]amino}-2,3-dihydroquinazolin-4(1*H*)-one (H-HAQ) Schiff base ligand

The metal complex was collected after filtration and copiously washed several times with 5% n-hexane containing methanol.

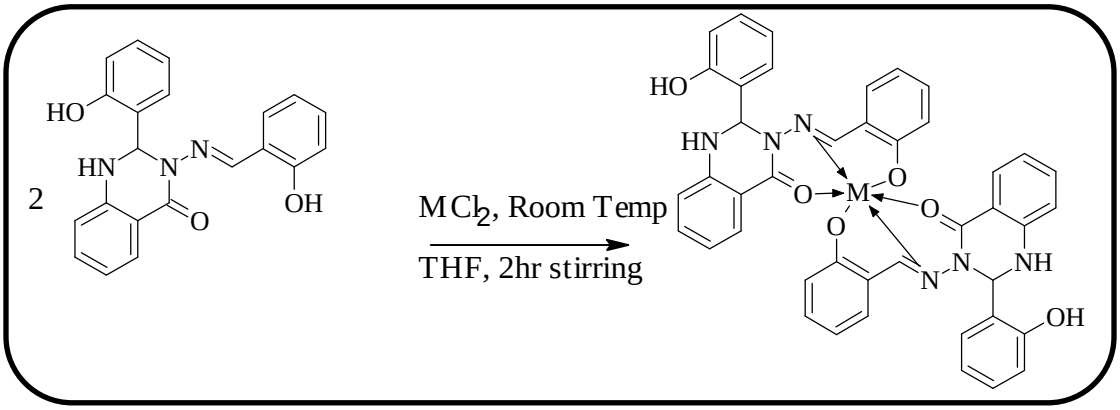

Scheme 2.11 Synthesis of metal complexes of (H-HAQ) Schiff base ligand

2.23 References

[1] G. M. Sheldrick, *Acta Crystallographica* Section *A*, **2008**, 64, 112-122.

[2] O. V. Dolomanov, L. J. Bourhis, R. J. Gildea, J. A. K. Howard and H. Puschmann, *J. Appl. Cryst.* **2009**, 42, 339.

[3] L. J. Bourhis, O. V. Dolomanov, R.J. Gildea, J. A. K. Howard, H. Puschmann, Olex2.refine in preparation, **2011**.

[4] G.L. Ellman, *Arch. Biochem. Biophys.*, **1958**, 74, 443.

[5] S.Schindler, *Eur.J. Inorg., Chem.* **2000**, 2311.

[6] R.J.P. Cannell, S.J. Kellam, A.M. Owsianka, J.M. Walker, *Planta Med.* **1988**, 54, 10.

[7] M. Arfan, , M. Ali, H. Ahmad, I. Anis, A. Khan, M. I. Choudhary, M. R. Shah, *J. Enz. Inh. Med. Chem.* **2010**, 25, 296.

[8] Atta-ur-Rahman, M. I. Choudhary and W. J. Thomsen, *Bioassay Techniques for Drug Development.* Amsterdam, The Netherlands: Harwood Academic, **2001.**

[9] H. H. Horowitz and G. Metzger, *Anal. Chem.* **1963**, 35(10), 1464.

[10] M. Olszak-Humienik, J. Mozejko, *Thermochim. Acta*, **2000**, 344, 73.

CHAPTER 3

3. RESULT AND DISCUSSION

3.1 Results and discussion of H-QMP series

3.1.1 Synthesis of 2-[(*E*)-(quinolin-3-ylimino)methyl]phenol (H-QMP)

Yield: 53%, M.p. 190-191 ^{o}C. IR, : 3200(bd), 1591(s), 1554(s), 1492(s), 1381w, 1361(s), 1338(s), 1319w, 1280(s), 1224(s), 1203(s), 1165(s), 1109(s), 927(s), 900(s), 848(s), 798(s), 780(s), 750(s), 736(s), 638(s), 610(w) cm^{-1} . ^{1}H-NMR (400.23 MHz, CD_3OD, 303k): δ = 11.0 (s, 1H, Ar-O<u>H</u>), 9.0 (s, 1H, -<u>H</u>C=N), 8.8 (s, 1H, H2), 8.10 (d, $^{3}J_{HH}$= 8.35Hz, 1H, H9), 8.0 (s,1H, H4), 7.8 (d, $^{3}J_{HH}$ = 7.72Hz, 1H, H6), 7.73(d, $^{3}J_{HH}$ = 7.9Hz, 1H, H8), 7.70(t, $^{3}J_{HH}$ = 7.55Hz,1H, H16), 7.4 (m, 1H, H17), 7.3 (d, $^{3}J_{HH}$ = 7.6, 1H, H18), 7.1(d, $^{3}J_{HH}$ = 8.03Hz, 1H, H15), 7.0 (d, $^{3}J_{HH}$ = 7.48Hz, 1H, H7) ppm, ^{13}C{^{1}H}-NMR (150.9 MHz, CD_3OD, 303k), 165(H<u>C</u>=N-, C12), 162(Aromatic <u>C</u>-OH, C14), 147(C, C10), 146 (CH, C2), 142(C, C5), 134(CH, C15), 133(CH, C18), 129.4(CH, C17), 129.2 (CH, C16), 128(C, C3), 127.8 (CH, C6), 127.4 (CH, C7), 124.7(CH, C8), 116(CH, C9) ppm. Elemental Analysis ($C_{16}H_{12}N_2O$), Calc. C: 77.40%, H: 4.87%, N: 11.28%, Exp. C: 76.80%, H: 5.10%, N: 10.89%. EI-MS: *m/z* (%) 249.1017 (100%) [$C_{16}H_{12}N_2O^{+}$].

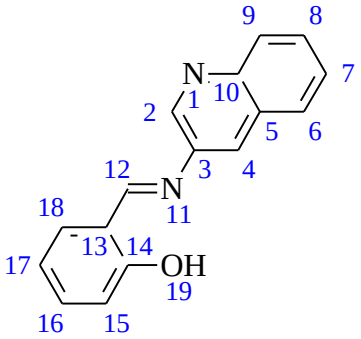

Scheme 3.1 Atoms numbering used for NMR signal

3.1.2 Bis(2-[(*E*)-(quinolin-3-ylimino)methyl]phenolato)nickel(II) (1)

Yield: 74%, IR: 1612(s), 1558(s), 1537(s), 1496(s), 1471(s), 1444(s), 1388(w), 1369(s), 1321(s), 1220w, 1155(s), 1136w, 1124(s), 1035(s), 999(w), 898(s), 819(s), 810(s), 750(s),732(s), 636(s), 596(w) cm^{-1}. λ_{max} = 720 nm (ε= 27.7$M^{-1}cm^{-1}$, $^1A_{1g}\rightarrow{}^1A_{2g}$). μ_{eff}: 2.7 B. M, Elemental analysis ($C_{32}H_{22}N_4O_2Ni$), Calcd. C: 69.47%, H: 4.01%, N: 10.13%, Ni: 10.61%, Exp. C: 70.43%, H: 3.88%, N: 11.56%, Ni: 10.50%. EI-MS: *m/z* (%) 554.2787 (15%) [$C_{32}H_{22}N_4O_2Ni^+$+$2H^+$], 249.5734 (100%) [$C_{16}H_{12}N_2O^+$], 145.3759 (5%) [$C_9H_8N_2^+$], $\wedge_m$= 0.01 Scm^{-1}.

3.1.3 Bis(2-[(*E*)-(quinolin-3-ylimino)methyl]phenolato)cobalt(II) (2)

Yield: 78%, IR Analysis: 2800-3300(bd), 1656(w), 1604(s), 1533(s), 1500(s), 1419(w), 1338(s), 1236(s), 1192(s), 1120(s), 1029(s), 980(s), 894(s), 800(w), 752(s), 667(s), 650(s) cm^{-1}. λ_{max}= 640nm (ε = 16.6 $M^{-1}cm^{-1}$, $^2A_{2g}\rightarrow{}^2B_{1g}$), μ_{eff}: 4.4 B. M. Elemental analysis ($C_{32}H_{22}N_4O_2Co$), Calcd. C: 69.44%, H: 4.01%, N: 10.12%, Co: 10.65%, Exp. C: 68.66%, H: 4.23%, N: 9.68%, Co: 11.12%. MS-ES+: *m/z* (%) 553.1060 (48%) [$C_{32}H_{22}N_4O_2Co^+$], 249.1078 (100%) [$C_{16}H_{12}N_2O^+$], 145.1128 (10%) [$C_9H_8N_2^+$], $\wedge_m$ = 0.03 S/cm.

3.1.4 2-[(*E*)-(quinolin-3-ylimino)methyl]phenolatoacetatoaquocopper(II) (3)

Yield: 65%, IR Analysis: 3290(bd), 1729(w), 1604(s), 1555(s), 1480(s), 1360(s), 1338(s),1280(w), 1200(s), 1160(w), 980(s), 848(s), 750(s), 650(s) cm^{-1}. λ_{max}= 850 nm (ε = 19.3 $M^{-1}cm^{-1}$, $^2E\rightarrow{}^2T_2$). μ_{eff}: 4.5B.M. Elemental analysis ($C_{18}H_{16}N_2O_4Cu$), Calcd. C: 55.74%, H: 4.16%, N: 7.22%, Cu: 16.38%, Exp. C: 55.44%, H: 4.10%, N: 8.22%, Cu: 15.88%. MS ES: *m/z* (%) = 387.8771 (10%) [$C_{18}H_{16}N_2O_4Cu^+$], (90%) [$C_{16}H_{12}N_2O^+$], $\wedge_m$ = 0.01 S/cm.

3.1.5 2-[(*E*)-(quinolin-3-ylimino)methyl]phenolatoacetatoaquozinc(II) (4)

Yield: 44%, IR Analysis: 3000-3400(bd), 1734(w), 1606(s), 1568(s), 1492(w), 1361(s), 1338(s), 1280(s), 1203(s), 1165(s), 977(s), 848(s), 750(s), 638(s) cm^{-1}. Elemental analysis

($C_{18}H_{16}N_2O_4Zn$), Calcd. C: 55.47%, H: 4.14%, N: 7.19%, Zn: 16.78%, Exp. C: 55.74%, H: 4.10%, N: 7.22%, Zn: 16.38%. MS-ES: *m/z* (%) = 389.7396 (5%) [$C_{18}H_{16}N_2O_4Zn^+$], 249.110 (100%) [$C_{16}H_{12}N_2O^+$], 145.1200 (2%) [$C_9H_8N_2^+$], $\wedge_m$ = 0.01 S/cm.

3.1.6 Analytical and spectroscopic characterization

The ligand H-QMP was synthesized by condensing salicyaldehyde with 3-aminquinoline to yield the phenolic Schiff base ligand. This was characterized by ^1H and $^{13}C\{^1H\}$ NMR spectroscopy which shows the expected resonances. The ^1H and $^{13}C\{^1H\}$ NMR peaks were assigned on the basis of scheme 2. Two singlets observed upfield at δ_H = 11.0ppm δ_H = 9.0ppm are assigned to the –HC=N- and phenolic protons, respectively. The remaining NMR spectrum shows the region for aromatic protons. The $^{13}C\{^1H\}$ spectrum also shows the azomethine peak at 165 ppm and the Ar-C-OH peak at 162 ppm, respectively. The aromatic resonances were explicitly assigned in the ^1H and $^{13}C\{^1H\}$ spectra. The ligand H-QMP was reacted with the divalent metal ions of Ni, Co, Cu and Zn as shown in scheme 3. The elemental composition of the ligand and metal complexes were unambiguously determined and reported which suggest the proposed composition for all compounds. This is further supported by ESI(+) mass spectrometry. All the complexes were found to be non-electrolyte in nature confirming coordination of the OAc^- ligands in **3** and **4**.

Since the IR spectra of all metal complexes are quite similar, the discussion is confined to the most important vibrations in the region of 4000-600 cm^{-1} in relation to the structure. The free ligand IR spectrum shows a broad peak around 3400 cm^{-1}, which is assigned to the –OH stretch. This absorption region either decreases in size or broadens to a large extent upon complexation with metal ions. Coordinated water in case of **3** and **4** shows a similar absorption band. The sharp band in the H-QMP spectrum at 1624 cm^{-1} is assigned to the $\upsilon_{(C=N)}$ vibration mode which was

found to be shifting by the difference of $\Delta\upsilon_{(C=N)}$ = 10-30 cm^{-1} in metal complexes. In **3** and **4** the C=O stretch for the coordinated acetate ion is observed at 1729 and 1734 cm^{-1}, respectively. The C-O stretch of acetate is observed at 1280cm^{-1} for both complexes **3** and **4**.

Except for the zinc complex all complexes show magnetic moments for spin only values. For **1**, **2**, and **3** the magnetic moment values suggest that the complexes are high spin.

The UV-visible spectra of compounds **1**, **2**, and **3** were measured in the region of 200-1000 nm. These spectra shows only one absorption band each for all of the compounds viz; for **1** the major absorption at 720 nm was assigned to a transition $^1A_1g \rightarrow {}^1A_2g$ since the other charge transfer bands caused by $^1A_1g \rightarrow {}^1B_1g$ and $^1A_1g \rightarrow Eg$ transitions are expected to be observed in the lower absorption region. However, no significant absorption of this kind was observed in rigorously purified samples, possibly because these transitions are buried beneath the absorption region for $^1A_1g \rightarrow {}^1A_2g$. The 2.7 B.M $\mu_{effective}$ value and the absorption band in the visible region confirm that the crystal field splitting between sets of dyz, dzx and dz^2 orbitals and dxy and dx^2-y^2 orbitals is large. Furthermore, the energies of the dxy and dx^2-y^2 orbitals ($\Delta E = 1.73x10^{-3}$ev) are similar enough to allow for their occupation with one single electron each.

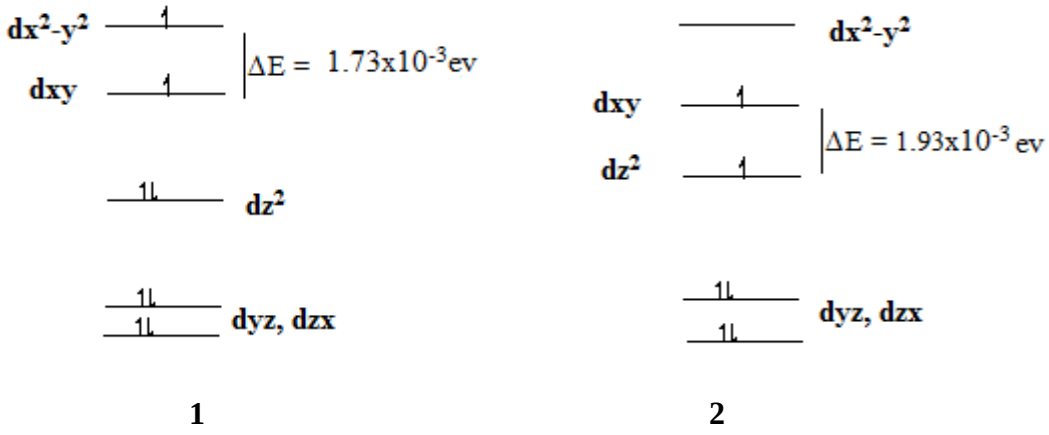

Figure 3.1 Crystal field splitting for 1 and 2 on the basis of UV-Visible and $\mu_{effective}$.

The splitting of orbitals is shown in fig.2. It was concluded by Gray and Ballhausen that for ligand-to-metal transitions (exhibited unambiguously by complexes without an intraligand π system) the two charge-transfer bands are separated by nearly 10,000 cm^{-1}, whereas for metal-to-ligand transitions (shown by complexes with an intraligand $\boldsymbol{\pi}$ system), the three charge-transfer bands shown by nickel square planar complexes are more closely spaced (approximately 2000-3000 cm^{-1} apart) [1,2]. The metal complexes formed with the aromatic monoanionic ligand H-QMP are therefore expected to yield transitions which will overlap in a narrow range.

For **2** the absorption occurs at 640 nm which was tentatively assigned to the $^2A_{2g} \rightarrow {}^2B_{1g}$ transitions on the basis of the 16.6 $M^{-1}cm^{-1}$ molar extinction coefficient value. It was presumed that for the C_{2v} symmetry of the cobalt complex the $^2A_{2g} \rightarrow {}^2B_{1g}$ transition is allowed whereas $^2A_2 \rightarrow {}^2A_1$ is forbidden. The 4.4 B.M $\mu_{effective}$ value and the visible absorption band for **2** shows that the dyz and dzx set of orbitals and the dz^2, dxy, dx^2-y^2 set of orbitals are spaced closely. The crystal filed splitting ($\Delta E = 1.93 \times 10^{-3}$ev) between dz^2 and the dxy, dx^2-y^2 set of orbitals is not very high as compared to complex **1** [see fig. 3.1 (2)]. Therefore each of dz^2 and dxy orbitals are occupied by a single electron resulting in a high spin cobalt complex. For **3** the visible band observed at 850 nm is assigned to the $^2E \rightarrow {}^2T_2$ tetrahedral transition.

All transitions are assigned to the excitation from pπ electrons from the phenolate ion to dπ* orbitals of the metal ion. The imine-nitrogen also donates pπ electrons to the dπ* orbital of the metal ion leading to transitions, which were presumed to be occurring in the region of 500-700 nm. However, these bands are obscured by the more intense phenolate to metal ion transitions [1].

3.1.7 Structural analyses

The ligand H-QMP co-crystalizes out from the concentrated THF solution in Pc space group. The cocrystallisation was handled with free variables but the atoms on identical positions were refined jointly (i.e. same position, same displacement factors but complementing occupation). About 70% is the wanted molecule and 30% of the bisquinoline is present in the crystals obtained. There is a lot of electron density between N and O which could be a partial carbon (about 35% according to an initial test) and oxygen is only about 65% oxygen and about 35% nitrogen and that affects the hydrogen attached to the oxygen as well, same for N(3) (mixture of carbon and nitrogen). In order to generate figures showing only the wanted molecule we have to either delete "Part 2" of the molecule or the individual atoms N(3), C(17) and H(17). Even though we are now in a more symmetrical space group the R-values have not increased compared to the old solution, which confirms that the current refinement is certainly the more correct one.

The ORTEP plot of H-QMP shows that the plane C(2)-C(3)-C(4)-C(5)-C(6)-C(7) is separated by 1.41^{o} from the plane produced by C(10)-C(11)-N(12)-C(13)-C(14)-C(15)-C(16)-C(17)-C(18) showing perfect coplanarity between the aromatic rings. The intramolecular hydrogen bonding between the imine nitrogen and the hydrogen of hydroxyl group results in the formation of non-planar six membered distorted ring. The bond length for this intra molecular hydrogen bond was found to be 2.156 A^{o}. A unique ladder type arrangement can be observed in the crystal lattice. The molecule possess 1,3 and 2,4 parallel arrangement for the next neighboring molecule. This unique arrangements is due to the hydrogen bonding explicitly connecting aminoquinoline nitrogen with H(19) (2.487 A^{o}), and hydroxyl group with H(8) hydrogen (2.478). The –CH=N bond distance is 1.337 A^{o} which was found to be longer than the normal bond length of imine

linkage as found in (E)-4-bromo-2-[(2-chloro-3-pyridyl)-iminomethyl]phenol(1.291 A^o) [3]. This may be due to presence of electron deficient aminoquinoline ring. The crystal data and the selected bond lengths are reported in table 1 and 2.

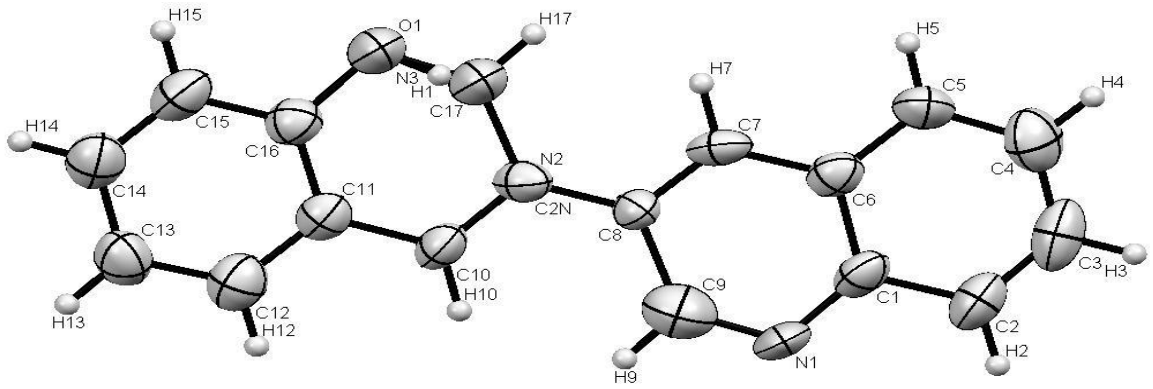

Figure 3.2 Molecular structure of H-QMP. Thermal ellipsoids are shown at 50% probability. H atoms are shown.

Table 3.1 Crystal data and structure refinement for H-QMP	
Identification code	H-QMP
Empirical formula	$C_{16}H_{12}N_2O$
Formula weight	248.27
Temperature/K	298
Crystal system	monoclinic
Space group	Pc
a/Å	8.9245(11)

b/Å	6.3535(7)
c/Å	12.318(2)
α/°	90.0
β/°	116.288(11)
γ/°	90.0
Volume/Å^3	626.22(16)
Z	1
ρ_{calc}mg/mm^3	1.33
m/mm^{-1}	0.083
F(000)	262.4
Crystal size/mm^3	0.31 × 0.11 × 0.07
2Θ range for data collection	6.42 to 56.16°
Index ranges	$-11 \leq h \leq 11$, $0 \leq k \leq 8$, $-15 \leq l \leq 15$
Reflections collected	5061
Independent reflections	4097[R(int) = 0.0297]
Data/restraints/parameters	4097/0/344
Goodness-of-fit on F^2	1.409528
Final R indexes [I>=2σ (I)]	R_1 = 0.092214, wR_2 = 0.2011
Final R indexes [all data]	R_1 = 0.142673, wR_2 = 0.204298
Largest diff. peak/hole / e Å^{-3}	1.039395/-0.369261
Flack Parameter	176

Table 3.2 Bond Lengths for H-QMP

Atom	Length/Å	Atom	Length/Å
C2- C3	1.402(9)	**C14-C15**	1.335(11)
C2-C7	1.379(10)	**C15-C16**	1.376(12)
C3-C4	1.377(12)	**C16-C17**	1.376(9)
C4-C5	1.415(12)	**C17-C18**	1.391(10)
C5-C6	1.398(9)	**C18-C19**	1.456(9)
C6-C7	1.386(11)	**N9-C8**	1.337(9)
C7-C8	1.406(9)	**N9-C10**	1.384(5)
C10-C11	1.540(9)	**N12-C11**	1.253(8)
C10-C19	1.320(9)	**N12-C13**	1.346(9)
C13-C14	1.402(9)	**O1-C2**	1.380(9)
C13-C18	1.428(10)		

Both **1** and **2** crystallize from dichloromethane/ether solutions at room temperature in the monoclinic space group $P2_1/c$, with one half of the symmetric monomer in the asymmetric unit (Figure 2 and 4). The structures of both complexes are, except for the central metal, identical. Therefore we are refraining from an in-depth study of the individual structures except where the difference is apparent enough to warrant discussion and instead focus predominantly on the structural evaluation of **1**. The ORTEP plots for **1** and **2** show that both central metals are coordinated by two ligands in *trans* fashion generating an almost perfect square planar coordination geometry (nickel and cobalt lie directly in the N_2O_2 plane with no deviation from it). The O(1)-M-O(1A) and N(1)-M-N(1A) [where M = Ni(II), and Co(II)] bond angles are (due to the space group symmetry) exactly 180^o and emphasize coplanarity (fig.3). The O(1)-Ni(1)-

N(1) is only slightly deviated from a perfect right angle with 90.37^{o}. The small difference of the bond angles C(1)-O(1)-Ni(1) (125.19^{o}) and N(1)-C(7)-Ni(1) (120.87^{o}) shows that the chelate ring formed by the anionic ligands and the metal is not symmetrical. This is further evidenced by the dihedral angle of 28.48^{o} between the planes N(1)-C(7)-C(6)-C(1)-O(1) (the chelate ring) and N(2)-C(16)-C(10)-C(15)-C(8) (the pendent quinoline group). The dihedral angle between planes O(1)-O(1A)-Ni(1)-N(1)-N(1A) and C(16)-N(2)-C(15)-C(10)-C(9)-C(8)-N(1) is 48.87^{o} showing significant non coplanarity of the NiO_2N_2 plane and the six membered chelate ring formed with the QMP anion and the metal. Aside from the planar complex core the ligands exhibit two further planar parts; i.e. the quinoline moiety and the phenyl moiety, which are both tilted slightly away from the central plane in opposite direction. For the two ligands the quinoline planes are (necessarily) coplanar as are the two phenyl moieties. In the crystal packing each quinoline nitrogen atom, which is not involved in direct bonding is pointing directly to one nickel or cobalt atom of a neighboring molecule creating a pseudo octahedral environment around the metal center, which is exposed to two such functional groups from different neighbors (fig. 4). The distance between these nitrogen atoms and the nickel centers is 2.973 Å (almost 1 Å longer than the direct Ni-N bond) emphasizing that this is a rather week interaction. By comparing the Ni-O [1.901 Å], Ni-N [2.032 Å] bond distances as well as the Co-O [1.905 Å], Co-N [2.037 Å] bond distances with those in related complexes that do not bear any N-heterocyclic rings, i.e. [1.833 and 1.902 Å] in ($C_{26}H_{24}O_6N_2Ni$) [28] and with [1.913 and 2.007 Å] in ($C_{26}H_{20}CoN_2O_2$) it becomes apparent that the metal chelate core MO_2N_2 is less tightly bound due to the quinolone-metal interactions forming the pseudo-octahedral geometry as shown in fig. 4 [4,5].

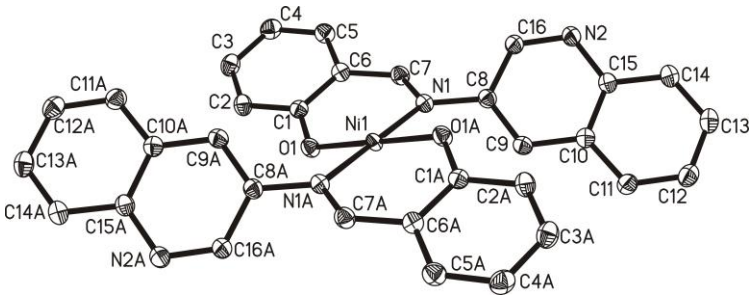

Figure 3.3 Molecular structure of 1. Thermal ellipsoids are shown at 50% probability. H atoms are omitted for clarity reasons. Selected bond lengths [Å] and angles [°]: Ni-O 1.9011(11); Ni-N 2.0323(13); O-Ni-O 180; N-Ni-N 180; O-Ni-N (intra) 90.37(5); O-Ni-N (inter) 89.63(5).

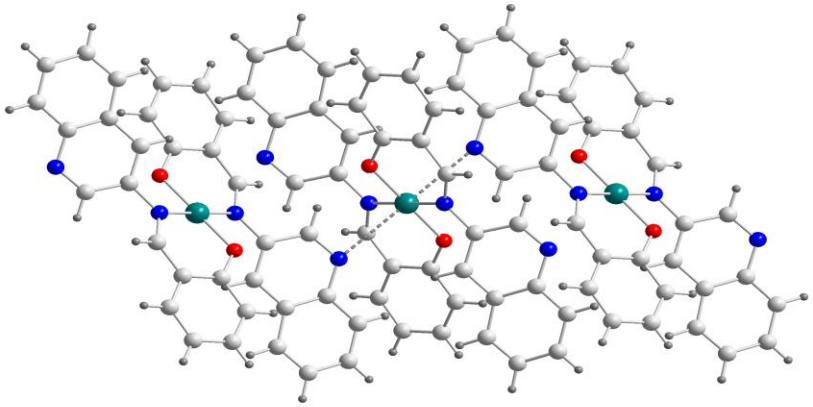

Figure 3.4 Intermolecular interactions between quinolone nitrogens and nickel in the crystal structure of 1 leading to the pseudo-octahedral coordination environment of nickel.

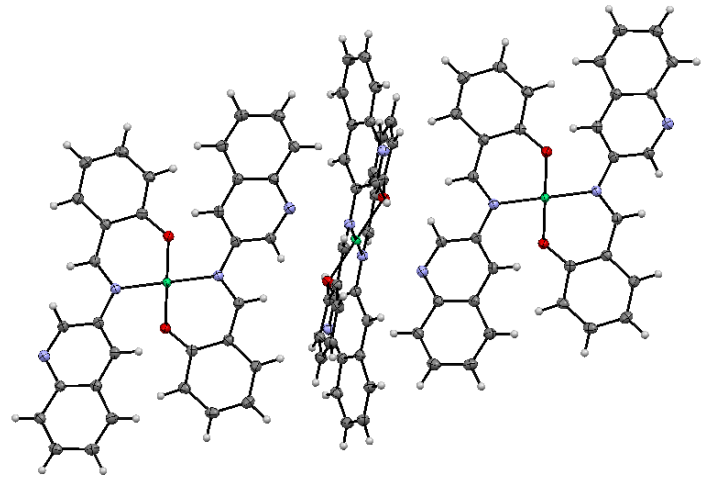

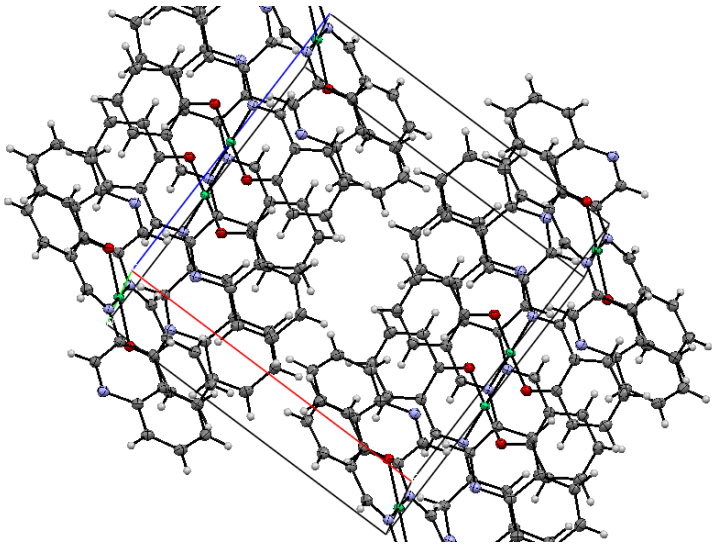

1

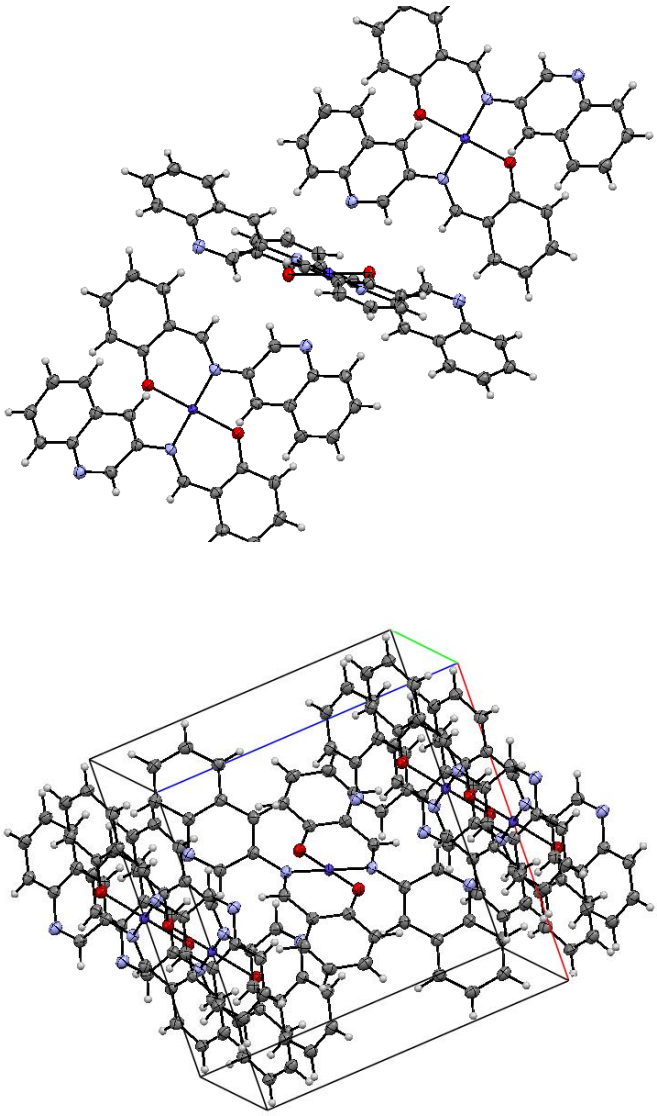

2

Figure 3.5 Crystal packing diagrams for 1 and 2

In complex **2** the C(1)-O(1)-Co(1) bond angle is 125.13^{o}, and the C(7)-N(1)-Co(1) bond angle is 120.84^{o} showing little difference to **1**. Similarly the dihedral angle between the planes produced by N(1)-C(7)-C(6)-C(1)-O(1) (the chelate ring) and N(2)-C(16)-C(10)-C(15)-C(8) (the pendent quinoline group) is equal to 28.83^{o} showing the same trend of non coplanarity of the chelate atoms and with the rest of the molecule.

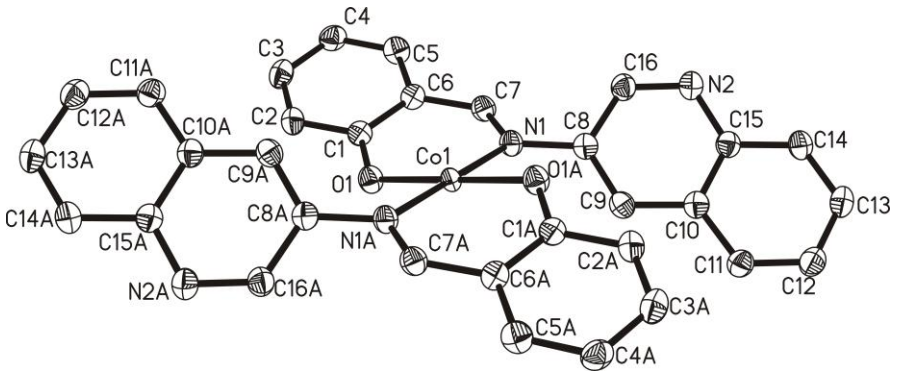

Figure 3.6 Molecular structure of 2. Thermal ellipsoids are shown at 50% probability. H atoms are omitted for clarity reasons. Selected bond lengths [Å] and angles [°]: Ni-O 1.905(11); Ni-N 2.037(13); O-Co-O 180; N-Co-N 180; O-Co-N (intra) 89.55(5); O-Co-N (inter) 90.45(5).

3.1.8 AChE and BChE inhibition

New cholinesterase inhibitors, in addition to their potential clinical importance if followed by proper pharmacological-investigations, would help in defining the role of BChE in brain development, health and aging and reveal the value of BChE inhibition as a novel strategy for the treatment of AD [6]. Here we report the AChE and BChE inhibition capabilities of the four synthesized metal complexes and their mutual relationships (Table 2). All compounds were found inactive against acetyl cholinesterase. The cobalt and copper QMP complexes were shown to be selectively inhibiting BChE, whereas the remaining compounds are inactive. It was previously reported that during the development of AD the activity of BChE increases by 40-90%. Examination of the amyloid plaque also show the increased concentration of BChE [7,8]. Therefore the selective BChE inhibitors like copper and cobalt QMP complexes may be good therapeutic agents. It has been shown that the amyloid protein precursor (APP) possesses specific selective Zn^{2+} and Cu^{2+} binding sites which mediate its physicochemical behavior and if occupied, may cause inhibition of AChE and BChE [9]. BChE inhibitors have been used to delay

symptoms of AD patients by virtue of their ability to enhance acetylcholine availability. Their involvement in a cholinergic anti-inflammatory pathway connect BChE and AChE with a possible marker of low-grade systemic inflammation observed in Type-2 diabetes, obesity, hypertension, coronary heart disease, and AD [10,11]. Thus, new metal based inhibitors for BChE are among the most sought after targets for therapeutic use in AD treatment [12,13]. Our results, as summarized in Table 2 clearly show that the copper complex is much more active than the cobalt complex, which is in accordance with senile plaque naturally containing copper. Due to the abundance of copper in particular in the brain, complexes are expected to be actively involved in decreasing the amyloid plaques in AD patients as well as eliminating oxidative stress from proactive metal ions, provided the metal binds at the targeted binding sites of APP [9]. It has been shown with potentiometric and spectroscopic studies that copper coordinates at the N-terminus of the Aβ-peptides, but in equilibrium with the internal histidyl (His13 and His14) sites. The binding based in both cases on the deprotonation of amide groups present on the surface of plaques, but the latter binding mode strongly favors copper over other metal ions [12].

3.1.9 Urease and α-Chymotrypsin activities

Compounds can be classified into two categories based on their urease inhibitory activities 1) organic compounds which include acetohydroxamic acid, humic acid etc and 2) heavy metal ions which include Cu^{2+}, Zn^{2+}, Pd^{2+}, and Cd^{2+}. Rarely metal complexes were tested for the inhibition of urease and α-Chymotrypsin. Table 3 enlists the inhibition of urease and α-Chymotrypsin by all the tested metal complexes. The results reveal that nickel complexes are much more active for urease inhibition than any other metal complex. At the same time it is observed that complex **1** is showing much lower activity against α-Chymotrypsin. Therefore

nickel centered metal complexes of the H-QMP ligand can help in designing selective drugs. This selectivity of the nickel containing compound to inhibit urease may be attributed to chelation by H-QMP. Other metal complexes with the same ligand were not found to be so much active against any of the tested enzyme. Cobalt centered complex of the ligand H-QMP is also showing activity which ranges from moderate inhibition of α-Chymotrypsin to the high activity for urease. By comparing **1** and **2** it can be concluded that nickel is selective inhibitor for urease. Previous study on the urease activities have shown that metal complexes of Sn(IV), Cu(II), Bi(III), Cu(II) and Cd(II) were found to be active [14]. Here we are extending the inhibition of urease by nickel(II) complex of H-QMP. The inhibition of urease by 1 may be explained by the possible interaction of the metal ion with –OH bridge group in the enzyme. This may either lead to Ni-Ni weak interactions as well which will affect the activity of enzyme. Therefore it can be presumed that metal ions which are involved in the interaction with the bridging –OH group will be active in the inhibition process [14]. Apart from it 2 is also showing inhibition of the urease enzyme up to some extent but unlike **1** is not selective by inhibiting chymotrypsin as well. Complexes 3 and 4 are not showing any convincing inhibition for both the tested enzymes. Therefore it can be concluded that square planar complexes are effective in inhibition process as compared to tetrahedral **3** and **4**.

3.1.10 Antimicrobial activities

Compounds H-QMP and its metal complexes were studied for their in Vitro antimicrobial activities against some Gram positive bacteria *Bacillus atrophaeus, Bacillus subtilis, Staphylococcus aureus,* Gram negative bacteria *Klebsiella pneumoniae*, *Salmonella typhus, Pseudomonas aeruginosa*, *Escherichia coli, Agrobacterium tumefaciens, Erwinia carotovora*, fungal Strain *Candida albican*. As revealed from the values of activities given in the

table 3.3, that the Schiff base ligand is not active against any of the pathogenic strain, whereas the complexes show low activities. From the table 3.3 it can be revealed that cobalt and copper complexes are also showing antibacterial and antifungal activities. Compound **1** is inactive against many Gram negative bacteria whereas showing weak activities against Gram positive and fungal strain. Compounds **2** and **3** are showing weak to moderate activities against all the tested species. Compound **4** is better in activities than the 1. Therefore metal complexes of H-QMP can be used for the design of metal based drugs.

Table 3.3 In vitro inhibitory activities (in terms of IC_{50} (µM)±SEM) of H-QMP and its metal complexes against acetyl cholinesterase, butyrylcholinesterase, Urease and α-Chymotrypsin

Sample	Acetyl cholinesterase IC_{50} (µM)±SEM	Butyrylcholinesterase IC_{50} (µM)±SEM	Urease IC_{50} (µM)±SEM	α-Chymotrypsin IC_{50} (µM)±SEM
H-QMP	---	---	---	---
1	---	---	9.9±0.124	---
2	---	69±0.0112	---	---
3	---	5±0.0004	---	---
4	---	---	---	---
Standard	0.5±0.01 **(galanthamine)**	8.5±0.5 **(galanthamine)**	21± 0.011 **(Thiourea)**	5.71± 0.13 **(Chymostatin)**

Table 3.4: In Vitro antimicrobial activities of H-QMP and its metal complexes against different animal and plant pathogens

Compounds	*Bacillus atrophaeus (cm)*	*Bacillus subtilis (cm)*	*Klebsiella pneumoniae (cm)*	*Salmonella typhus (cm)*	*Pseudomonas aeruginosa (cm)*	*Escherichia coli (cm)*	*Staphylococcus aureus (cm)*	*Candida albican (cm)*	*Agrobacterium tumefaciens (cm)*	*Erwinia carotovora (cm)*
H-QMP	—	—	—	—	—	—	—	—	—	—
1	1.2	1.1	—	—	1.0	1.0	—	1.2	—	2.2
2	2.8	1.6	1.7	1.5	1.6	2.1	1.3	2.3	2.1	1.4
3	2.2	2.1	2.8	1.4	1.8	2.1	1.9	1.9	1.9	2.5
4	1.4	2.1	1.2	1.3	1.8	1.0	2.0	2.1	1.8	1.2
Standard	2.5	2.6	2.9	4.2	3.6	3.8	3.4	1.6	1.5	2.6

Gram positive bacteria: *Bacillus atrophaeus*, *Bacillus subtilis*, *Staphylococcus aureus*, standard used was erythromycin in 6 µM

Gram negative bacteria: *Klebsiella pneumoniae*, *Salmonella typhus*, *Pseudomonas aeruginosa*, *Escherichia coli*, *Agrobacterium tumefaciens*, *Erwinia carotovora*, standard used was ciprofloxacin in 6 µM

Fungal Strain: *Candida albican*, standard used was clothrimazol in 6 µM

3.1.11 Thermodynamics and Thermal studies

Thermal pyrolysis of H-QMP ligand and its metal complexes were evaluated in the range of 30-1000 ^{o}C in static air. The TG and DTA curves are shown in figure 3.7 and 3.8 respectively. The complexes exhibited endothermic peaks corresponding to melting points and transition temperatures. The table 3.6 represents DTA and TG data for Schiff base ligand and its transition metal complexes. The TG curves for all the compounds are shown in figure 3.7. TG curve for H-QMP shows that the compound is stable up to 200 ^{o}C and then follows the degradation process. The temperature at which a compound starts its decomposition is represented by Td. Td for **1, 2, 3** and **4** are 240, 310, 190 and 180 ^{o}C respectively. The kinetic and thermodynamic data of the compounds are shown in table 3.5, whereas the species evolved in the decomposition is shown in table 3.6.

Table 3.5 Kinetic and thermodynamic parameters of H-QMP and its metal complexes

Compound	**Ts in K**	**E*, KJ/mol**	**ΔH*, KJ/mol**	**ΔG*, KJ/mol**	**ΔS*, Jmol^{-1}K^{-1}**	**Order of reaction, n**
H-QMP	608.7	61.01	55.94	184.14	-210.62	1
1	727	51.85	48.01	240.81	-265.21	3/2
2	697	11.30	5.50	179.93	-250.26	2
3	588.1	13.79	8.90	163.41	-262.74	5
4	562	10.50	5.82	138.53	-236.15	5

By looking into table 3.6, it is apparent that the ligand exhibit five DTA peaks marking the five products of pyrolysis. The very large negative value for entropy, shown in table aaa, explains the stable nature of the ligand, also confirmed by high activation energy value. H-QMP follows

single degradation step, producing the benzene, quinolone, nitric oxide, carbon monoxide and acetylene, without any residue left at the end of process. The degradation process completes at 610 ^{o}C. The degradation is shown in scheme 3.2.

$C_{16}H_{12}N_2O \rightarrow C_2H_2 + C_7H_5N + C_6H_6 + 1/2NO + 1/2CO$

Scheme 3.2 Thermal degradation of H-QMP

Both **1** and **2** are nickel and cobalt complexes of the H-QMP ligand having identical crystal structures, follow the same trend in degradation phenomenon. Both the complexes bear ethanol and methanol molecules in their crystal lattice respectively, which is evolved first when the sample is heated. In the second step hydrogen cyanide moiety is produced with two DTA peaks for **1** and one for **2**. In the third step both compounds exhibit identical behavior and produced two moles of quinolone in the form of free radicals and two moles of phenol moieties. The quinolone free radical moiety combined with each other to produce the stable bisquinoline species. The two DTA peaks for this fragmentation substantiate the results of TG data. In the last step both the compounds produces their corresponding oxides which are stable up to 1000 ^{o}C, the temperature to which compounds were heated. The negative entropy values for both the compounds differ only by $\Delta S^{\#}$= 15 J/molK. **1** follow 3/2 order of pyrolysis whereas **2** show 2nd order reaction process. By comparing the activation free energies for both the complexes, it is apparent that H-QMP produces more stable complex with nickel than cobalt. This is further evidenced by the values for enthalpy change and activation energy terms.

$C_{32}H_{22}N_4NiO_2 \rightarrow C_2H_5OH$ in crystal lattice $+ C_{32}H_{22}N_4NiO_2$ I Stage

$C_{32}H_{22}N_4NiO_2 \rightarrow C_{30}H_{20}N_2NiO_2 + 2HCN$ II Stage

$C_{30}H_{20}N_2NiO_2 \rightarrow C_{18}H_{14}N_2 + 2C_6H_6O + NiO$(Residue) III Stage

Scheme 3.3 Thermal degradation of 1

The degradative routes for both **1** and **2** are shown below in scheme 3.3 and 3.4 respectively:

$C_{32}H_{22}CoN_4O_2 \rightarrow CH_3OH$ in crystal lattice $+ C_{32}H_{22}CoN_4O_2$ I Stage

$C_{32}H_{22}CoN_4O_2 \rightarrow C_{30}H_{20}CoN_2O_2 + 2HCN$ II Stage

$C_{30}H_{20}CoN_2O_2 \rightarrow C_{18}H_{14}N_2 + 2C_6H_6O + CoO$(Residue) III Stage

Scheme 3.4 Thermal degradation of 2

Table 3.6 Thermo analytical results of H-QMP and its complexes

Compound	TG Temp. range/ ^oC	Stage	Mass loss		DTA	Moiety evolved
			% Calc.	% Found		
H-QMP	30-610	I	101.4	100	(-)26, (-)18, (-)26.5, (+)0.30, (+)10.78	1/2NO, 1/2CO, C_2H_2, C_7H_5N, C_6H_6
1	30-140	I	7.6	8.2	(-)10	C_2H_5OH(in crystal lattice
	140-320	II	9.3	8.0	(-)13, (-)15	2HCN
	320-400	III	77.0	79.8	(-)12, (+)118	$C_{18}H_{12}N_2$, $2C_6H_6O$
	>400	Res	13.3	13.1	---	NiO
2	30-120	I	5.5	5.5	(+)2	CH_3OH
	120-300	II	9.8	9.7	(-)2	2HCN
	300-400	III	67	71.5	(-)9, (+)81.5	$C_{18}H_{12}N_2$, $2C_6H_6O$
	>400	Res	12.8	12.9	---	CoO

3	30-210	I	16.0	16.7	(-)0.5, (-)5.6, (-)9.3	H_2O, HOCN
	210-390	II	22.7	23.4	(-)19.0	$2CO_2$
	390-520	III	56.3	49.2	(+)120	C_6H_6O, C_9H_7N
	>520	Res	16.2	15.3	---	Cu
4	30-100	I	5.6	6.0	(+)2, (-)6	$1/2H_2O$, 1/2NO
	100-370	II	57.2	55.3	(-)10, (-)9	C_9H_6N, C_6H_6O
	370-560	III	26.3	25	(+)46	2CO, CO_2, $2H_2$
	>560	Res	16.0	15.0	---	ZnO

For **3** the thermal degradation process starts at 140 ^oC and ends at 210 ^oC. The initial products are coordinated water and the hydrogen isocyanic acid, an intermediate for cyanoric acid. In the second stage of degradation, started at about 230 ^oC, two moles of carbon dioxide is produced. In the third step ranging from 390 ^oC to 520 ^oC, the ligand based degradation occur, producing quinolone and phenol. Copper metal remain as residue. DTA peaks are consistent with the degradative products produced. There are three DTA peaks for first stage of pyrolysis, one for second and one for third. All the DTA peaks are negative except for the third stage which is +120. The value of entropy, for **3,** is -262.74 $Jmol^{-1}K^{-1}$ indicating that the degradation reactions are slower than the normal reactions. The low activation energy value for **3** may be attributed to less stable complexes of the H-QMP ligand. The high value of activation free energy shows that the degradation process is endergonic with almost zero enthalpy change. The degradation is following the 5^{th} order reaction process and is shown in scheme 3.5:

$$C_{18}H_{16}CuN_2O_4 \rightarrow H_2O + HOCN + C_{17}H_{13}CuNO_2 \qquad \text{I Stage}$$

$C_{17}H_{13}CuNO_2 \rightarrow 2CO_2 + C_{15}H_{13}CuNO$ II Stage

$C_{15}H_{13}CuNO \rightarrow C_9H_7N + C_6H_6O + Cu$ (Residue) III Stage

Scheme 3.5 Thermal degradation of 3

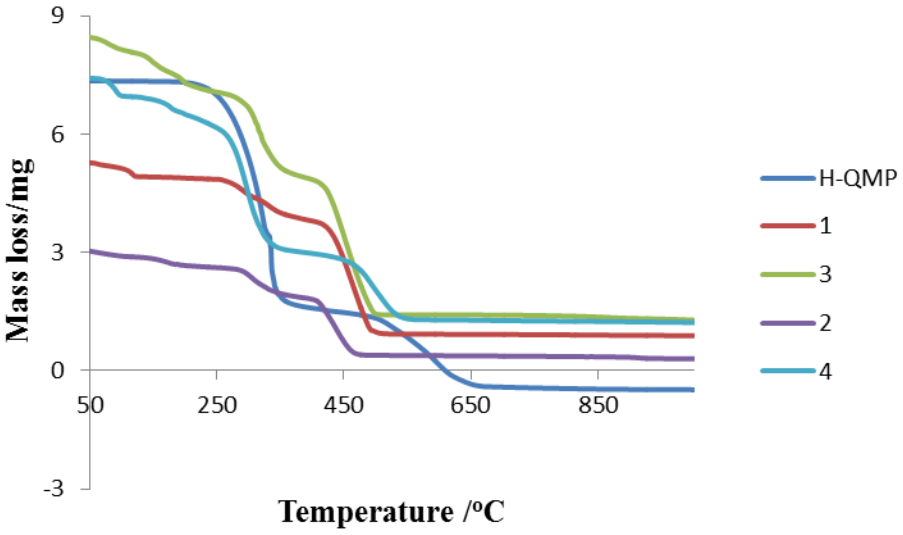

Figure 3.7. Thermogravimetric plots of H-QMP and its metal complexes

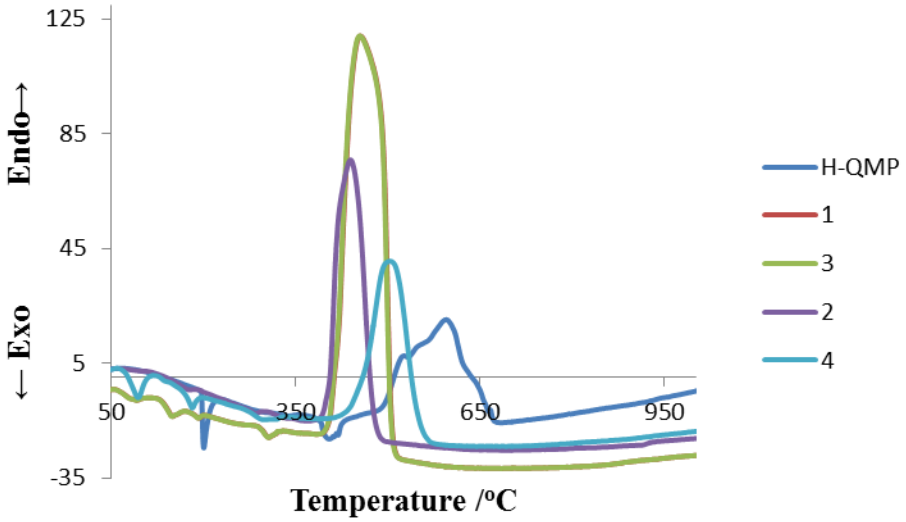

Figure 3.8. Differential thermogravimetric curves for H-QMP and its metal complexes

At about 100 °C, thermal degradation process of **4** was started, releasing 0.5 moles of water and the same amount of nitric oxide. The second stage completes at 370 °C, quioline and phenol

moieties are released at that stage. Two moles of carbon monoxide, one mole of each of the hydrogen gas and carbon dioxide are produced leaving zinc oxide residue. Five DTA peaks are observed during the complete degradation process. In the first stage one endothermic as well as one exothermic peak is observed. Both the peaks are exothermic in the second stage, whereas in the third step endothermic peak can be seen. Fifth order kinetics is followed during the degradation process of **4**. -236.15 $Jmol^{-1}K^{-1}$ represents entropy of the process. The free energy term is low with negative enthalpy value, representing exogonic process. This is further supported by the low activation energy value. The degradation is shown in scheme 3.6:

$C_{18}H_{16}N_2O_4Zn \rightarrow 1/2H_2O + 1/2NO + C_{18}H_{14}NO_2Zn$ I Stage

$C_{18}H_{14}NO_2Zn \rightarrow C_9H_7N + C_6H_6O + C_3H_4O_2Zn$ II Stage

$C_3H_4O_2Zn + O_2 \rightarrow 2CO + CO_2 + 2H_2 + ZnO$ (Residue) III Stage

Scheme 3.6 Thermal degradation of 4

3.1.12 Conclusion

The modified amino quinoline Schiff base ligand was found to produce metal complexes with two different geometries depending on the metal center. The nickel and cobalt complexes were assigned square planar geometries on the basis of spectrometric studies whereas the copper and zinc complex were assigned distorted tetrahedral geometries. The geometries of nickel and cobalt complexes were further confirmed by diffraction studies. The Schiff base and its complexes were studied for acetyl cholinesterase and butyrylcholinesterase inhibition activities for a possible therapeutic activity in Alzheimer's disease. The copper and cobalt complexes with QMP were found to be active in inhibiting the butyrylcholinesterase only. This selectivity may be used for designing drugs, which control dementia more specifically and consequently more successfully. The inhibitory concentration needed for the copper complex is considerably lower

than for the cobalt complex, emphasizing its superiority in this respect, which is in accordance with previous metal to Aβ binding studies and the natural abundance of copper in the brain. Here we have shown that the easily accessible QMP^- ligand in combination with copper might be reasonable alternative drugs, which have been used and are being used for the inhibition of butyrylcholinesterase in order to treat Alzheimer's disease and for related illnesses.

Novel nickel based urease inhibitor has been reported here which is found to be selectively involved in the urease inhibition with low inhibition of the chymotrypsin. Therefore a new metal based therapeutic agent can be developed for the treatment of various diseases like ulcers, kidney related diseases, coma etc. This selective inhibitory behavior of **1** was assigned to the possible interaction of nickel with the bridged –OH group. Complex **2** was also found to be moderately active, therefore it was concluded that geometry of the complex has profound role in inhibition process. Cobalt and copper centered metal complexes were also found to be moderately active against chymotrypsin whereas the nickel and zinc complexes of the same ligand were inactive al mostly.

The thermal data of the complexes reveal that the order of the stability for metal complexes of H-QMP will be Ni(II)>Co(II)>Cu(II)>Zn(II) based on the activation parameter.

3.2 Results and discussion of CIMP and BIMP series

3.2.1 2-{(*E*)-[(4-chlorophenyl)imino]methyl}phenol (CIMP)

Yield; 75%, M.P: 93-95 ^{o}C IR analysis: 3400 (bd), 1683 (s), 1608(s), 1485(s), 1456(s), 1394(w), 1271(s), 1149(s), 1010(s), 908(w), 835(s), 813(s), 754(s), 698(s), 630(w) cm^{-1}, ^{1}H-NMR (300.13MHz, $CDCl_3$, 303k) δ = 6.9 (d, $^{3}J_{HH}$= 7.2Hz , 1H, H12), 7.04 (d, $^{3}J_{HH}$ = 7.23Hz , 1H, H15), 7.1(d, $^{3}J_{HH}$ = 7.56Hz ,1H, H14 and H13), 7.4 (d, $^{3}J_{HH}$ = 7.01Hz, 1H, H3 and H5), 7.5 (d, $^{3}J_{HH}$ = 7.25Hz , 1H, H2 andH6), 8.6 (s, Ar-HC=N), 13.0 (s, OH), ^{13}C{^{1}H}-NMR (75.47 MHz, $CDCl_3$, 303k), 117.3 (CH, C15), 119.0 (CH, C13), 119.2 (CH, C14), 122.4 (CH, C2 & C6), 129.5 (CH, C3 & C5), 132.4 (CH, C12), 133.48 (C, C4), 147.0 (C, C1), 161.1(C, C11), 162.9 (CH, Ar-HC=N), Elemental Analysis, $C_{13}H_{10}ClNO$, Calc. C: 67.39%, H: 4.35%, N: 6.05%, Exp. C: 67.90%, H: 4.30%, N: 6.57%,

3.2.2 Bis(2-{(*E*)-[(4-chlorophenyl)imino]methyl}phenolate)nickel(II) (5)

Yield; 55% M.P: 248-250 ^{o}C, IR analysis: 3303(bd), 1611(s), 1531(s), 1466(s), 1444(s),1418(s), 1349(s), 1330(s), 1258(s), 1220(s), 1188(s), 1142(s), 1142(s), 1116(s), 1023(w), 976(s), 938(s), 901(s), 862(w), 812(s), 806(s), 759(s), 748(s), 721(s), 698(s), 667(s) cm^{-1}, λ_{max} = 710 nm (ε= 27.7M^{-1}cm^{-1}, $^{1}A_{1g}\rightarrow{}^{1}A_{2g}$), μ_{eff}: 2.03 B.M. Elemental Analysis, $C_{26}H_{18}Cl_2N_2NiO_2$, Calc. C: 60.05%, H: 3.49%, N: 5.39% Ni: 11.29%, MS-ES^{+}: *m/z* (%) = 540.9997 (100%) [$C_{26}H_{18}Cl_2N_2NiO_2$+Na],

3.2.3 Bis(2-{(*E*)-[(4-chlorophenyl)imino]methyl}phenolate)cobalt(II) (6)

Yield; 75% M.P: 270-272 ^{o}C, IR analysis: 1606(s), 1537(s), 1485(s), 1463(s), 1440(s), 1379(s), 1325(s), 1178(s), 1149(s), 1126(s), 1089(s), 1012(s), 979(s), 925(s), 856(s), 831(s), 759(s), 696(s) cm^{-1}, λ_{max}= 890 nm (ε = 16.6 M^{-1}cm^{-1}, $^{2}A_{2g}\rightarrow{}^{2}B_{1g}$), μ_{eff}: 3.23 B.M. Elemental analysis, $C_{26}H_{18}Cl_2CoN_2O_2$, Calc. C: 60.02%, H: 3.49%, Co: 11.33% N: 5.38%, MS-ES^{+}: *m/z* (%) = 519.0075 (100%) [$C_{26}H_{18}Cl_2CoN_2O_2^{+}$],

3.2.4 Bis(2-{(*E*)-[(4-chlorophenyl)imino]methyl}phenolate)copper(II) (7)

Yield; 68%, M.P: 219-220^{o}C, IR analysis: 1598(s), 1573(s), 1519(s), 1489(s), 1431(s), 1390(s), 1348(s), 1321(s), 1300(s), 1249(s), 1211(w), 1170(s), 1147(s), 1126(s), 1093(s), 1029(s), 1006(s), 975(s), 923(s), 852(s), 827(s), 756(s), 696(s), 610(s) cm^{-1}, λ_{max}= 690 nm (ε = 220.6 $M^{-1}cm^{-1}$ $d_Z^2 \rightarrow d_{X^2-Y^2}$), μ_{eff}: 1.89 B.M. Elemental Analysis, $C_{26}H_{18}Cl_2CuN_2O_2$, Calc. C: 59.49%, H: 3.46%, Cu: 12.11%, N: 5.34%, MS-ES$^+$: *m/z* (%) = 545.9939 (100%) [$C_{26}H_{18}CuCl_2N_2O_2$+Na],

3.2.5 Bis(2-{(*E*)-[(4-chlorophenyl)imino]methyl}phenolate)zinc(II) (8)

Yield; 55%, M.Pt. 278-280^{o}C, IR analysis: 1598(s), 1581(s), 1521(s), 1460(s), 1435(s), 1394(s), 1348(s), 1325(s), 1249(s), 1170(s), 1147(s), 1093(s), 1029(s), 1006(s), 923(s), 827(s), 786(s), 756(s), 698(s), 590(s) cm^{-1}, Elemental analysis, $C_{26}H_{18}Cl_2N_2O_2Zn$, Calc. C: 59.28%, H: 3.44%, N: 5.32%, Zn: 12.42%, MS-ES$^+$: *m/z* (%) = 524.0063 (80%) [$C_{26}H_{18}Cl_2N_2O_2Zn^+$],

3.2.6 2-{(*E*)-[(4-bromophenyl)imino]methyl}phenol (BIMP)

Yield; 80%, M.P: 90-92 ^{o}C, IR analysis: 3400(bd), 1606(s), 1568(s), 1481(s), 1409(s), 1359(s), 1280(s), 1184(s), 1151(s), 1107(s), 1006(s), 983(s), 910(s), 852(s), 752(s), 678(s) cm^{-1}. ^{1}H-NMR(300.13 MHz, $CDCl_3$, 303k) δ = 6.9 (d, $^3J_{HH}$= 7.01Hz , 1H, H12), 7.03 (d, $^3J_{HH}$ =7.2Hz , 1H, H15), 7.1(d, $^3J_{HH}$ = 7.34Hz,1H, H14 and H13), 7.4 (d, $^3J_{HH}$ = 6.8Hz, 1H, H3 and H5), 7.5 (d, $^3J_{HH}$ = 7.9Hz, 1H, H2 andH6), 8.6 (s, Ar-<u>H</u>C=N), 13.0 (s, OH), ^{13}C{^{1}H}-NMR (75.47 MHz, $CDCl_3$, 303k), 117.3 (CH, C3 & C5), (CH, C15), 119.0 (CH, C13), 119.2 (CH, C14), 122.8 (CH, C2 & C6), 132.4 (CH, C12), 133.5 (C, C4), 147.4 (C, C1), 161.1(C, C11), 162.9 (CH, Ar-<u>HC</u>=N).Elemental Analysis, $C_{13}H_{10}BrNO$, Calc. C: 56.55%, H: 3.65%, N: 5.07%,

3.2.7 Bis(2-{(*E*)-[(4-bromophenyl)imino]methyl}phenolate)nickel(II) (9)

Yield; 83%, M.P: 100-102 ^{o}C, IR analysis: 1611(s), 1531(s), 1466(s), 1444(s),1418(s), 1349(s), 1330(s), 1258(s), 1220(s), 1188(s), 1142(s), 1142(s), 1116(s), 1023(w), 976(s), 938(s), 901(s),

862(w), 812(s), 806(s), 759(s), 748(s), 721(s), 698(s), 667(s) cm^{-1}, λ_{max}= 890 nm (ε = 16.6 $M^{-1}cm^{-1}$, $^2A_{2g} \rightarrow {}^2B_{1g}$), μ_{eff}: 1.98 B.M. Elemental analysis, $C_{26}H_{18}Br_2N_2NiO_2$, Calc. C: 51.28%, H: 2.98%, N: 4.60%, Ni: 9.64%, *m/z* (%) = 605.5830 (100%) $[C_{26}H_{18}Cl_2N_2NiO_2^+]$,

3.2.8 Bis(2-{(*E*)-[(4-bromophenyl)imino]methyl}phenolate)cobalt(II) (10)

Yield; 75%, M.P: 230-232 ^oC, IR analysis: 1683 (w), 1653(s), 1604(s), 1533(s), 1483(w), 1463(s), 1446(s), 1379(s), 1348(s), 1327(s), 1253, 1180(s), 1149(s), 1072(s), 1010(s), 925(s), 856(s), 831(s), 761(s), 711(s), 678(s) cm^{-1}, λ_{max}= 890 nm (ε = 16.6 $M^{-1}cm^{-1}$, $^2A_{2g} \rightarrow {}^2B_{1g}$), μ_{eff}: 4.91 B.M. Elemental analysis, $C_{26}H_{18}Br_2CoN_2O_2$, C: 51.26%, H: 2.98%, Co: 9.67%, N: 4.60%, *m/z* (%) = 606.7541 (100%) $[C_{26}H_{18}Cl_2CoN_2O_2^+]$,

3.2.9 Bis(2-{(*E*)-[(4-bromophenyl)imino]methyl}phenolate)copper(II) (11)

Yield; 71%, M.P: 276-278 ^oC, IR analysis:1597(s), 1570(s), 1521(s), 1490(s), 1460(s), 1429(s), 1388(s), 1348(s), 1321(s), 1249(s), 1209(s), 1170(s), 1147(s), 1126(s), 1078(s), 1029(s), 1002(s), 975(s), 925(s), 852(s), 823(s), 786(s), 756(s), 677(s) cm^{-1}. λ_{max}= 690 nm (ε = 220.6 $M^{-1}cm^{-1}$ $d_Z^2 \rightarrow d_{X^2-Y^2}$), μ_{eff}: 2.3 B.M. Elemental analysis, $C_{26}H_{18}Br_2CuN_2O_2$, Calc. C: 50.88%, H: 2.96%, Cu: 10.35%, N: 4.56%, *m/z* (%) = 611.1259 (90%) $[C_{26}H_{18}Br_2CuN_2O_2+H]^+$,

3.2.9 Bis(2-{(*E*)-[(4-bromophenyl)imino]methyl}phenolate)zinc(II) (12)

Yield; 45%, M.P: 278-280 ^oC IR analysis: 1595(w), 1523(w), 1460(s), 1436(s), 1394(s), 1325(w), 1301(w), 1170(w), 1147(s), 1078(w), 983(w), 923(w), 825(w), 758(s), 667(s), 634(s) cm^{-1}, Elemental analysis, $C_{26}H_{18}Br_2N_2O_2Zn$, Calc. C: 50.72%, H: 2.95%, N: 4.55%, Zn: 10.62%, *m/z* (%) = 611.3404 (100%) $[C_{26}H_{18}Br_2N_2O_2Zn^+]$,

3.2.10 Analytical and spectroscopic characterization

Schiff base of the pharmacologically important salicyldehyde were prepared by condensing one equivalent of 4-chloro or bromo substituted anilines with one equivalent of the

aldehyde. The two ligands were isolated in 75-80% yields. The uncorrected melting points for both the ligands were found to be in the range of 90-95 ^{o}C. Both these Schiff base ligands were reacted with transition metal ions like Co(II), Ni(II), Cu(II) and Zn(II) in 2:1 equivalent ratios and obtained their corresponding metal complexes with composition $[M(L_{(1or\ 2)})_2]$ as shown in scheme 3.7.

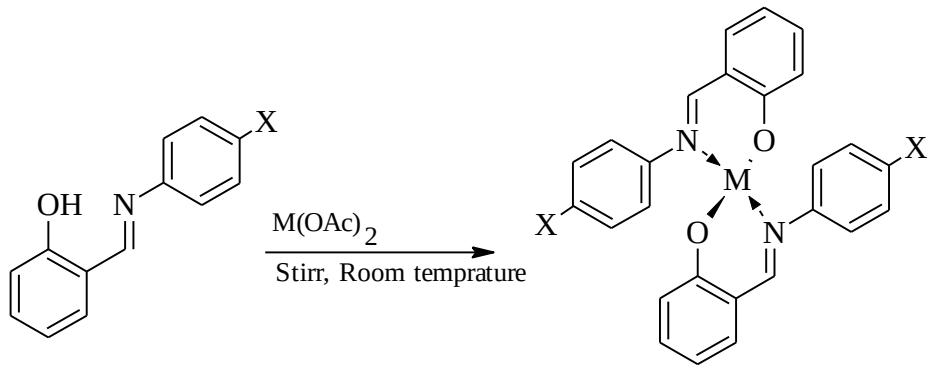

Where X = Cl-, Br- and M = Co, Ni, Cu and Zn

Scheme 3.7 Metal complexes of the Schiff bases BIMP and CIMP

The two Schiff base ligands and their metal complexes were completely characterized by various characterization techniques. Elemental analysis and ES(+) mass spectral data suggest the characteristic compositions in which the metal center is surrounded by two anionic ligands. ^{1}H and ^{13}C{^{1}H}-NMR for both the Schiff base ligands were measured and all the peaks assigned unambiguously. The representative imine linkage peak was observed at 8.6 ppm in ^{1}H-NMR of both the ligands. The peak for the imine carbon is observed at 162.9 ppm in ^{13}C{^{1}H}-NMR. Rest of the splitting pattern peak values for all the protons and carbons are assigned and given. Fig.1 represents the atomic numbering scheme for the ligands. Infrared spectra for the ligands and metal complexes were measured in the region of 4000-600 cm^{-1} in relation to the structure. The infrared spectral data show the disappearance of broad hydroxyl peak in the free ligands and also

a change in the –C=N absorption frequency. Therefore it is unambiguously assigned that the skeleton of the complexes is produced by these two coordinating sites. All the complexes were found to be non-electrolyte as the values suggest which is attributed to the absence of free acetate ions.

The UV-visible spectra of compounds **5, 7, 9,** and **11** were measured in spectrophotometric grade ethanol within the region of 400-800 nm whereas these were measured in spectrophotometric grade within the range of 400-1000 nm for **6** and **8** respectively. **5** and **9** compounds show the same trend of absorption which was assigned to $^1A_{1g} \rightarrow {}^1A_{2g}$ square planar transition, whereas the other absorption transitions $^1A_1g \rightarrow {}^1B_1g$ and $^1A_1g \rightarrow Eg$ were considered to be buried in the same $^1A_{1g} \rightarrow {}^1A_{2g}$ transition. Similarly for **6** and **10** the absorption was assigned to the transition $^2A_{2g} \rightarrow {}^2B_{1g}$ for C_{2v} symmetry. In case of copper as may be seen by looking into the absorption band in **7** and **11**, the transition band is assigned to $d_Z^2 \rightarrow d_{X^2-Y^2}$. In all of the compounds the transitions were assigned as ligand to metal charge transfer (LMCT) transitions.

3.2.11 Enzyme inhibitory studies

The metal complexes have been extensively used as therapeutics in many physiological disorders. Bismuth complexes is one of them widely used for the treatment of peptic ulcers and *Helicobacter pylor*i infections as urease inhibitors [15]. Bismuth has exhibited many side effect such as darkening of tongue, vomiting, diarrhea, dizziness. To overcome these side effects we have synthesized various metal complexes of Schiff-base and they were checked for their potential inhibition against urease enzyme and the results are shown in table 3.7. The most interesting and excellent activity were shown by Cu-complexes with both ligands CIMP and BIMP which reveal that Cu based complexes of both series will be excellent in this therapy. The Cu-complex of first series ($[Cu(CIMP)_2]$) have IC_{50} 10.66±0.19 while the Cu-complex of second

series ([Cu(BIMP)$_2$] have IC_{50} 5±0.047 which are two and four time more better than our standard thiourea (IC_{50} 21±0.011) the results are in table 3.7. As we know that α-chymotrypsin is also involved in ulcer healing [16] so, we subjected the same complexes to the α-chymotrypsin inhibitory activity. Bare Schiff-base ligands were found to be inactive to moderately active in urease and α-chymotrypsin, respectively. Only copper complexes of both the ligands showed inhibition towards urease enzyme. Neither ligand nor their complexes found to be inhibiting acetylcholinesterase (AChE) and butyrylcholinesterase (BChE) enzymes. The results are shown in table 3.7.

3.2.12 Antimicrobial activities

The ligands CIMP and BIMP and their corresponding divalent metal complexes were studied for their antimicrobial activities against Gram positive bacteria *Bacillus atrophaeus*, *Bacillus subtilis*, *Staphylococcus aureus,* Gram negative bacteria *Klebsiella pneumoniae*, *Salmonella typhus*, *Pseudomonas aeruginosa*, *Escherichia coli*, *Agrobacterium tumefaciens*, *Erwinia carotovora,* fungal Strain *Candida albican*. The table 3.8 enlists the results, revealing that metal complexes are more active than the neat ligand but the activities are lower than the standard drugs used. Compound 6 was found to be more active than the other metal complexes of the CIMP series which may be attributed to the copper electronic effects and also the distortion created in the geometry. Compound 8 also show good results against *Escherichia coli* and *Agrobacterium tumifaciens*. The other compounds of the series are either weakly active or do not show any activity at all. In the BIMP series again the results are good for the copper and zinc based metal complexes like the CIMP but weaker in activity than **7** and **8**. Compounds **9** and **10** are showing very low activities.

Table 3.7: Enzyme inhibitory efficacy of the Schiff base and their metal complexes

Compound	Urease (IC_{50} ± S.E.M) µM	α-Chymotrypsin (IC_{50} ± S.E.M) µM	Acetyl cholinesterase (IC_{50} ± S.E.M) µM	Butyrylcholinesterase (IC_{50} ± S.E.M) µM
CIMP	NA	305.04± 3.24	NA	NA
5	NA	NA	NA	NA
6	NA	NA	NA	NA
7	10.66±0.19	NA	NA	NA
8	NA	NA	NA	NA
BIMP	NA	330.55± 1.60	NA	NA
9	NA	NA	NA	NA
10	NA	NA	NA	NA
11	5.0±0.05	NA	NA	NA
12	NA	NA	NA	NA
Thiourea[a]	21± 0.011	-	-	-
Chymostatin[b]	-	5.71± 0.13	-	-
Galanthamine			0.5±0.01	8.5±0.5

NA = not active, i.e., % of inhibition is less than 50% at 500 µM; S.E.M = Standard Error of Mean;

[a] **Standard inhibitor of urease;** [b] **Standard inhibitor of α-chymotrypsin**

Table 3.8 In Vitro antimicrobial activities of CIMP and BIMP and its metal complexes against different animal and plant pathogens

Compounds	*Bacillus atrophaeus (cm)*	*Bacillus subtilis (cm)*	*Klebsiella pneumoniae (cm)*	*Salmonella typhus (cm)*	*Pseudomonas aeruginosa (cm)*	*Escherichia coli (cm)*	*Staphylococcus aureus (cm)*	*Candida albican (cm)*	*Agrobacterium tumefaciens (cm)*	*Erwinia carotovora (cm)*
CIMP	1	1.1	---	---	1.0	---	1.1	1.0	1.0	1.1
5	1.4	2.2	2.6	2	1.5	1.4	2.1	2.5	2.6	1.9
6	3.0	2.8	3.6	2.4	2.0	2.4	1.7	2.5	2.6	1.8
7	1.9	2.1	---	---	1.2	---	2.6	1.8	1.6	1.2
8	2.6	2.6	1.4	1.4	2.1	3.2	2.1	1.9	3.2	1.7
BIMP	0.3	0.6	---	1.2	1.1	0.9	---	1.0	1.0	---
9	1.2	1.1	1.7	2.1	2.0	0.7	---	1.3	1.1	1.2
10	---	---	---	1.7	1.3	1.1	0.8	0.2	1.1	---
11	2.2	2.4	1.1	1.5	---	1.7	1.7	1.3	1.0	1.3
12	2.9	3.4	3.0	3.2	2.0	2.1	2.1	1.5	1.0	2.1
Standard	2.5	2.6	2.9	4.2	3.6	3.8	3.4	1.6	1.5	2.6

Gram positive bacteria: *Bacillus atrophaeus*, *Bacillus subtilis*, *Staphylococcus aureus*, standard used was erythromycin in 6 µM

Gram negative bacteria: *Klebsiella pneumoniae*, *Salmonella typhus*, *Pseudomonas aeruginosa*, *Escherichia coli*, *Agrobacterium tumefaciens*, *Erwinia carotovora*, standard used was ciprofloxacin in 6 µM

Fungal Strain: *Candida albican*, standard used was clothrimazol in 6 µM

3.2.13 Thermodynamics and Thermal studies

Thermal degradation of Schiff base ligands CIMP and BIMP and their corresponding metal complexes were studied in the range of 30-1000 ^{o}C except **5** and **6** metal complexes, studied up to 1200 ^{o}C. Table 3.9 show the temperature at which maximum loss of the species under study occurred, this temperature is called temperature at maximum slope and represented by Ts. Activation energies of all the compounds were calculated using Horrowitz and Mettzger method of calculations. From this data order of degradation was calculated using the relationship between reaction order and concentration at maximum slope [12]. Thermodynamic parameters were calculated using the relationships given in section 2.9.

Table 3.9 Thermodynamic parameters of metal complexes

Compound	**Ts in K**	**Ea, KJ/mol**	**ΔH, KJ/mol**	**$\Delta G^{\#}$, KJ/mol**	**$\Delta S^{\#}$, $Jmol^{-1}K^{-1}$**	**Order of reaction, n**
CIMP	524.9	89.09	84.72	209.71	-238.13	1
5	603	9.06	4.04	167.31	-254.19	5
6	517.6	26.95	22.64	164.89	-258.19	4
7	636.7	11.80	6.50	170.73	-257.94	∞
8	649	8.75	3.35	168.39	-254.30	∞
BIMP	543	13.00	8.48	124.73	-214.10	∞
9	837	16.89	9.93	220.19	-251.18	½
10	617	12.97	7.84	167.04	-258.03	∞
11	678	8.79	3.15	173.05	-250.59	5
12	821.8	25.26	18.42	222.04	-247.78	3

TG and DTA curves for metal complexes of both BIMP and CIMP are shown in figures 3.9, 3.10, 3.11 and 3.12 resectively. Table 3.10 depicts the species which are evolved during each thermo gravimetric step. Differential thermo gravimetric values for each thermo gravimetric step are given. By looking into table 2 it is apparent that both the Schiff base ligands are pyrolysed in a single step producing 4-halo substituted biphenol and hydrogen cyanide. Degradation starts at 190 ^{o}C in CIMP, whereas in BIMP it starts at 210 ^{o}C. The theoretical and experimental calculated weights of the moieties are similar with three DTA peaks. CIMP follow 1st order degradation kinetics whereas BIMP infinite order, clearly points to the electronic effects of the halogen groups. CIMP has 89.09 KJ/mol activation energy value, whereas the activation energy for BIMP is 13.0 KJ/mol. This type of difference can also be seen in the values of enthalpy change and Gibb's free energy change. Both the ligands have negative entropies depicting that the degradation is less favorable of the parent compounds. By observing the clear demarcated change in the values of entropy change, enthalpy change, Gibb's free energy change, activation energy and most importantly the order of the degradation it becomes apparent that chloro substituted Schiff base ligand is more stable than the bromo analog. This type of change in behavior can be observed in other properties as well. The degradation of CIMP and BIMP follow the following scheme 3.8 and 3.9 respectively:

$C_{13}H_{10}ClNO \rightarrow C_{12}H_9ClO + HCN$

Scheme 3.8 Thermal degradation of CIMP

$C_{13}H_{10}BrNO \rightarrow C_{12}H_9BrO + HCN$

Scheme 3.9 Thermal degradation of BIMP

In **5** Ts is around 603 ^{o}C which depicts the loss of 4-chlorobiphenol, produced by the fusion of two free radicals i.e. chlorobenzene free radical and hydroxybenzene free radical. This fusion is

shown by -26 DTA peak. The activation energy for **5** is 14.04KJ/mol and follow 5th order kinetics of degradation. In the first step two moles of carbon monoxide, one mole of nitrogen and hydrogen molecules along with one mole of 4-chlorobiphenol are released. The second stage starts around 400 ^{o}C and completes at 1000 ^{o}C. This stage is associated with the release of one mole of 4-chlorobiphenol moiety. Nickel oxide remains as residue. Collectively there are three DTA peaks which support the formation of three intermediate products i.e. chlorobenzene free radical, hydroxybenzene free radical and hydrogen cyanide molecule. Chlorobenzene free radical and hydroxybenzene free radical bonds together and produce 4-chlorobiphenol, whereas hydrogen cyanide is converted to carbon monoxide, hydrogen gas and nitrogen gas. The low enthalpy change, large Gibb's free energy and negative entropy depicts the stable nature of parent compounds rather the degradation products. The degradation is shown below in scheme 3.10.

$C_{26}H_{18}Cl_2N_2NiO_2 + O_2 \rightarrow C_{12}H_9ClO + 2CO + H_2 + N_2 + C_{12}H_9ClNiO$ I Stage

$C_{12}H_9ClNiO + O_2 \rightarrow C_{12}H_9ClO + NiO$ II Stage

Scheme 3.10 Thermal degradation of 5

Compound **6** degrades in three steps unlike **5**. The degradation starts around 360 ^{o}C and completes at 1000 ^{o}C. The decomposition of **6** occur around 370 ^{o}C along with the release of two moles of carbon monoxide, two moles of water and one mole of dinitrogen gas. Second stage of decomposition is associated with the release of two moles of 4-chlorobiphenol. In the third stage the decomposition of the cobalt oxide produced the residual cobalt metal by the release of oxygen molecule. First stage is associated with exothermic DTA peak at -40 and two endothermic peaks at -20 and -23. The exothermic peak represents the initiation of decomposition whereas the two shoulder peaks represent the intermediate hydrogen cyanide

which reacts with air to produce one mole each of diatomic gases of nitrogen and hydrogen and two moles of carbon monoxide. The third stage is associated with the weak exothermic peak at -58. The degradation follows the 4th order kinetics.

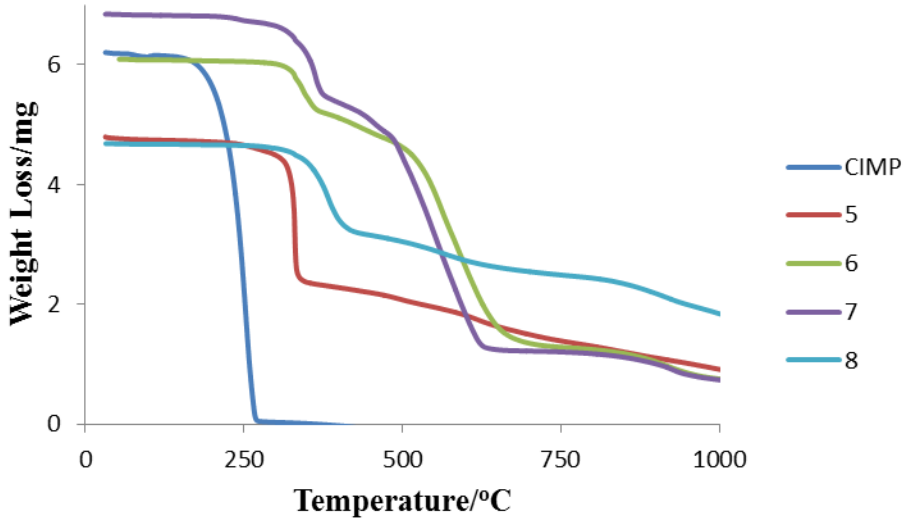

Figure 3.9. Thermogravimetric plots of CIMP and its metal complexes

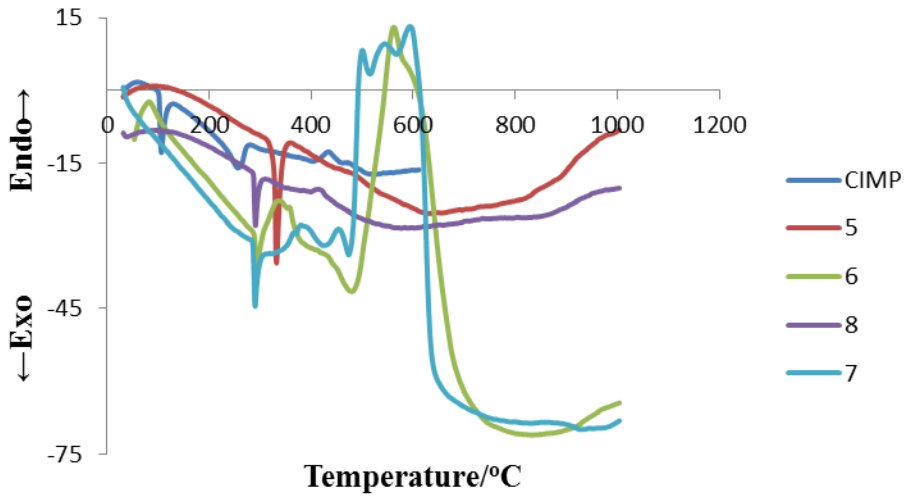

Figure 3.10. Differential thermogravimetric curves for CIMP and its metal complexes

The activation energy for the thermal degradation is also higher than **5** i.e. 27 KJ/mol. Gibb's free energy change is high, entropy is negative and almost equal to **5** but enthalpy is higher than

5 representing the stable nature of the parent compound. Thermal degradation of **6** is shown in scheme 3.11.

$C_{26}H_{18}Cl_2CoN_2O_2 + O_2 \rightarrow 2CO + 2H_2O + N_2 + C_{24}H_{18}Cl_2CoO$ I Stage

$C_{24}H_{18}Cl_2CoO + O_2 \rightarrow 2C_{12}H_9ClO + CoO$ II Stage

$CoO + 1/2O_2 \rightarrow Co\ (Res) + O_2$ III Stage

Scheme 3.11 Thermal degradation of 6

In **7** the thermal degradation starts around 280 ^oC and completes at 1000 ^oC leaving copper as residue. Thermal degradation of the compound is comprised of three stages. First stage is represented by the formation of two moles of carbon monoxide, one mole each of dihydrogen and dinitrogen. This stage show three DTA peaks, one exothermic around -38 and two shoulder endothermic peaks around -19. Second stage starts at 410 ^oC and completes around 670 ^oC with three DTA peaks. This stage is represented by the release of two moles of 4-chlorobiphenol. There is one large endothermic peak for this stage. The third stage like **6**, is comprised of the CuO degradation releasing dioxygen. There is no DTA peak for this stage. In table 3.9, 11.80 KJ/mol is the activation energy for **7**, and follow infinite order of degradation. The entropy is negative than **5** and almost equal to **6**. Similar behavior is followed in Gibb's free energy, but enthalpy change is contrasting in nature. These thermodynamic parameters reveal that copper complex of CIMP ligand is stable than its nickel and cobalt analogs. Thermal degradation for **7** is shown in the form of scheme 3.12:

$C_{26}H_{18}Cl_2CuN_2O_2 + O_2 \rightarrow 2CO + H_2 + N_2 + C_{24}H_{18}Cl_2CuO$ I Stage

$C_{24}H_{18}Cl_2CuO + O_2 \rightarrow 2C_{12}H_9ClO + CuO$ II Stage

$CuO + 1/2O_2 \rightarrow Cu\ (Res) + O_2$ III Stage

Scheme 3.12 Thermal degradation of 7

Compound **8** of the CIMP series is behaving differently than other compounds with different metal centers. Thermal degradation is completed in two steps with zinc as residue. The first stage is marked and clear, starts at almost 400 ^{o}C and completes 440 ^{o}C. In this stage two moles of carbon monoxide, two moles of dihydrogen, one mole of dinitrogen and one mole of phenol ion are produced. The second stage of thermal degradation is comprised of many encompassing steps which may be partly due to the formation of free radicals and partly because of fusion of these free radicals with each other. This stage show two DTA peaks both of them are endothermic, clearly reveal the presence of two major intermediate products. These two products are two 4-chlorobenzene free radicals and one phenolic free radical. All these may combine and rearrange to produce 4,4"-dichloro-1,1':3',1"-terphenyl-2'-ol, a stable product produced by the ortho substituting effect of phenolate ion. Compound **8** has negative entropy which is almost equal to **5**. This change in entropy value suggests that parent compound is much more favourable than the degradation. Subsequent trend in Gibb's free energy change and enthalpy change were observed. The thermal degradation of **8** follows the following scheme 3.13:

$C_{26}H_{18}Cl_2N_2O_2Zn + O_2 \rightarrow 2CO + 2H_2 + N_2 + C_6H_6O + C_{18}H_{12}Cl_2OZn$ I Stage

$C_{18}H_{12}Cl_2OZn \rightarrow C_{18}H_{12}Cl_2O + Zn$ (Residue) II Stage

Scheme 3.13 Thermal degradation of 8

Overall based upon the Td values it become clear that Cu(II)>Co(II)>Ni(II)<Zn(II) whereas based on the activation energies it is clear that $Ea_6 > Ea_5 > Ea_7 > Ea_8$.

Compound **9** starts decomposition at around 220^{o}C which subsequently completes at 610 ^{o}C. The overall decomposition takes two steps to complete. In the first step two moles of water molecules and two moles of hydrogen cyanide molecules from the Schiff base linkage are produced. Only one endothermic peak is observed in this stage due to the melting of the parent compound. The

second and final stage of pyrolysis is comprised of production of two moles of 4-bromobiphenolate ion. This stage of decomposition starts after the end of the first stage and completes at 610 ^{o}C. This stage of decomposition is comprised of small encompassing steps due to the intermediate free radicals formation. These free radicals are 4-bromobenzene and 2-hyroxybenzene ion. They bond together to produce the 4-bromobiphenolate ion and evaporates without further decomposition leaving behind residue in the form of nickel. This free radical reaction is represented by the appearance of a huge endothermic DTA peak at 12.

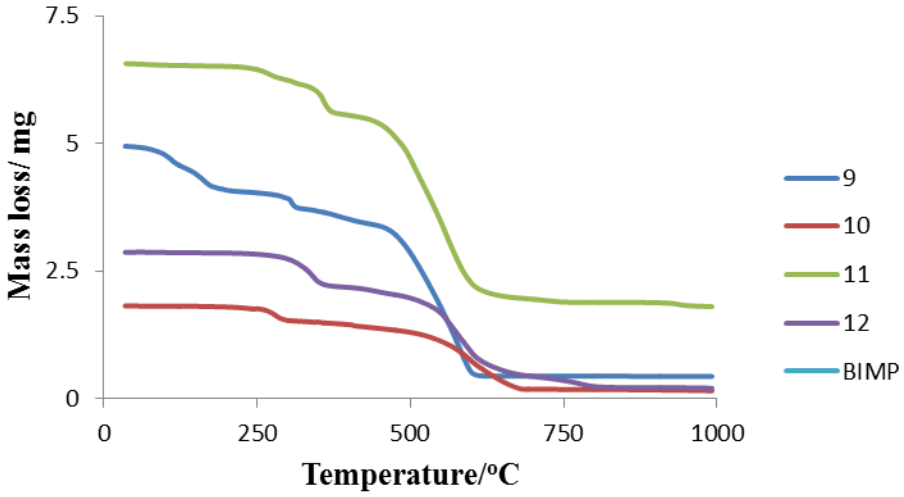

Figure 3.11. Thermogravimetric plots of BIMP and its metal complexes

Table 3.9 depicts the ½ order of reaction with comparative activation energy with its close analog of CIMP nickel complex. The enthalpy change is smaller whereas the Gibb's free energy change is large with very negative entropy change. The degradation occurs as shown in scheme 3.14:

$C_{26}H_{18}Br_2N_2NiO_2 + O_2 \rightarrow 2H_2O + 2HCN + C_{24}H_{12}Br_2NiO_2$ I Stage

$C_{24}H_{12}Br_2NiO_2 \rightarrow C_{24}H_{12}Br_2O_2 + Ni$ (Residue) II Stage

Scheme 3.14 Thermal degradation of 9

Compound **10** following the same trend of its analogs, degrades in two steps. The first step starting at 240 ^{o}C completes 380 ^{o}C with the release of two moles of carbon monoxide, two mole of dihydrogen and one mole of dinitrogen gases. This stage is supported by the appearance of one endothermic DTA peak. The second stage starts at 480 ^{o}C and completes at 640 ^{o}C, releasing the same 4-bromobiphenolate ion with a huge exothermic peak of 40µV. the residue was calculated to be Co_2O_3. The pyrolysis follows infinite order of kinetics and 4.06 KJ/mol of activation energy. The rest parameters are almost following the same trend. The stepwise degradation of **10** is shown below in scheme 3.15:

$C_{26}H_{18}Br_2CoN_2O_2 + O_2 \rightarrow 2CO + 2H_2 + N_2 + C_{24}H_{12}Br_2CoO_2$ I Stage

$C_{24}H_{12}Br_2CoO_2 + O_2 \rightarrow C_{24}H_{12}Br_2O_2 + Co_2O_3$ (Residue) II Stage

Scheme 3.15 Thermal degradation of 10

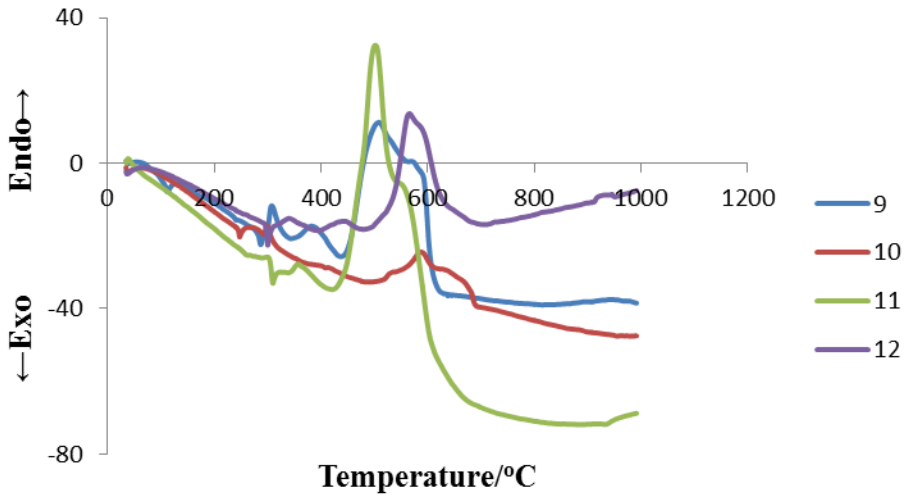

Figure 3.12. Differential thermogravimetric curves for BIMP and its metal complexes

Compounds **11** and **12** are following the same trend of degradation with the difference in the starting and ending temperature points. The first step in compound **11** is comprised of evolution of two moles carbon monoxide, and dihydrogen molecules, one mole of dinitrogen whereas this

stage in **12** is marked with the release of two moles of hydrogen cyanide formation along with the release of one mole of chloroform molecule came from solvent of recrystallization. Both the compounds show endothermic DTA peaks for this stage. Stage two in both the compounds is identical with the same parental difference of temperature limits. This stage starts at 280 ^{o}C in **11** and at 360 ^{o}C in **12** and ends at 640 ^{o}C in **11** and 800 ^{o}C in **12**. The moiety evolved during this stage is the same 4-bromobiphenolate ion produced by the fusion of the two free radicals. Both these compounds show of -26 and 40 µV in the DTA graph. In **11** the residue remaining was assigned to be copper oxide whereas in **12** the residue was found out to be zinc metal. The former is following 5th order kinetics whereas the latter 3rd order kinetics. The activation energy for **12** is also very high than that of **11**. The rest of the thermodynamic parameters, calculated, are comparable with each other. The degradation for **11** and **12** are shown in scheme 3.16 and 3.17 respectively.

$C_{26}H_{18}Br_2CuN_2O_2 + O_2 \rightarrow 2CO + 2H_2 + N_2 + C_{24}H_{12}Br_2CuO_2$ I Stage

$C_{24}H_{12}Br_2CuO_2 + O_2 \rightarrow C_{24}H_{12}Br_2O_2 + CuO$ (Residue) II Stage

Scheme 3.16 Thermal degradation of 11

$C_{26}H_{18}Br_2N_2O_2Zn.CHCl_3 + O_2 \rightarrow 2HCN + CHCl_3 + C_{24}H_{12}Br_2O_2Zn$ I Stage

$C_{24}H_{12}Br_2O_2Zn \rightarrow C_{24}H_{12}Br_2O_2 + Zn$ (Residue) II Stage

Scheme 3.17 Thermal degradation of 12

From the thermal degradation data of the series of meta complexes of BIMP, it becomes clear that the order of stability on the basis of Td is Co(II)>Zn(II)>Cu(II)>Ni(II) whereas the order of decreasing activation energy is $Ea_{12}>Ea_9>Ea_{10}>Ea_{11}$.

Table 3.10: Thermo analytical results of CIMP and BIMP and its complexes

Compound	TG Temp. range/ ^{o}C	Stage	Mass loss		DTA	Moiety evolved
			% Calc.	% Found		
CIMP	30-280	I	100	100	(-)12.3, (-)15.14, (-)13.5	HCN, $C_{12}H_9ClO$
5	30-390	I	55.8	55.6	(-)36, (+)2	$C_{12}H_9ClO$, 2CO, H_2, N_2
	390-1000	II	39.1	38.21	(-)26	$C_{12}H_9ClO$
	>1000	Res	11.1	10.72	---	NiO
6	30-410	I	22.9	22.5	(-)40, (-)23, (-)20	2CO, $2H_2O$, N_2
	410-670	II	78.6	70.4	(-)19.0, (+)18, (+)20, (+)23	2 $C_{12}H_9ClO$
	670-980	III	5.8	6.1	(-)58	O_2
	>980	Res	11.2	11.0	---	Co
7	30-360	I	16.7	17.8	(-)2, (-)34, (-)18	2CO, H_2, N_2
	360-660	II	77.8	73.8	(+)20	2 $C_{12}H_9ClO$
	660-910	III	6.0	6.5	(-)59	O_2
	>910	Res	11.9	11.5	---	Cu
8	30-430	I	34.1	34.2	(-)8, (-)28	2CO, H_2, N_2, C_6H_6O

	430-970	II	61.9	59.6	(-)18, (-)29	$C_{17}H_{12}Cl_2O$
	>970	Res	12.2	9.0	---	Zn
BIMP	30-880				(-)5.4, (-)4.5, (-)8.5, (-)7.4, (-)6, (-)9.8	HCN, $C_{12}H_9BrO$
9	30-220	I	15.4	16.0	(-)8	$2H_2O$, 2HCN
	220-480	II	80.2	79.8	(-)23, (-)21, (-)26	2 $C_{12}H_9BrO$
	>480	Res	9.5	9.1	(+)12	Ni
10	30-380	I	14.2	15.0	(-)28	2CO, N_2, H_2
	380-960	II	82.1	80.3	(+)43	$2C_{12}H_9BrO$
	>960	Res	28.9	27.5	---	Co_2O_3
11	30-380	I	15.0	17.1	(-)2, (-)20, (-)18	2CO, N_2, H_2
	380-700	II	80.7	76.8	(-)36, (+)24	$2C_{12}H_9BrO$
	>700	Res	13.4	14.9	---	CuO
12	30-380	I	24.1	23.1	(-)2, (-)24	CH_3Cl, 2HCN
	380-800	II	78.4	75.3	(-)18, (-)17, (+)14, (-)14	$2C_6H_5Br$, $2C_6H_6O$
	>800	Res	10.5	9.8	---	Zn

3.2.14 Conclusion

Metal complexes of the two very important Schiff base ligands were prepared following different approaches of the synthesis. All the metal complexes were assigned the square planar geometries

basing on the results obtained from different analytical and spectroscopic measurements. All the compounds were tested for their inhibiting activities for enzymes like urease, α-chymotrypsin, acetyl cholinesterase, and butyrylcholinesterase. Both the ligands CIMP and BIMP were found to be active against α-chymotrypsin whereas their copper complexes were found to be active against urease. The rest of metal complexes were found to be inactive against any of the tested enzyme. The unique nature of the copper square planar complexes may be due to the interactions of the complex with carbonyl group of the glycine located on enzyme. This interaction can be established due to the geometric strain in the copper complex i.e. the complex may either attain square pyramidal or octahedral geometry which is much more favorable than the distorted square planar geometry. All of the compounds are inactive against acetyl cholinesterase and butyrylcholinesterase. Overall based upon the Td values it become clear that the order of stability for the complexes of CIMP series is Cu(II)>Co(II)>Ni(II)<Zn(II) whereas based on the activation energies it is clear that Ea_6>Ea_5>Ea_7>Ea_8. From the thermal degradation data of the series of metal complexes of BIMP, it becomes clear that the order of stability on the basis of Td is Co(II)>Zn(II)>Cu(II)>Ni(II) whereas the order of decreasing activation energy is Ea_{12}>Ea_9>Ea_{10}>Ea_{11}.

3.3 Results and discussion of H-HMAC series

3.3.1 Synthesis of [1-({[(*Z*)-(2-hydroxynaphthalen-1-yl)methylidene]amino}methyl)cyclohexyl]acetic acid (H-HMAC)

Yield: 1.2 g, 55%, D. pt: 209 ^{o}C, Elemental Analysis, $C_{20}H_{23}NO_3$, Calc. C: 73.82%, H: 7.12%, N: 4.30%, Exp. C: 73.80%, H: 7.13%, N: 4.43%, IR analysis. 3400(bd), 2922(s), 2868(w), 1683(m), 1635(s), 1595(w), 1544(s), 1506(m), 1463(w), 1402(m), 1319(s), 1240(s),1180(s), 1139(s), 1004(s), 927(s), 825(s), 740(s), 732(s), 680(s), 648(s) cm^{-1}, ^{1}H-NMR (400.23 MHz, d^{6}-DMSO, 303k): δ = 14.28 (s, 2H, Ar-O<u>H</u>, COO<u>H</u>), 9.10 (s, 1H, -<u>H</u>C=N), 8.18 (m, 1H, H12), 8.05 (d, $^{3}J_{HH}$ = 8, 1H, H13), 7.95 (d, $^{3}J_{HH}$ = 7, 1H, H15), 7.72 (d, $^{3}J_{HH}$ = 8, 1H, H16), 7.63(d, $^{3}J_{HH}$ = 8.05, 1H, H17), 7.50 (m, 1H, H17), 6.72(d, $^{3}J_{HH}$ = 7.98, 1H, H18), 5.64, 5.49, 3.72(s, 2H, H7), 3.61(s, 2H, H20), 3.58 (m, 2H, H6), 2.98 (m, 2H, H1) , 2.39 (m, 2H, H3 and H5), 1.98(m, 2H, H4) ppm, ^{13}C{^{1}H}-NMR (150.9 MHz, d^{6}-DMSO, 303k), 190.14 (C, C21), 177.62 (C, C11), 159.75 (H<u>C</u>=N-, C9), 137.07 (CH, C12), 136.42 (CH, C13), 134.21(C, C10), 128.82(C, C14 and C19), 127.9 (CH, C18), 125.70 (CH, C17), 125.05(CH, C16), 122.12 (CH, C15), 105.55 (CH_2, C7), 36.44 (CH_2, C20), 36.01 (C, C1) 32.94 (CH_2, C2 and C6), 25.49 (CH_2, C3 and C5), 20.78(CH_2, C4) ppm, EI-MS: *m/z* (%) 326.1762 (100%) $[C_{20}H_{23}NO_3 + H]^{+}$, ∧m = 123 μS.

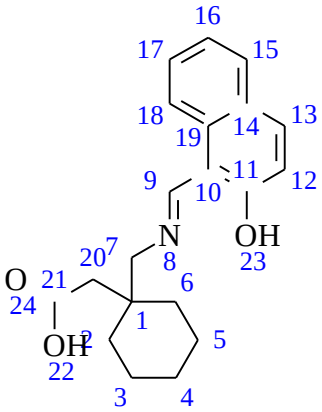

Scheme 3.18 Atoms numbering for NMR assignment

3.3.2 Synthesis of transition metal complexes [$M(L)_2$] where M = Co, Ni, Cu and Zn (II) acetates

3.3.3Bis[1-({[(*Z*)-(2-hydroxynaphthalen-1-yl)methylidene]amino}methyl)cyclohexyl]aceticacid]nickel(II) (13)

Yield: 87%, D. pt: 240 ^{o}C, Elemental Analysis, $C_{40}H_{44}N_2NiO_6$, Calc. C: 67.91%, H: 6.27%, N: 3.96%, Ni: 8.30%, Exp. C: 67.11%, H: 7.21%, N: 4.26%, Ni: 8.10%, IR analysis. 3400(bd), 2922(s), 2848(m), 1581(s), 1456(s), 1390(s), 1184(s), 1035(m), 952(w), 821(s), 742(s), 653(s) cm^{-1}. λ_{max}= 480 nm (ε = 112.6 $M^{-1}cm^{-1}$, $^3T_1$ (F) $\rightarrow$$^4T_1$ (P), μ_{eff}: 2.89 B.M. EI-MS: *m/z* (%) 382.0953 (10%) $[C_{20}H_{22}NNiO_3]^+$, 706.2547 (91%) $[C_{40}H_{44}N_2NiO_6]^+$, $\wedge_m$ = 212µS.

3.3.4Bis[1-({[(*Z*)-(2-hydroxynaphthalen-1-yl)methylidene]amino}methyl)cyclohexyl]aceticacid]cobalt(II) (14)

Yield: 56%, D. pt: 196 ^{o}C, Elemental Analysis, $C_{40}H_{44}CoN_2O_6$ C: 67.88%, H: 6.27%, Co: 8.33%, N: 3.96%, Exp. C: 68.08%, H: 6.77%, Co: 8.67%, N: 3.86%, IR analysis. 3400(bd), 2927(s), 2854(m), 1635(s), 1544(s), 1456(s), 1357(s), 1315(m), 1261(w), 1193(m), 1010(w), 833(s), 744(s) cm^{-1}. λ_{max}= 520nm, 635nm [ε = 102 and 234.6 $M^{-1}cm^{-1}$, $^4A_2(F)\rightarrow{}^4T_1(p)$, $^4A_2(F)\rightarrow{}^4T_1(F)$, $^4A_2$ (F) $\rightarrow$$^4A_1$ (F)], μ_{eff} = 4.21 B.M. EI-MS: *m/z* (%) 707.2525 (100%) $[C_{40}H_{44}CoN_2O_6]^+$, $\wedge_m$ = 243 µS.

3.3.5Bis[1-({[(*Z*)-(2-hydroxynaphthalen-1-yl)methylidene]amino}methyl)cyclohexyl]aceticacid]copper(II) (15).

Yield: 67%, D. pt: 205 ^{o}C, Elemental Analysis, $C_{40}H_{44}CuN_2O_6$, C: 67.44%, H:6.23%, Cu: 8.92%, N:3.93%, Exp. C: 67.98%, H: 6.66%, Cu: 8.54%, N: 3.87%, IR analysis, 3400(bd), 2927(s), 2854(w), 1635(s), 1544(s), 1456(m), 1357(s), 1315(s), 1261(w), 1193(m), 1010(w),

833(s), 744(s), 620(s) cm^{-1}, λ_{max}= 730nm (ε = 98.7 $M^{-1}cm^{-1}$, Eg→T_2g), μ_{eff} =1.73 B.M. EI-MS: *m/z* (%) 711.2495 (60%) $[C_{40}H_{44}CuN_2O_6]^+$, $\wedge_m$ = 232 µS.

3.3.6Bis[1-({[(*Z*)-(2-hydroxynaphthalen-1-yl)methylidene]amino}methyl)cyclohexyl]aceticacid]zinc(II) (16)

Yield: 53%, D. pt: 234 ^oC, Elemental Analysis, $C_{40}H_{44}N_2O_6Zn$, C: 67.27%, H: 6.21%, N: 3.92%, Zn: 9.16%, Exp. C: 66.98%, H: 6.78%, N: 3.22%, Zn: 9.98%, IR analysis. 3633(w), 2926(s), 2839(m),1585(s), 1541(s), 1463(m), 1417(s), 1367(s), 1307(s), 1188(s), 1138(s), 1037(w), 979(s), 837(s), 746(s), 692(s), 659(s) cm^{-1}, ^{1}H-NMR (400.23 MHz, d^6-DMSO, 303k): δ = 14.28 (s, 1H, COO<u>H</u>), 12.4 (s, 1H, -<u>H</u>C=N), 8.18 (m, 1H, H12), 8.05 (d, $^3J_{HH}$ = 8, 1H, H13), 7.95 (d, $^3J_{HH}$ = 7, 1H, H15), 7.72 (d, $^3J_{HH}$ = 8, 1H, H16), 7.63(d, $^3J_{HH}$ = 8.05, 1H, H17), 7.50 (m, 1H, H17), 6.72(d, $^3J_{HH}$ = 7.98, 1H, H18), 5.64, 5.49, 3.72(s, 2H, H7), 3.61(s, 2H, H20), 3.58 (m, 2H, H6), 2.98 (m, 2H, H1) , 2.39 (m, 2H, H3 and H5), 1.98(m, 2H, H4) ppm, EI-MS: *m/z* (%) 735.2389 (10%) $[C_{40}H_{44}N_2O_6Zn+Na]^+$, 326.1806 (5%) $[C_{20}H_{23}NO_3 + H]^+$ 712.2485 (45%) $[C_{40}H_{44}N_2O_6Zn]^+$, $\wedge_m$: 202 µS.

3.3.7 Analytical and spectroscopic characterization

Keeping in view the importance of gabapentene, it was reacted with 2-hydroxynaphthaldehyde to yield the novel Schiff base ligand which was fully characterized by various analytical and spectroscopic techniques which include EI^+-MS and elemental analysis, ^{1}H, ^{13}C{^{1}H}-NMR and most importantly by single crystal diffraction study. The EI^+-MS and elemental analysis confirm the composition of the compound, which is further approved by the ^{1}H, ^{13}C{^{1}H}-NMR studies.

^{1}H and ^{13}C NMR of the ligand show the characteristic peak at 9.2 ppm whereas the –OH group come at 14.3 ppm. Rest of the NMR spectrum shows the respective peaks for each and every

proton. Similarly ^{13}C-NMR shows the carboxyl carbon at 177 ppm and the imine carbon fall at 159 ppm. Respective aromatic and non-aromatic peaks are unambiguously assigned. The zwitterionic Schiff base ligand was complexed with metal (II) centers of Co, Ni, Cu and Zn to produce the respective coordination compounds. These compounds were also characterized by mass spectrometry, elemental analyses and IR studies along with UV-visible and conductance measurements.

The elemental analyses and ES^+ mass spectra of all the complexes suggest the attachment of two ligands to the same metal center. Corresponding molecular ion peak with reasonable abundances were observed. Infrared studies suggest the attachment of the ligand through –CH=N and hydroxyl group of the naphthaldehyde producing six membered chelate ring. In all of these complexes the vibratory frequency was found to be changing by 40-60 cm^{-1}. Carboxyl frequency may be seen at 3400 cm^{-1} in the form of broad peak. The complementary C-O frequency was found at 1170-1300 cm^{-1} in all of the compounds which show that in all of the transition metal complexes the carboxyl group is not coordinating to the metal center.

Conductance studies show the electrolyte nature of the compounds therefore the carboxylic protons are available which may correspond to the conductance values. Therefore it was proved that ligand is coordinating in 2:1 molar ratio to the metal center.

UV visible absorption spectra were measured and compared to the magnetic susceptibilities in order to assign the different transitional bands to their respective excitations. UV-Visible spectra were taken for **13, 14,** and **15** in the range 200-800 nm in a 1cm matched quartz glass cuvette. The solvent used for the measurement was acetonitrile. For **13** the band observed around 480nm was assigned to the transition of electron from $Eg \rightarrow T_2g$ in a tetrahedral environment for the complex. Tetrahedral geometry can be assigned because the ligand H-HMAC is flexible and can

twist around cyclohexane linked carbon (C-7). Both the ligands attached to the same metallic center therefore produces tetrahedral metal complexes unlike N,N,O,O type of coordination by the other similar nonflexible ligands. The single band observed for **13** may be assigned to the transition $^3T_1$ (F) $\rightarrow ^4T_1$ (P). The other band which may be arising due to the transition $^3T_1$ (F) $\rightarrow ^3T_2$ (F) is not observed due to its forbidden nature. For **14** there must be three bands which could be observed in the UV-Visible region, but actually the two bands viz; $^4A_2$ (F) $\rightarrow ^4T_1$ (p) and the weakly observed $^4A_2$ (F) $\rightarrow ^4T_1$ (F) are observed. The former is broader band which might be encompassing the low energy band arising from $^4A_2$ (F) $\rightarrow ^4A_1$ (F). The only absorption band observed for **15** is assigned to the Eg$\rightarrow T_2$g transition occurring in the form energy holes. The visible band for **15** is a broad band which might be carrying several electronic transitions. Therefore based on the UV-Visible assignments, the assigned geometries are tetrahedral for all the complexes [1,2]. The magnetic susceptibilities values are also in close agreement with this assignment. For **13**, the μ_{eff} value is 2.89 B.M. which suggest the existence of free electrons and low energy gap between the Eg and T_2g orbitals. According to Pauli Exclusion Principle the T_2g electrons will be filled leaving two electrons unpaired which ultimately corresponds to the spin only values. Similarly for **14** the μ_{eff} = 4.21 B.M., suggesting the presence of three unpaired electrons which arises by considering the tetrahedral geometry around cobalt. For copper based metal complex i.e.**15**, the μ_{eff} corresponds to 1.73 B.M. values representing the d^9 system of the metal center. Thus UV-Visible spectroscopy and the magnetic susceptibilities count for the tetrahedral geometries. Due to the paramagnetic nature of the **13, 14** and **15** the ^{1}H and ^{13}C{^{1}H}-NMR signals were observed as undistinguishable broad bands. For **16** which is diamagnetic the ^{1}H and ^{13}C{^{1}H}-NMR recorded gave values with a strong gallop for the HC=N proton and the

disappearance of the hydroxyl group frequency. Therefore same geometry can be assigned to **16** as well like the other metal complexes of the same series.

3.3.8 Crystal structure study of H-HMAC

The Schiff base ligand H-HMAC was crystalized from the concentrated solution of THF in *P1* space group. The ORTEP plot of the H-HMAC is shown in figure 3.13. and the corresponding crystal data table 3.11. Table 3.12 and 3.13 are enlisting the selected bond lengths and bond angles respectively. The plane produced by C(1)-C(2)-C(4)-C(5) is lying at 44.89^{o} to the plane produced by C(1)-C(5)-C(6), while the angle between the planes C(1)-C(2)-C(4)-C(5) and C(2)-C(3)-C(4) is 51.41^{o}. The former is lower by Δ = 6.52^{o} which may be due to the involvement of the C(7) in the Schiff base linkage. The torsion angles for C(6)-C(7)-N(8)-C(9) and C(7)-N(8)-C(9)- C(10) are -117.38^{o} and 177.94^{o} respectively which clearly represent the twist in the attachment of cyclohexane ring for the formation of Schiff base linkage. The bond distance between C(9)-N(8) is 1.296 A^{o} like linkage as found in (E)-4-bromo-2-[(2-chloro-3-pyridyl)-iminomethyl]phenol (1.291 A^{o}) [17]. There is intra molecular hydrogen bonding between H(8)-O(23) in the crystal structure of the ligand which is of 1.908 A^{o} length. An intermolecular hydrogen bonding between O(22)-H(23) is 2.549 A^{o}.

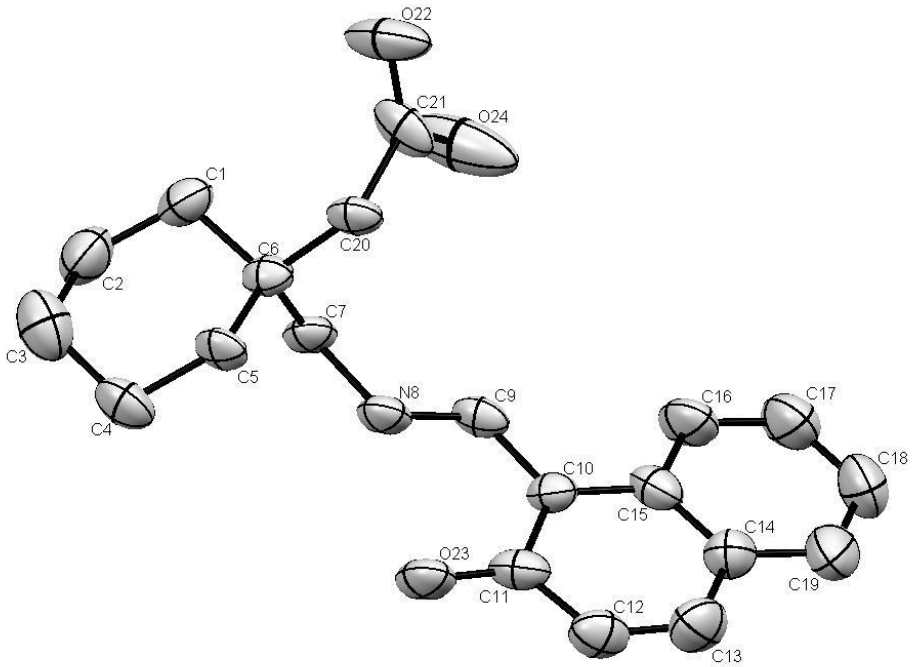

Figure 3.13 Molecular structure of H-HHMAC. Thermal ellipsoids are shown at 50% probability. H atoms are omitted for clarity reasons.

Table 3.11: **Crystal data and structure refinement for H-HMAC**	
Identification code	H-HMAC
Empirical formula	$C_{20}H_{23}NO_3$
Formula weight	325.4
Temperature / K	298
Crystal system	triclinic
Space group	P-1
a / Å, b / Å, c / Å	9.1610(11), 9.8202(15), 10.0079(14)
α/°, β/°, γ/°	88.430(12), 83.227(11), 71.868(13)
Volume / $Å^3$	849.6(2)
Z	2
Crystal size / mm^3	0.2279 × 0.065 × 0.0248
2Θ range for data collection	6.02 to 55.12°
Index ranges	$-11 \leq h \leq 11, -12 \leq k \leq 12, 0 \leq l \leq 12$
Reflections collected	5573
Independent reflections	3600[R(int) = 0.1160]
Data/restraints/parameters	3600/0/231
Goodness-of-fit on F^2	0.908600

Final R indexes [I>2σ (I)]	R_1 = 0.133823, wR_2 = N
Final R indexes [all data]	R_1 = 0.339499, wR_2 = 0.236766
Largest diff. peak/hole / e $Å^{-3}$	1.103803/-1.199478

Table 3.12: Bond lengths for single crystal structure of H-HMAC

Atom	Atom	Length/Å	Atom	Atom	Length/Å
O	C13	1.285(8)	C9	C10	1.540(9)
N	C3	1.296(8)	C9	C11	1.522(9)
N	C10	1.470(8)	C11	C20	1.531(10)
C3	C6	1.414(9)	C12	C23	1.408(10)
O0aa	C16	1.262(9)	C12	C24	1.419(10)
C5	C9	1.527(8)	C13	C14	1.435(9)
C5	C15	1.512(9)	C14	C24	1.340(10)
C6	C7	1.436(9)	C15	C22	1.510(10)
C6	C13	1.427(9)	C16	O1aa	1.182(9)
C7	C12	1.419(9)	C17	C18	1.383(10)
C7	C17	1.400(9)	C18	C21	1.391(11)
C8	C9	1.555(9)	C20	C22	1.518(11)
C8	C16	1.533(9)	C21	C23	1.369(11)

Table 3.13 Selected bond angles for molecular structure of H-HMAC

Atom	Atom	Atom	Angle/°	Atom	Atom	Atom	Angle/°
C10	N	C3	126.0(6)	C23	C12	C7	119.6(8)
C6	C3	N	125.2(6)	C24	C12	C7	119.2(7)
C15	C5	C9	114.8(6)	C24	C12	C23	121.1(8)
C7	C6	C3	119.8(6)	C6	C13	O	122.3(7)
C13	C6	C3	118.6(7)	C14	C13	O	121.1(7)
C13	C6	C7	121.5(7)	C14	C13	C6	116.7(7)
C12	C7	C6	118.1(7)	C24	C14	C13	122.0(7)

C17	C7	C6	123.6(8)	C22	C15	C5	110.0(6)
C17	C7	C12	118.2(7)	C8	C16	O0aa	113.5(7)
C16	C8	C9	114.7(6)	O1aa	C16	O0aa	123.4(7)
C8	C9	C5	106.8(6)	O1aa	C16	C8	122.4(8)
C10	C9	C5	111.3(5)	C18	C17	C7	120.6(8)
C10	C9	C8	111.0(6)	C21	C18	C17	121.2(9)
C11	C9	C5	109.2(6)	C22	C20	C11	111.4(8)
C11	C9	C8	110.6(5)	C23	C21	C18	119.3(9)
C11	C9	C10	107.8(6)	C20	C22	C15	110.6(8)
C9	C10	N	112.7(6)	C21	C23	C12	121.0(9)
C20	C11	C9	113.7(6)	C14	C24	C12	122.1(8)

3.3.9 Enzyme Inhibitory activities

The gabapentene based Schiff base ligand and its divalent metal complexes were also screened for their inhibitory activities against urease, α-chymotrypsin, acetyl cholinesterase and butyrylcholinesterase activities. Table 3.14 enlists the activities result for all the tested compounds of H-HHMAC series. The ligand is showing interesting results against the tested

enzymes. It was found inactive against α-Chymotrypsin, but show some inhibition against the other enzymes. Whereas all the metal complexes of the Schiff base ligand were found inactive except **14** which show weak activity against butyrylcholinesterase. Therefore ligand H-HMAC is a good inhibitor rather than its metal complexes.

Table 3.14: In Vitro inhibition activities of H-HMAC and its metal complexes against urease, α-chymotrypsin, acetyl cholinesterase and butyrylcholinesterase

Compounds	**IC_{50} for urease (µM)±SEM**	**IC_{50} for α-Chymotrypsin (µM)±SEM**	**IC_{50} for acetyl cholinesterase (µM)±SEM**	**IC_{50} for butyrylcholinesterase (µM)±SEM**
H-HHMAC	86.7±0.021	---	98.3±0.001	56.3±0.231
13	---	---	---	---
14	---	---	---	103±0.003
15	---	---	---	---
16	---	---	---	---
Standard	0.5±0.01 **(galanthamine)**	8.5±0.5 **(galanthamine)**	21± 0.011 **(Thiourea)**	5.71± 0.13 **(Chymostatin)**

3.3.10 Antimicrobial activities

Table 3.15 depicts the antimicrobial activities for H-HMAC and its metal complexes against Gram positive bacteria *Bacillus atrophaeus*, *Bacillus subtilis*, *Staphylococcus aureus*, Gram negative bacteria *Klebsiella pneumoniae*, *Salmonella typhus*, *Pseudomonas aeruginosa*, *Escherichia coli*, *Agrobacterium tumefaciens*, *Erwinia carotovora*, fungal Strain *Candida albican*. As the table show that the ligand is acting as weak to moderate active against Gram

positive and Gram negative bacterial strains along the only fungal strain Candida albican. Compound **13** is not found active whereas the compounds **15** and **16** are also showing similar activities against these tested microbial strains. Compound **14** show very weak activity against all the tested microbial strains.

Table 3.15: In Vitro antimicrobial activities of H-HMAC and its metal complexes against different animal and plant pathogens

Compounds	*Bacillus atrophaeus (cm)*	*Bacillus subtilis (cm)*	*Klebsiella pneumoniae (cm)*	*Salmonella typhus (cm)*	*Pseudomonas aeruginosa (cm)*	*Escherichia coli (cm)*	*Staphylococcus aureus (cm)*	*Candida albican (cm)*	*Agrobacterium tumefaciens (cm)*	*Erwinia carotovora (cm)*
H-HMAC	1.2	1.9	1.0	---	0.9	---	1.1	1.9	1.6	1.1
13	---	---	---	---	0.8	---	1.0	---	---	---
14	---	---	1.3	0.6	1.0	---	---	1.2	1.5	0.9
16	2.1	2.1	1.4	1.6	1.8	2.5	2.2	2.2	2.3	0.9
15	1.9	1.5	---	0.6	1.4	1.7	2.6	1.8	1.7	---
Standard	2.5	2.6	2.9	4.2	3.6	3.8	3.4	1.6	1.5	2.6

Gram positive bacteria: *Bacillus atrophaeus*, *Bacillus subtilis*, *Staphylococcus aureus*, standard used was erythromycin in 6 µM

Gram negative bacteria: *Klebsiella pneumoniae*, *Salmonella typhus*, *Pseudomonas aeruginosa*, *Escherichia coli*, *Agrobacterium tumefaciens*, *Erwinia carotovora*, standard used was ciprofloxacin in 6 µM

Fungal Strain: *Candida albican*, standard used was clothrimazol in 6 µM

3.3.11 Thermodynamics and Thermal studies

Thermal decomposition of H-HMAC and its metal complexes was studied in the range of 30-1000 ^{o}C. The first decomposition temperature values are 220 ^{o}C, 250 ^{o}C, 225 ^{o}C, 200 ^{o}C, and 250 ^{o}C for H-HMAC, **13, 14, 15**, and **16** respectively. Table 3.16 and enlists the kinetic and thermodynamic parameters whereas table 3.17 is comprised of the thermal degradation mechanistic study of the H-HMAC and its metal complexes. Figure 3.14 and 3.15 show TG and DTA curves of the series H-HMAC.

Table 3.16: Kinetic and thermodynamic parameters of H-HMAC and its metal complexes

Compound	**Ts in K**	**Ea, KJ/mol**	**ΔH, KJ/mol**	**$\Delta G^{\#}$, KJ/mol**	**$\Delta S^{\#}$, $Jmol^{-1}K^{-1}$**	**Order of reaction, n**
H-HMAC	518	30.78	26.47	153.19	-244.64	5
13	530.8	26.53	22.14	151.40	-245.36	5
14	509.7	46.56	41.18	210.19	-261.43	3/2
15	560	22.48	17.79	156.10	-245.23	5
16	634	65.49	60.21	233.73	-273.71	1

The zwitterionic Schiff base ligand H-HMAC was studied for its thermal degradation and was found to be decomposing in two stages of thermal degradation. First stage of degradation is ranging from 30-520 ^{o}C and the second stage is in the range 520-850 ^{o}C. The ligand decomposes completely without leaving any residue. In the first stage of degradation two species are produced as a result of degradation, including 1-(prop-2-en-1-yl)naphthalen-2-ol and ethene. In the second stage the thermal degradation is completed by the release of cyanobutanoic acid produced by the fusion of free radicals of cyanide and the butanoic acid. It means that the

hexacyclic ring is decomposed whereas the aromatic naphthalene ring remains intact. There are three endothermic DTA peaks observed for the first stage of degradation whereas the second stage carries two exothermic DTA peaks. It has 30.7 KJ/mol of activation energy. The decomposition is of 5^{th} order kinetics with very high Gibb's free energy and enthalpy values. The change in entropy of activation is also very high representing that the degradation is rather very difficult. The degradation is shown in scheme 3.19:

$C_{20}H_{23}NO_3 \rightarrow C_{13}H_{12}O + C_2H_4 + C_5H_7NO_2$ Stage I

$C_5H_7NO_2 \rightarrow C_5H_7NO_2$ Stage II

Scheme 3.19 Thermal degradation of H-HMAC

Compound **13** follow thermal degradation in a single step lying in the range 250-500 ^oC leaving nickel oxide as residue. The degradation products include the formation of 1,1'-binaphthalene-2,2'-diol, two moles of butene, two moles of 3-butenoic acid and two moles of acetonitrile. The whole degradation is comprised of four DTA peaks consisting of two exothermic and two endothermic peaks. The huge endothermic peak may be due to the formation of stable conjugated product like butadiene. The activation energy is 26.5 KJ/mol and it is following 5^{th} order kinetics. The change in entropy of activation is very low whereas the change in enthalpy of activation and change in Gibb's free energy of activation are large representing stable nature of the complex. The schematic thermal degradation is given below in scheme 3.20:

$C_{40}H_{44}N_2NiO_6 \rightarrow C_{20}H_{14}O_2 + 2C_4H_6 + 2C_4H_6O_2 + 2CH_3CN + NiO$

Scheme 3.20 Thermal degradation of 13

Compound **14** starts degradation around 225 ^oC and completes around 870 ^oC leaving cobalt oxide as residue. In the first stage of decomposition one mole of 1,1'-binaphthalene-2,2'-diol is produced with two endothermic and one exothermic peaks. Second stage of decomposition starts

Table 3.17: Thermo analytical results of H-HMAC and its complexes

Compound	TG Temp. range/ ^{o}C	Stage	Mass loss		DTA	Moiety evolved
			% Calc.	% Found		
H-HMAC	30-520	I	63.7	63.5	(-)19, (-)20, (-)34	C_2H_4, $C_{13}H_{12}O$
	520-850	II	38.9	38.3	(+)21, (+)5	$C_4H_6O_2$, CH_3CN
13	30-500	I	90.9	90.4	(+)0.1, (-)18, (-)10, (-)24,	$C_{20}H_{18}O_2$, $2C_4H_6$, $2C_4H_6O_2$, $2CH_3CN$, H_2
	>500	Res	10.6	10.4	---	NiO
14	30-390	I	38.4	39.7	(-)30, (-)40, (+)25	$C_{20}H_{18}O_2$
	390-880	II	50.2	49.5	(+)30	$2C_4H_6$, $2C_4H_6O_2$, $2CH_3CN$, H_2
	>880	Res	12.0	10.5	---	CoO
15	30-390	I	83.6	83.3	(+)4, (-)10, (-)6, (+)64	$C_{20}H_{18}O_2$, $2C_4H_6$, $2C_4H_6O_2$, $2CH_3CN$, H_2
	>390	Res	10.4	12.9	---	CuO
16	30-430	I	54.3	53.8	(-)22, (-)40	$C_{20}H_{18}O_2$, C_2H_4
	430-620	II	23.0	22.4	(-)18	$2C_8H_{12}O_2$,
	620-910	III	11.7	11.5	(-)52	2HCN
	>910	Res	11.5	13.1	---	ZnO

around 380 ^{o}C, producing several products which include the production of two moles of butene, two moles of 3-butenoic acid and two moles of acetonitrile. This stage is comprised of a huge

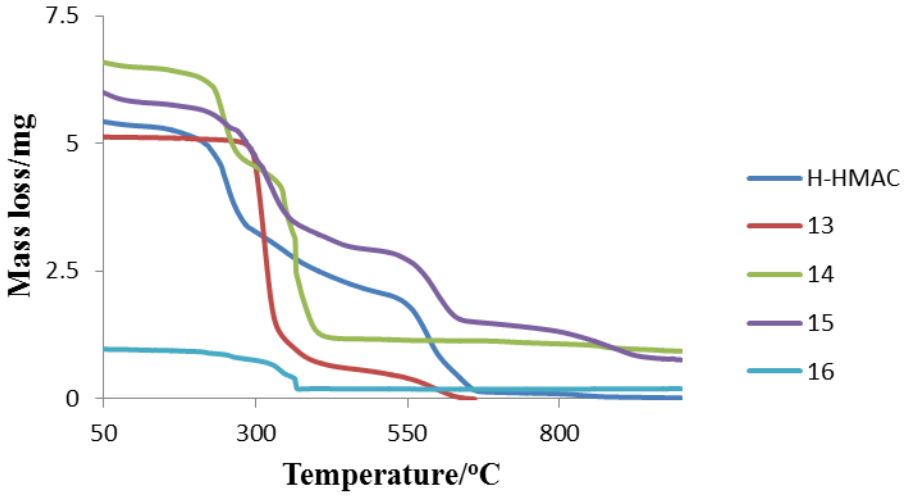

Figure 3.14. Thermogravimetric plots of H-HMAC and its metal complexes

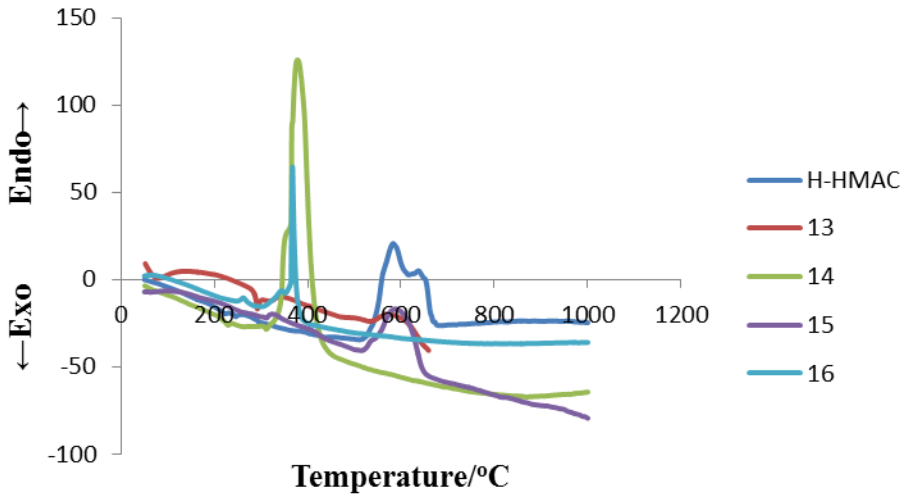

Figure 3.15. Differential thermogravimetric curves for H-HMAC and its metal complexes

exothermic DTA peak. The percentage compositions calculated for each step are in agreement with the observed values. The activation energy for **14** is 46.56 KJ/mol, higher than **13** therefore representing the stable nature of the cobalt complex with H-HMAC ligand. The same trend is followed in change in entropy of activation, change in Gibb's free energy of activation and change in enthalpy of activation. As whole the degradation was observed to be proceeding with 1.5 order of reaction. The overall degradation is represented in the form of scheme 3.21 as given below:

$C_{40}H_{44}CoN_2O_6 \rightarrow C_{20}H_{14}O_2 + C_{20}H_{30}CoN_2O_4$ Stage I

$C_{20}H_{30}CoN_2O_4 \rightarrow 2C_4H_6 + 2C_4H_6O_2 + 2CH_3CN + CoO$ Stage II

Scheme 3.21 Thermal degradation of 14

Compound **15** was observed to stable upto around 190 ^oC and then starts degradation by following the single route of decomposition like the **13**. Cupric oxide remains as residue at the end of the process above 380 ^oC. The products are identical to the degradation of **13**, like one mole of 1,1'-binaphthalene-2,2'-diol, two moles each of butene, 3-butenoic acid, and acetonitrile. There are four exothermic DTA peaks observed for the degradation of **15**. The same trend is followed in degradation kinetics, producing these products by following the 5^{th} order degradative kinetics. Similar behavior is shown in change in entropy of activation, whereas the change in Gibb's free energy of activation is higher but the change in enthalpy of activation is low. The schematic representation is shown in the following scheme 3.22:

$C_{40}H_{44}CuN_2O_6 \rightarrow C_{20}H_{14}O_2 + 2C_4H_6 + 2C_4H_6O_2 + 2CH_3CN + CuO$

Scheme 3.22 Thermal degradation of 15

Compound **16** unlike the other compounds of the same series degrades in three steps. The first step starts around 210 ^oC and completes at 430 ^oC with the production of one mole of 1,1'-

binaphthalene-2,2'-diol and one mole of ethene. This step is comprised of two endothermic peaks. The second stage of degradation starts around 500 ^{o}C and completes around 620 ^{o}C with the release of two moles of (2*E*)-octa-2,7-dienoic acid. This stage is comprised of one endothermic DTA peak. The third stage of degradation starts around 790 ^{o}C and completes around 910 ^{o}C leaving behind zinc oxide. In the third stage two moles of hydrogen cyanide is produced. This stage encompasses one huge exothermic DTA peak. The scheme of degradation is given below in scheme 3.23:

$C_{40}H_{44}N_2O_6Zn \rightarrow C_{20}H_{14}O_2 + 2C_2H_4 + C_{18}H_{26}N_2O_4Zn$ Stage I

$C_{18}H_{26}N_2O_4Zn \rightarrow 2C_8H_{12}O_2 + C_2H_2N_2Zn$ Stage II

$C_2H_2N_2Zn \rightarrow 2HCN + ZnO$ Stage III

Scheme 3.23 Thermal degradation of 16

By looking into the activation energy it becomes clear that zinc has the highest activation energy i.e. 65.5 KJ/mol. Similarly the change in enthalpy of activation and change in Gibb's free energy of activation are also very high from the other samples of the same series. Therefore it can be said that based on activation energy parameter the metal ions can be arranged on the basis of decreasing activation energy as, $E^*_{Zn} > E^*_{Co} > E^*_{Ni} > E^*_{Cu}$.

3.3.12 Conclusion

The interesting and novel Schiff base ligand derived from gabapentene H-HMAC and its divalent metal complexes with Co(II), Ni(II), Cu(II) and Zn(II) were synthesized and fully characterized using different analytical and spectroscopic techniques. All the techniques reveal that the metal complexes are formed in 2:1 molar ratio of the ligand and the corresponding metals. The ligand was found to be coordinating through hydroxyl group of salicyldehyde and azomethine group of Schiff base. Apart from it the ligand was also characterized by single

crystal analysis. The ligand crystalizes in *P1* space group and was completely characterized. All the compounds were studied for their for their inhibiting activities for enzymes like urease, α-chymotrypsin, acetyl cholinesterase, and butyrylcholinesterase. The ligand was found to be showing activities against urease, acetyl cholinesterase, and butyrylcholinesterase. Whereas all the metal complexes were found inactive except **14** which is showing weak activity against butyrylcholinesterase**.** All the compounds were found to be weakly active against the tested pathogenic microbes. From the thermal and thermodynamic data it becomes clear that the metal complexes are following the order $E^*_{Zn} > E^*_{Co} > E^*_{Ni} > E^*_{Cu}$ in activation energies and Co(II) >Cu(II) >Ni(II) >Zn(II) in the stability temperatures.

3.4 Results and discussion of H-HAB series

3.4.1 Synthesis of methyl 2-{[(*E*)-(2-hydroxyphenyl)methylidene]amino}benzoate (H-HAB)

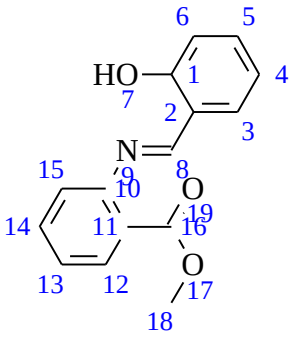

Scheme3.24 Atoms numbering for NMR peak assignment

Yield: 88%, D. pt: 256 ^{o}C, IR: 3043(m), 1791(w), 1683(w), 1618(s), 1570(s), 1485(s), 1446(s), 1386(s), 1317(s), 1269(s), 1197(s), 1147(s), 1105(s), 1031(s), 983(s), 943(m), 893(s), 852(m), 783(s), 746(s), 727(s), 682(s), 610(m) cm^{-1}, ^{1}H-NMR (400.23 MHz, CD_3OD, 303k): δ = 11.0 (s, 1H, Ar-O<u>H</u>), 10.2 (s, 1H, <u>H</u>C=N), 8.02 (d, $^{3}J_{HH}$= 8.35Hz, 1H, H12), 7.95 (d, $^{3}J_{HH}$= 7.8Hz, 1H, H15), 7.4 (d, $^{3}J_{HH}$= 7.35Hz, 1H, H6), 7.2 (d, $^{3}J_{HH}$= 8.21Hz, 1H, H13), 7.11 (d, $^{3}J_{HH}$= 8.13Hz, 1H, H5), 7.0 (d, $^{3}J_{HH}$= 7.83Hz, 1H, H13), 6.5 (d, $^{3}J_{HH}$= 7.1Hz, 1H, H4), 4.2 (s, 3H, H18), ^{13}C{^{1}H}-NMR (150.9 MHz, CD_3OD, 303k): δ = 178 (<u>C</u>=O, C, C10), 158(CH=N, CH, C8), 156 (aromatic <u>C</u>–OH, C1), 150 (C, C10), 143 (C, C11), 142.7 (CH, C6), 141 (CH, C12), 139 (CH, C15), 137 (CH, C3), 133 (CH, C13), 126 (CH, C5), 123 (CH, C4), 120 (CH, C14), 76 (CH_3, C18), Elemental Analysis ($C_{15}H_{13}NO_3$), Calc. C: 70.58%, H: 5.13%, N: 5.49%, Exp. C: 70.11%, H: 4.78%, N: 5.38%, EI-MS: *m/z* (%)255.0889 (100%) [$C_{15}H_{13}NO_3^{+}$], $\wedge_m$ = 54.3 µS

Synthesis of [M(HAB)$_2$] where M=Ni, Co, Cu and Zn (II) acetates

3.4.2.Bis(methyl 2-{[(*E*)-(2-hydroxyphenyl)methylidene]amino}benzoate)nickel(II) (17)

Yield: 34%, D. pt: 202 ^{o}C, IR: 3437(s), 3294(m), 3078(w), 1614(s), 1581(s), 1529(s), 1469(s), 1446(m), 1417(m), 1361(m), 1321(s), 1298(w), 1267(s), 1192(s), 1147(s), 1099, (s) 1022, 952(s), 896(s), 860(w), 802(s), 752(s), 704(s), 671(s), 640(s), 602(m) cm^{-1}, λ_{max}= 520, 590, 700

nm [ε = 220.6, 134, 13.7 $M^{-1}cm^{-1}$ ^3A_2g (F) $\rightarrow$ ^3T_1g (P), ^3A_2g (F) $\rightarrow$ ^3T_1g (F), ^3A_2g (F) $\rightarrow$ ^3T_2g (F)], μ_{eff} = 2.30 B.M. Elemental Analysis ($C_{30}H_{24}N_2NiO_6$), Calc. C: 63.52%, H: 4.26%, N: 4.94%, Ni: 10.35%, Exp. C: 63.22%, H:4.89%, N: 4.90%, Ni: 10.30%, EI-MS: *m/z* (%) 566.0982 (100%) [$C_{30}H_{24}N_2NiO_6^+$], $\wedge_m$ = 0.31 µS

3.4.3 bis(methyl 2-{[(*E*)-(2-hydroxyphenyl)methylidene]amino}benzoate)cobalt(II) (18)

Yield: 64%, D. pt: 228 ^oC, IR. 3280(s), 3138(w), 1620(s), 1591(s), 1544(s), 1446(s), 1420(s), 1300(s), 1199(s), 1103(s), 1031(s), 956(s), 889(s), 804(s), 740(s), 644(s), 560(s) cm^{-1}, λ_{max}= 430, 680 nm (ε = 331.8, 13.4 $M^{-1}cm^{-1}$, ^4T_1g (F) $\rightarrow$ ^4A_2g and the ^4T_1g (F)$\rightarrow$ ^4T_1g (P), ^4T_1g (F) $\rightarrow$ ^4T_2g, μ_{eff} = 3.92 B.M. Elemental Analysis ($C_{30}H_{24}CoN_2O_6$), Calc. C: 63.50%, H: 4.26%, Co: 10.39%, N: 4.94%, Exp. C: 63.40 %, H: 4.96%, Co:10.41%, N: 4.60%, EI-MS: *m/z* (%) 567.096088 (100%) [$C_{30}H_{24}CoN_2O_6^+$], $\wedge_m$ = 0.11 µS

3.4.4 bis(methyl 2-{[(*E*)-(2-hydroxyphenyl)methylidene]amino}benzoate)copper(II) (19)

Yield: 55%, D. pt: 254 ^oC, IR: 1651(s), 1589(s), 1556(s), 1492(s), 1456(s), 1408(s), 1348(s), 1303(s), 1267(s), 1199(m), 1138(s), 1076(m), 1020(w), 935(m), 898(w), 854(s), 817(s), 767(s), 748(s), 729(s), 694(s), 632(s) cm^{-1}, λ_{max}= 780 nm (ε = 12.7 $M^{-1}cm^{-1}$,$T_2g\rightarrow eg$), μ_{eff} = 2.02 B.M. Elemental Analysis ($C_{30}H_{24}CuN_2O_6$), Calc. C: 62.99%, H: 4.23%, Cu: 11.11%, N: 4.90%, Exp. C: 62.77%, H: 4.21%, Cu: 11.87%, N: 4.30%, EI-MS: *m/z* (%) 571.0930 (100%) [$C_{30}H_{24}CoN_2O_6^+$], $\wedge_m$ = 0.01 µS

3.4.5 bis(methyl 2-{[(*E*)-(2-hydroxyphenyl)methylidene]amino}benzoate)zinc(II) (20)

Yield: 44%, D. pt: 190 ^oC, IR: 3437(s), 3307(w), 1614(s), 1587(s), 1537(s), 1469(s), 1446(m), 1361(m), 1311(s), 1269(s), 1193(s), 1147(s), 1089(s), 1033(m), 974(s), 935(w), 908(s), 860(s), 796(s), 754(s), 705(s), 667(s), 610(s) cm^{-1}, ^{1}H-NMR (400.23 MHz, CD_3OD, 303k): δ = 14.1 (s, 1H, HC=N), 8.02 (d, $^3J_{HH}$= 8.35Hz, 1H, H12), 7.95 (d, $^3J_{HH}$= 7.8Hz, 1H, H15), 7.4 (d, $^3J_{HH}$=

7.35Hz, 1H, H6), 7.2 (d, $^{3}J_{HH}$= 8.21Hz, 1H, H13), 7.11 (d, $^{3}J_{HH}$= 8.13Hz, 1H, H5), 7.0 (d, $^{3}J_{HH}$= 7.83Hz, 1H, H13), 6.5 (d, $^{3}J_{HH}$= 7.1Hz, 1H, H4), 4.2 (s, 3H, H18), Elemental Analysis ($C_{30}H_{24}N_2O_6Zn$), Calc. C: 62.78%, H:4.21%, N:4.88%, Zn:11.40%, Exp. C: 62.18%, H:4.73%, N:4.67%, Zn:11.32%, EI-MS: *m/z* (%) 572.0920 (100%) [$C_{30}H_{24}N_2O_6Zn^{+}$], $\wedge_m$ = 0.11 µS

3.4.6 Analytical and spectroscopic characterization

The Schiff base ligand H-HAB was fully characterized using the spectroscopic techniques which include the ^{1}H and ^{13}C{^{1}H}-NMR. The ^{1}H-NMR was assigned on the basis of the expected analytical techniques including the elemental analysis and EI-MS. ^{1}H-NMR of the ligand show an up field peak at 11 ppm which was assigned to hydroxyl proton. The Schiff base proton appeared at 10.2 ppm. The methyl group of the ester appeared at 4.3 ppm. Rest of the ^{1}H-NMR was in good agreement with the aromatic protons and their corresponding coupling constants. The ^{13}C{^{1}H}-NMR was also studied for the H-HAB ligand. The ester carbonyl appeared at 178 ppm, the Schiff base carbon appeared at 158 ppm whereas the hydroxyl group appeared at 156 ppm. Rest of the spectrum was assigned to the aromatic carbon atoms. The methyl group of the ester appeared at 76 ppm. The ^{1}H and ^{13}C{^{1}H}-NMR spectra support the formation of the Schiff base ligand derived from methyl anthranilate and salicyldehyde. The ES(+) MS was also recorded for the ligand which gave the respective peak for the ligand. The mass spectral data was also supported by the elemental analyses, confirming the composition considered for the condensation reaction between the methyl anthranilate and salicyldehyde. The characterization was further supported by the IR analysis. The IR spectrum was recorded in the range 500-4000 cm^{-1}. The hydroxyl peak was not observed because of the probable involvement of the group in the production hydrogen bonding with the nitrogen of CH=N, thus producing the zwitterionic Schiff base ligand. The ester carbonyl was observed to be vibrating at 1791 cm^{-1},

whereas the Schiff base vibration was observed at 1618 cm^{-1} as strong stretching band. In metal complexes the IR bands of the hydroxyl groups was either observed as strong band or not observed at all. The esteric carbonyl frequency diminished and was not observed in either of the complex. Similarly the C=N vibrating frequency was observed to be shifting by $\Delta\upsilon$ = 15-40 cm^{-1}. Hence it can be suggested that the ligand H-HAB is acting as tridentate monoanionic ligand which is attacking the metal center through hydroxyl group, carbonyl group and the Schiff base nitrogen group. Thus the ligand can be classified as one of the representative in the category of N, O, and O^- group of ligands. All the metal complexes were found to be paramagnetic in nature except zinc therefore the NMR recorded for them gave broad peaks which were found to be non-interpretable. The zinc complex shown the broadening of the HC=N proton frequency whereas the hydroxyl group diminished as a result of loss of the proton. Therefore zinc was also assigned the same geometry based on the NMR, mass and elemental studies.

The UV-Visible spectra for all the compounds were recorded in the 200-800 nm range. Compound **17** exhibit two clear bands, one is observed around at 520 nm and the other at 590 nm. Whereas the third broader ones is weakly observed at about 700 nm. The peak at 520 nm can be assigned to the ^3A_2g (F) $\rightarrow{}^3T_1g$ (P) and the peak at 590 nm can be assigned to the ^3A_2g (F) $\rightarrow{}^3T_1g$ (F). The broad peak is of ^3A_2g (F) $\rightarrow{}^3T_2g$ (F) transition. The spin only value is 2.30 B.M. which is also in close agreement with the octahedral geometry around nickel center. Similarly 18 show two asymmetric bands i.e. at 430nm and 680nm. The peak at 430 nm may be due to the two spin allowed transitions such as ^4T_1g (F) $\rightarrow{}^4A_2g$ and the ^4T_1g (F) $\rightarrow{}^4T_1g$ (P). Whereas the latter corresponds to the $^4T_{1g}$ (F) $\rightarrow{}^4T_2g$. The spin only value for this complex is 3.92 B.M. which corresponds to the three unpaired electrons in the e.g. level of the orbitals. Copper based metal complex of H-HAB show one broad peak around 780 nm which is

considered to be carrying many overlapping peaks [1,2]. This transition was assigned to the $T_2g \rightarrow eg$. The magnetic susceptibility for the complex is 2.02 B.M., which shows the only unpaired electron. The complexes were also found to be non-electrolyte because the molar conductance values are very lower than 50 µS. Therefore the presence of free ions from the ligand or that from the complexes are completely ruled out.

3.4.7 Enzyme inhibitory activities

The compounds H-HAB and its divalent metal complexes were tested for their enzyme inhibition against urease, α-Chymotrypsin, acetyl cholinesterase and butyrylcholinesterase and the results are shown in table 3.18.

Table 3.18: In Vitro inhibition activities of H-HHMAC and its metal complexes against urease, α-chymotrypsin, acetyl cholinesterase and butyrylcholinesterase

Compounds	**IC_{50} for urease (µM)±SEM**	**IC_{50} for α-Chymotrypsin (µM)±SEM**	**IC_{50} for acetyl cholinesterase (µM)±SEM**	**IC_{50} for butyrylcholinesterase (µM)±SEM**
H-HAB	---	---	---	---
17	---	---	---	---
18	53.4±0.02	103±0.001	---	93±0.0023
19	---	32±0.013	47±0.025	86±0.11
20	---	---	77±0.04	57±0.23
Standard	0.5±0.01 **(galanthamine)**	8.5±0.5 **(galanthamine)**	21± 0.011 **(Thiourea)**	5.71± 0.13 **(Chymostatin)**

It was found that ligand did not show activity against any tested enzyme, but the complexes were active against one or more enzymes. **17**, which is nickel based metal complex, was found

completely inactive like the ligand, whereas the copper base metal complex of the same ligand show interesting activities. It was found to be inhibiting α-Chymotrypsin, acetyl cholinesterase and butyrylcholinesterase with high IC_{50} values. Therefore copper based metal complex of the H-HAB ligand is unable to achieve selectivity in inhibiting one or more enzymes. Similarly the cobalt based metal complex of the same ligand was also found to be moderately inhibiting the enzymes.

3.4.8 Antimicrobial activities

The Schiff base ligand and its divalent metal complexes were exposed for their antibacterial and antifungal activities to different pathogenic microbes including Gram positive bacteria *Bacillus atrophaeus, Bacillus subtilis*, *Staphylococcus aureus,* Gram negative bacteria *Klebsiella pneumoniae*, *Salmonella typhus*, *Pseudomonas aeruginosa*, *Escherichia coli*, *Agrobacterium tumefaciens*, *Erwinia carotovora,* fungal Strain *Candida albican*. Table enlists the activities, which reveal that neither the ligand nor its divalent metal ion complexes are active against any of the bacterial or fungal strain tested. Compound **17** show very weak activities. Therefore it can be stated that H-HAB is not effecting so much the steric of the metal complexes that it can enhance the activities.

Table 3.19: In Vitro antimicrobial activities of H-HAB and its metal complexes against different animal and plant pathogens

Compounds	*Bacillus atrophaeus (cm)*	*Bacillus subtilis (cm)*	*Klebsiella pneumoniae (cm)*	*Salmonella typhus (cm)*	*Pseudomonas aeruginosa (cm)*	*Escherichia coli (cm)*	*Staphylococcus aureus (cm)*	*Candida albican (cm)*	*Agrobacterium tumefaciens (cm)*	*Erwinia carotovora (cm)*
H-HAB	---	---	---	---	---	---	1.3	---	---	1.2
17	1.6	2.1	1.6	1.5	1.0	1.9	1.0	2.1	1.4	---
19	1.2	---	---	---	0.8	---	1.1	0.8	---	---
18	---	---	---	---	---	---	1.1	1.5	1.3	1.2
20	---	---	---	---	0.9	1.1	1.6	0.7	2.0	---
Standard	2.5	2.6	2.9	4.2	3.6	3.8	3.4	1.6	1.5	2.6

Gram positive bacteria: *Bacillus atrophaeus*, *Bacillus subtilis*, *Staphylococcus aureus*, standard used was erythromycin in 6 µM

Gram negative bacteria: *Klebsiella pneumoniae*, *Salmonella typhus*, *Pseudomonas aeruginosa*, *Escherichia coli*, *Agrobacterium tumefaciens*, *Erwinia carotovora*, standard used was ciprofloxacin in 6 µM

Fungal Strain: *Candida albican*, standard used was clothrimazol in 6 µM

3.4.9 Thermodynamics and Thermal studies

The Schiff base ligand H-HAB was derived by the condensation of methylanthranilate with salicyldehyde. The thermo analytical, the thermodynamic and kinetic data of the ligand and its transition metal complexes is given in table 3.20 and table 3.21 respectively. The Td temperature for the ligand H-HAB is 210 ^{o}C whereas for its octahedral metal complexes the Td temperatures are 235 ^{o}C, 250 ^{o}C, 258 ^{o}C and 200 ^{o}C for **17, 18, 19** and **20** respectively. The TG and DTA curves for all the compounds are shown in figure 3.16 and 3.17 respectively.

Table 3.20: Kinetic and thermodynamic parameters of H-HAB and its metal complexes

Compound	**Ts in K**	**Ea, KJ/mol**	**ΔH, KJ/mol**	**$\Delta G^{\#}$, KJ/mol**	**$\Delta S^{\#}$, Jmol^{-1}K^{-1}**	**Order of reaction, n**
H-HAB	566	36.49	31.28	171.16	-247.14	3/2
17	530.8	29.04	24.62	154.84	-245.34	5
18	509.7	39.75	35.51	159.42	-243.09	∞
19	544	14.02	9.50	142.1	-243.7	5
20	498.5	26.86	22.71	112.25	-179.63	5

The Schiff base ligand H-HAB was decomposed in the temperature range of 30-580 ^{o}C. The whole decomposition process was completed in two stages, in the first stage of decomposition one mole of biphenylene, one mole of carbon monoxide and ½ mole of hydrogen were released. This stage is comprised of three endothermic peaks as given in table 2. The second stage of pyrolysis releases one mole each of methane and carbon monoxide gas along with ½ mole of oxygen gas. The whole compound was consumed leaving no residue behind. The second stage is comprised of one huge exothermic peak which may be due to the production of methane gas. By

looking into table 1, it is clear that the degradation follows 3/2 order kinetics with 6.49KJ/mol activation energy. The change in entropy of activation like the other Schiff base ligands and their complexes are negative. Similar trends in the values of change in enthalpy of activation and change in Gibb's free energy of activation were followed. The decomposition of the H-HAB compound is shown below in scheme 3.25.

$C_{15}H_{13}NO_3 \rightarrow C_{12}H_8 + CO + 1/2N_2 + 1/2H_2 + C_2H_4O_2$ I Stage

$C_2H_4O_2 + O_2 \rightarrow CH_4 + 1/2O_2 + CO$ II Stage

Scheme 3.25 Thermal degradation of H-HAB

Compound **17** starts decomposition at 200 ^oC and completed at 600 ^oC the whole process of degradation was completed in two stages. The first stage was comprised of the release of one mole each of dioxygen and ethane, and two moles of hydrogen cyanide and carbon dioxide. The second stage of decomposition started at 300 ^oC and was finished with the release of two moles of biphenylene produced by the fusion of two benzene radicals. Non-stoichiometric nickel oxide remains as a residue after the complete release of all the gaseous products. The decomposition is following 5^{th} order kinetics and has reasonable activation energy. Similar trend in entropy of activation, Gibb's free energy of activation and enthalpy of activation can be observed. The degradation is shown below in scheme 3.26:

$C_{30}H_{24}N_2NiO_6 + O_2 \rightarrow 2CO_2 + O_2 + 2HCN + C_2H_6 + C_{24}H_{16}NiO$ I Stage

$C_{24}H_{16}NiO \rightarrow 2C_{12}H_8 + NiO$ II Stage

Scheme 3.26 Thermal degradation of 17

Compound **18** was studied for its thermal degradation studies in the same range viz; 30-1000 ^oC and was found to be decomposing at 250 ^oC. It is also following the same trend in decomposition like the compound **17**. The whole degradation is a two steps process first stage of decomposition

Table 3.21: Thermo analytical results of H-HAB and its complexes

Compound	TG Temp. range/ ^{o}C	Stage	Mass loss		DTA	Moiety evolved
			% Calc.	% Found		
H-HAB	30-370	I	77.5	77.5	(-)8, (-)25, (-)18	1//2N_2, CO, $C_{12}H_{8,}$ 1/2H_2
	370-580	II	23.5	23.3	(-)18, (-)2	CH_4, CO, 1/2O_2
17	30-300	I	35.8	36.9	(+)2, (+)18, (+)28	CO_2, 2HCN, $O_{2,}$ C_2H_6
	300-380	II	52.6	48.1	(+)150	2 $C_{12}H_8$
	>380	Res	9.6	18.7	---	Ni not calc.
18	30-280	I	24.2	22.4	(-)1, (-)3	2CO, 2HCN, $O_{2,}$ C_2H_6
	280-440	II	52.9	53.8	(+)1, (-)8, (-)17	2 $C_{12}H_8$
	>440	Res	10.5	11.4	---	Co_2O_3
19	30-450	I	55.6	56.0	(-)5.8, (-)5.6, (-)15.3, (-)18	$C_{12}H_{8,}$ 1/2N_2, 2CO, 2$C_2H_{2,}$ N_2O_4
	450-600	II	48.2	48.2	(-)12.0	2 $C_{12}H_{10}O_2$
	>600	Res	10.1	10.9	---	CuO
20	30-280	I	24.4	25.3	(-)2, (+)1	2CO, 2HCN, $O_{2,}$ C_2H_6
	280-530	II	54.2	54.9	(-)2.0, (+)38	2 $C_{12}H_8$

>530	Res	20.2	20.9	---	$ZnCO_3$

releases two moles of carbon dioxide and hydrogen cyanide, and one mole each for dioxygen and ethane. Similar trend in DTA was also observed in the first stage of decomposition. Both the DTA peaks are exothermic in nature. The second stage is comprised of the release of biphenylene leaving behind Co_2O_3 as residue. The theoretical and experimental calculated compositions, for each of the released moiety are well in agreement with each other. All of the three observed DTA peaks exothermic in nature. The degradation of compound **18** is shown in scheme 3.

$C_{30}H_{24}N_2CoO_6 + O_2 \rightarrow 2CO_2 + O_2 + 2HCN + C_2H_6 + C_{24}H_{16}CoO_3$ I Stage

$C_{24}H_{16}CoO_3 \rightarrow 2C_{12}H_8 + Co_2O_3$ II Stage

Scheme 3.27 Thermal degradation of 18

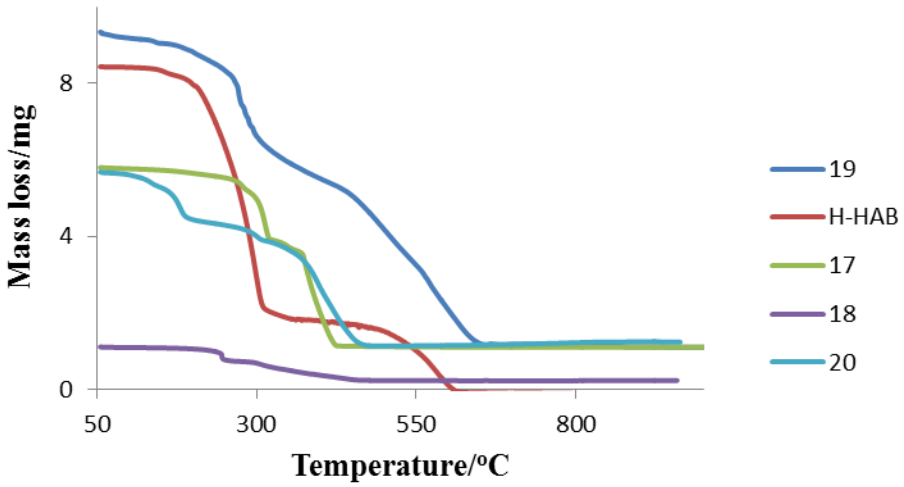

Figure 3.16. Thermogravimetric plots of H-HAB and its metal complexes

In **19** the thermal degradation starts at 230 ^oC and ends at 650 ^oC. The whole process take two stages to complete the pyrolysis. The Td temperature is around 263 ^oC. The first stage of pyrolysis starts around 115 ^oC and completes around 440 ^oC releasing one mole of biphenylene,

two moles of carbon dioxide and one mole of water. This stage is comprised of four endothermic and one exothermic DTA peaks. The second stage of decomposition starts around 440 ^{o}C and completes around 865 ^{o}C. This stage releases one mole of biphenylene, one mole of acetylene, two moles of hydrogen cyanide and one mole of water. This stage represent two exothermic and one endothermic DTA peaks. The degradation is following 5th order kinetics and has 14.02 KJ/mol activation energy. The degradation is following negative entropy representing that the decomposition process is hard to follow. The degradation has high Gibb's free energy of activation and moderate enthalpy change of activation. The degradation is shown below in scheme 3.28:

$C_{30}H_{24}N_2CuO_6 + O_2 \rightarrow C_{12}H_8 + 2CO_2 + H_2O + C_{16}H_{14}N_2CuO_2$ I Stage

$C_{16}H_{14}N_2CuO_2 \rightarrow C_{12}H_8 + C_2H_2 + 2HCN + CuO$ II Stage

Scheme 3.28. Thermal degradation of 19

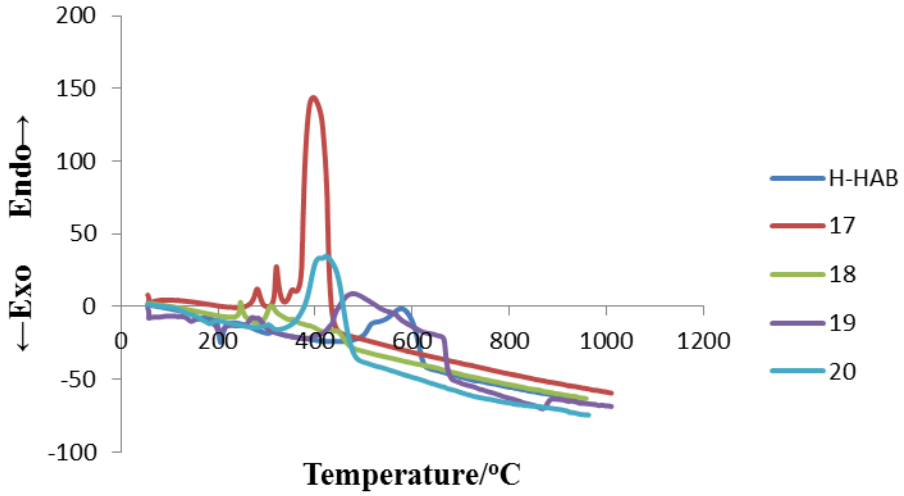

Figure 3.17. Differential thermogravimetric curves for H-HAB and its metal complexes

Thermal decomposition of **20** starts around 200 ^{o}C and completes at 550 ^{o}C. The whole decomposition process is completed in two step degradation process. Unlike the other complexes of the same series zinc carbonate remained as residue. The first stage of degradation releases one mole each of carbon monoxide, dioxygen and ethane accompanied with two moles of hydrogen cyanide gas. Two DTA peaks were observed including one endothermic and the other is exothermic process. The second stage of decomposition is represented by the release of biphenylene moiety. This stage is comprised of one endothermic and one exothermic peak. The exothermic peak may be assigned to the fusion process of two phenylene biradicals. By looking into table 1 it becomes apparent that degradation process is faster unlike the other metal complexes of the same series. Change in enthalpy of activation and Gibb's free energy of activation are also lower than the other compounds. Therefore it can be concluded that zinc complex of H-HAB produces less stable complex with zinc metal ion. The degradation is shown in scheme 3.29.

$C_{30}H_{24}N_2O_6Zn + O_2 \rightarrow CO + O_2 + 2HCN + C_2H_6 + C_{25}H_{16}O_3Zn$ I Stage

$C_{25}H_{16}O_3Zn \rightarrow 2C_{12}H_8 + ZnCO_3$ II Stage

Scheme 3.29 Thermal degradation of 20

From the thermal degradation studies it becomes apparent the order of increasing activation energy is $E^*_{Cu} < E^*_{Zn} < E^*_{Ni} < E^*_{Co}$ and increasing stability is Zn(II) <Ni(II) <Co(II) <Cu(II).

3.4.10 Conclusion

The ligand H-HAB was synthesized by reacting methyl anthranilate with salicyldehyde to yield Schiff base ligand which was characterized by spectroscopic and analytical methods. The ligand was complexed with Co(II), Ni(II), Cu(II) and Zn(II) metal ions to yield $M(HAB)_2$ metal complexes in which the ligand is acting as anionic tridentate O,O,N type of chelating agent. The

ligand and its metal complexes were studied for their enzyme inhibitory activities against acetylcholinesterase, butyrylcholinesterase, urease and α-chymotrypsin enzymes. The Ni^{2+} containing metal complexes is acting as good inhibitor of urease whereas the Cu^{2+} containing metal complex is selective inhibitor of α-chymotrypsin therefore metal based urease and α-chymotrypsin inhibitors using the chelating agent H-HAB can be designed. The copper based metal complex is also acting as good inhibitor of acetylcholinesterase. Zinc complex of HAB^- is found active against butyrylcholinesterase. All the compounds including the Schiff base ligand were found to be weakly active against various pathogenic Gram positive, Gram negative and a fungal strain. The thermal degradation of all the compounds was studied in the temperature range 30-1000 ^oC under static air flow. From this study it is approved that the increasing activation energy order is $E^*_{Cu} < E^*_{Zn} < E^*_{Ni} < E^*_{Co}$ and increasing stability is Zn(II) <Ni(II) <Co(II) <Cu(II).

3.5 Results and discussion of H-HHAQ series

3.5.1 Synthesis of 2-(2-hydroxyphenyl)-3-{[(*E*)-(2-hydroxyphenyl)methylidene]amino}-2,3-dihydroquinazolin-4(1*H*)-one (H-HHAQ)

Yield: 76%, D. pt: 223 ^{o}C, IR: 3500(s), 3387(s), 3155, 3020, 1620(s), 1573(s), 1548, 1514(s), 1450(s), 1367(s), 1325(s), 1280(s), 1257(s), 1172(s), 1132(s), 1060(s), 1035(s), 960(s), 902(s), 866(s), 812(s), 786(s), 740(s), 698(s), 621(s) cm^{-1}, ^{1}H-NMR (400.23 MHz, CD_3OD, 303k): δ = 11.45 (s, 1H, Ar-O<u>H</u>, H27), 9.54 (s, 1H, CH=N, H12), 8.27(s, 1H, NH, H3), 7.54 (d, $^{3}J_{HH}$ = 8, aromatic), 7.29 (s, 1H, N-CH-N, H2) 7.19 (t, $^{3}J_{HH}$ = 7.5, aromatic),7.05(d, $^{3}J_{HH}$ = 7.5, aromatic), 6.83 (d, $^{3}J_{HH}$ = 7.5, aromatic), 6.74 (d, $^{3}J_{HH}$ = 8.5, aromatic), 6.56 (t, $^{3}J_{HH}$ = 7.5, aromatic), 6.35 (s, 1H, Ar-O<u>H</u>, H26), ^{13}C{^{1}H}-NMR (150.9 MHz, CD_3OD, 303k), δ = 165 (C=O, C6), 160.3 (H<u>C</u>=N-, C12), 153(C, C20) , 149.8(CH, C2) , 148.7 (CH, C24), 147.9 (CH, C7), 147.5 (C, C14), 133.8 (C, C4), 132 (CH, C21), 128.1 (C, C5), 127.8 (C, C13), 125.9 (CH, C15), 121.9 (CH, C10), 116.2 (CH, C21), 115.3 (CH, C18) , 115.4 (C, C19), 113.8 (CH, C16, C17, C22, & C23), 108.7 (CH, C8 & C9), Elemental analyses ($C_{21}H_{17}N_3O_3$) Calc. C: 70.18%, H: 4.77%, N: 11.69%, EI-MS *m/z* (%): 382.1168 (88%) $[C_{21}H_{17}N_3O_3+Na]^{+}$, $\wedge_m$ = 0.10 µS.

2.4 Synthesis of [M(HHAQ)$_2$] where M= Co, Ni, Cu and Zn (II) acetates

3.5.2 Bis(2-(2-hydroxyphenyl)-3-{[(*E*)-(2-hydroxyphenyl)methylidene]amino}-2,3-dihydroquinazolin-4(1*H*)-one)cobalt(II) (21)

Yield: 38%, D. pt: 201 ^{o}C, IR: 3240(bd), 3126(bd), 2970(w), 2872(w), 1640(s), 1614(s), 1562(s), 1555(s), 1510(s), 1454(s), 1427(s), 1377(s), 1338(s), 1253(s), 1207(s), 1155(s), 1124(s), 1028(s), 970(s), 893(s), 860(s), 783(s), 750(s), 692(s), 621(s) cm^{-1}, λ_{max}= 480, 590, 640 nm (ε = 67.4, 12.7 M^{-1}cm^{-1}, $^{4}T_1g(F)\rightarrow{}^{4}A_2g$ and the $^{4}T_1g(F)\rightarrow{}^{4}T_1g(P)$, $^{4}T_1g(F)\rightarrow{}^{4}T_2g$), μ_{eff} = 4.98 B.M. Elemental Analysis ($C_{42}H_{32}CoN_6O_6$), Calc. C: 65.03%, H: 4.16%, N: 10.83%, Co: 7.60%, Exp. C: 66.30%,

H: 4.60%, N: 9.59%, Co: 8.12%, EI-MS: *m/z* (%): 775.1709(67%) $[C_{42}H_{32}CoN_6O_6]^+$, $\wedge_m$ = 10.0µS.

3.5.2 Bis(2-(2-hydroxyphenyl)-3-{[(*E*)-(2-hydroxyphenyl)methylidene]amino}-2,3-dihydroquinazolin-4(1*H*)-one)nickel(II) (22)

Yield: 47%, D. pt: 278 ^oC, IR: 3224(bd), 1635(w), 1612(s), 1550(s), 1506(s), 1490(s), 1425(w), 1382(w), 1338(w), 1280(s), 1255(s), 1213(w), 1155(s), 1126(s), 1028(s), 972(s), 931(w), 860(w), 825(w), 792(w), 750(s), 692(s), 615(s), 586(w), 553(w) cm^{-1}, λ_{max}= 780(bd) nm [ε = 12.7 $M^{-1}cm^{-1}$, ^3A_2g (F) $\rightarrow ^3T_1g$ (P), ^3A_2g (F)$\rightarrow ^3T_1g$ (F), ^3A_2g (F) $\rightarrow ^3T_2g$ (F)], μ_{eff} = 2.88 B.M. Elemental Analysis ($C_{42}H_{32}N_6NiO_6$), Calc. C: 65.05%, H: 4.16%, N: 10.84%, Ni: 7.57%, Exp. C: 65.12%, H: 4.32%, N: 9.96%, Ni: 7.12%, EI-MS: *m/z* (%): 774.1731 $[C_{42}H_{32}N_6NiO_6]+$, $\wedge_m$ = 4.3 µS.

3.5.3 bis(2-(2-hydroxyphenyl)-3-{[(E)-(2-hydroxyphenyl)methylidene]amino}-2,3-dihydroquinazolin-4(1H)-one)copper(II) (23)

Yield: 37%, D. pt: 310 ^oC, IR: 3196(bd), 3066(bd), 2972(bd), 2870(w), 1640(s), 1608(s), 1585(w), 1544(s), 1512(s), 1460(w), 1429(s), 1382(bd), 1278(s), 1201(s), 1155(s), 1124(s), 1053(s), 1028(s), 975(s), 893(s), 856(s), 819(s), 781(s), 750(s), 690(s), 665(s), 615(s), 563(s) cm^{-1}, λ_{max}= 820 nm (ε = 34.7 $M^{-1}cm^{-1}$, $T_2g \rightarrow eg$), μ_{eff} = 1.67 B.M. Elemental Analysis ($C_{42}H_{32}CuN_6O_6$), Calc. C: 65.65%, H: 4.13%, N: 10.77%, Cu: 7.57%, Exp. C: 65.12%, H: 4.32%, N: 9.96%, Ni: 7.12%, EI-MS: *m/z* (%): 779.167934 Da, $\wedge_m$ = 87 µS.

3.5.4 bis(2-(2-hydroxyphenyl)-3-{[(E)-(2-hydroxyphenyl)methylidene]amino}-2,3-dihydroquinazolin-4(1H)-one)zinc(II) (24)

Yield: 32%, D. pt: 210 ^oC, IR: 3251(bd), 2968(w), 2870(w), 2366(w), 1687(w), 1614(s), 1585(s), 1564(s), 1510(s), 1427(s), 1384(s), 1334(w), 1278(w), 1253(s), 1205(s), 1155(s), 1124(s),

1028(s), 970(s), 896(s), 858(s), 821(s), 783(s), 748(s), 692(s), 665(s), 615(s), 582(s), 543(s) cm^{-1}, Elemental Analysis ($C_{42}H_{32}N_6O_6Zn$), Calc. C: 64.50%, H: 4.12%, N: 10.74%, Zn: 8.36%, Exp. C: 64.67%, H: 4.82%, N: 10.44%, Zn: 8.12%, EI-MS: *m/z* (%): 780.1669(23) $[C_{42}H_{32}N_6O_6Zn]^+$, $\wedge_m$ = 54 µS.

3.5.5 Analytical and spectroscopic characterization

The novel Schiff base ligand and its first row divalent metal complexes were characterized using different spectroscopic and analytical methods. By looking into the structure of the ligand, it become apparent that the aromatic protons are in the same environment, therefore the ^{1}H-NMR spectrum of the ligand show four doublets and two triplets in the region 6.5-7.6 ppm. Five singlets were also observed along with these aromatic bands. Singlets at 11.45 ppm and 6.34 ppm were assigned to the two hydroxyl groups. The difference in the values was assigned to the probable involvement of one of the hydroxyl group in hydrogen bonding with the nitrogen of the Schiff base linkage. The other hydroxyl group is considered to be freely available as may also be seen in the crystal structure. The HC=N proton appear at 9.45 ppm as expected. A singlet at 8.25 ppm was assigned to cyclic NH group. A singlet at 7.29 ppm was assigned to the cyclic N-CH-N proton. The ^{13}C{^{1}H}-NMR recorded also shown the similar peaks for the secondary and tertiary carbon atoms. The ketonic carbon was observed at 165 ppm, whereas the –CH=N was observed around 160 ppm. C14 and C20 were observed at 147 and 153 ppm respectively which were assigned to the carbon atoms with the hydroxyl groups. Rest of the C-13 spectrum was assigned unambiguously to the respective secondary and tertiary carbon atoms.

The ligand H-HHAQ was reacted with divalent metal ions like Co(II), Ni(II), Cu(II) and Zn(II) and obtained bis-complexes as may be seen in scheme 3.30.

All the complexes were characterized by elemental analyses, ES^+-MS, UV-visible and IR spectroscopic techniques. The elemental analyses supported by the ES^+-MS results confirmed the mentioned compositions.

The IR spectra were also recorded in the region 4000-600 cm^{-1}, which show that the complex formation occur through coordination from Schiff base linkage, hydroxyl group and the cyclic ketone group. In the free ligand and the complexes these linked groups were found to be varying in the range of $\Delta\upsilon$= 40-60 cm^{-1}. In the free ligand the –OH group was observed in the region 3500 cm^{-1} which is further broadened and moved to 3200 cm^{-1} after formation of the complexes. The cyclic ketone group was observed around 1620 cm^{-1} which was moved to 1640cm^{-1} in **21, 22** and **23** whereas in **24** it is moved to 1680 cm^{-1}. Similarly the Schiff base linkage was observed around 1573 cm^{-1} as strong peak which was found around 1620 cm^{-1} in all the complexes. Therefore it was confirmed that these functional groups are involved in the formation of the octahedral metal complexes.

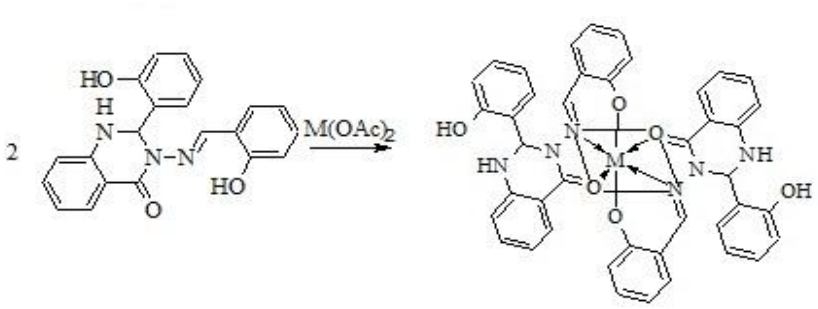

Scheme 3.30 Formation of Octahedral complexes of HHAQ with M(II) ions where M = Co, Ni, Cu and Zn

The UV-Visible spectra of **21, 22** and **23** were recorded in the range 200-800 nm in 1 cm matched quartz cuvette. Compound **21** was found to be absorbing the visible light and gave three peaks at 480, 590 and 640 nm. These peaks were assigned to the ^4T_1g (F) $\rightarrow{}^4A_2g$ and the ^4T_1g (F) $\rightarrow{}^4T_1g$ (P), ^4T_1g (F) $\rightarrow{}^4T_2g$ transitions, respectively. It means that carbonyl group,

hydroxyl ion and the Schiff base linkage are involved in the formation of octahedral. The ligand is responsible for high spin electronic configuration of the complex as suggested by the magnetic susceptibility value. Compound **22** was found to be absorbing in the range of 780 nm as a broad peak which might be encompassing the overlapping peaks. Therefore this broad spectral line may be assigned to the possible transition caused by ^3A_2g (F) $\rightarrow ^3T_1g$ (P), ^3A_2g (F) $\rightarrow ^3T_1g$ (F), and ^3A_2g (F) $\rightarrow ^3T_2g$ (F). The magnetic susceptibility value of the compound shows that the complex is high spin having two unpaired electrons in the eg level. Similarly the copper complex **23** of this ligand is absorbing in the form broad peak in the range of 820 nm. This transition may be due to $T_2g \rightarrow eg$ [2,3]. The complex has μ_{eff} = 1.67 B.M. representing the paramagnetic nature with one unpaired electron in the e.g. level. Complex **24** was found to be diamagnetic in nature, therefore did not correspond to the magnetic effects.

Compounds **21** and **22** were found to be non-electrolyte in nature as depicted from their molar conductance values. Whereas compounds **23** and **24** show small values for the conductance which may be due to the free availability of proton on the non-coordinating hydroxyl group.

3.5.6 Crystal Structure of H-HHAQ

H-HHAQ was crystallised from THF in $C222_1$ space group after keeping the solution for 12hrs at room temperature, yellow block single crystal were isolated. The ORTEP plot (figure 3.18) of H-HHAQ show a Schiff base linkage at C(12) and N(11). C(2), a chiral carbon, may be seen in the formation of distorted heterocyclic ring system connecting both N(3) and N(1). Due to this unique linkage the three aromatic rings lie at angle less than 180^o, creating a three dimensional orientation. The plane produced by aromatic ring C(13)-C(14)-C(15)-C(16)-C(17)-C(18) is therefore lying at 32.45^o to the plane produced by C(4)-C(5)-C(7)-C(8)-C(9)-C(10) aromatic

ring. C(2) was found to be 32.49^{o} below the plane produced by C(5)-C(7)-C(8)-C(9)-C(10) aromatic ring.

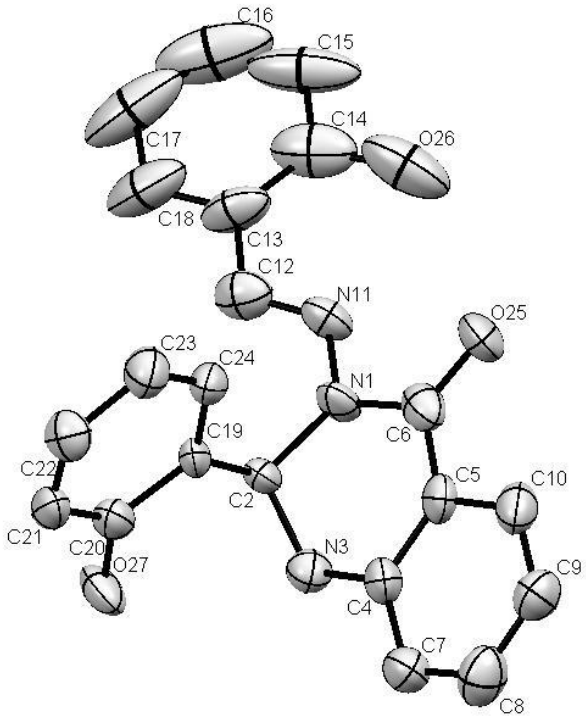

Figure 3.18. Molecular structure of H-HHAQ. Thermal ellipsoids are shown at 50% probability. H atoms are omitted for clarity reasons.

Therefore it can be concluded that C(2) is involved in the distortion of both the aromatic rings. Similarly the plane produced by N(3)-C(4)-C(5)-C(6)-N(1) is also 32.49^{o} above than C(2). The distance between C(12)-N(11) is 1.292 A^{o} which is equal to the normal bond length of imine linkage as found in (E)-4-bromo-2-[(2-chloro-3-pyridyl)-iminomethyl]phenol (1.291 A^{o}) [14]. The C(2)-N(1) and C(2)-N(3) bond lengths are 1.458 A^{o} and 1.452 A^{o} respectively with a 0.006

A^o difference. These bond lengths may be compared with 1.437 A^o in 2,2',2",2"'-(1,4-Phenylenedinitrilo)tetraacetic acid dehydrate [18].

3.5.7 Enzyme inhibitory activities

The H-HHAQ and its complexes were studied for their inhibitory activities against each selected enzymes in optimum conditions and the results are shown in table 3.22. Based upon metallic center the enzymes were chosen, like copper and zinc were found to be inhibiting acetyl cholinesterase and butyrylcholinesterase, cobalt can also be included in this category, whereas the nickel enzymes are always inhibitory in nature to urease (if in case they are active). α-Chymotrypsin was chosen to see the selectivity of the inhibition by the nickel complex, if nickel complex is only inhibiting urease then the ligand if inhibits the α-Chymotrypsin**,** the drug will be selective urease inhibitor and hence a better antiulcer agent. Here we are reporting the enzyme inhibitory activities of the metal complexes of H-HHAQ series. The table show that nickel complex **22**, is acting as selective inhibitor for the inhibition of α-Chymotrypsin and butyrylcholinesterase. Copper based metal complex **23**, is showing promising inhibition of the butyrylcholinesterase with weak activities against acetyl cholinesterase. Compound **24** is a zinc based metal complex of H-HHAQ, inhibits acetyl cholinesterase but the activities are very low. Therefore compound **22** and **23** may act as drug for the treatment of diseases related to urease and butyrylcholinesterase adding to the metal based drugs.

Table 3.22: In Vitro inhibition activities of H-HHAQ and its metal complexes against urease, α-chymotrypsin, acetyl cholinesterase and butyrylcholinesterase

Compounds	IC_{50} for urease (µM)±SEM	IC_{50} for α-Chymotrypsin (µM)±SEM	IC_{50} for acetyl cholinesterase (µM)±SEM	IC_{50} for butyrylcholinesterase (µM)±SEM
H-HHAQ	---	---	---	---
21	---	---	---	---
22	13±1.22	---	---	53±0.023
23	---	---	169±0.025	87±0.136
24	---	---	137±4.32	---
Standard	0.5±0.01 **(galanthamine)**	8.5±0.5 **(galanthamine)**	21± 0.011 **(Thiourea)**	5.71± 0.13 **(Chymostatin)**

3.5.8 Antimicrobial activities

Following the trend in enzyme inhibition compounds **22, 23** and **24** were also found to be active against one or more tested microbial strains. These strains included the Gram positive, Gram negative and a fungal strain. Compound 21 was tested and found to be active against Candida and Bacillus atrophies. **22** was found active against Candida and Bacillus, whereas compound **23** demonstrated good results against E. coli and Agrobacterium. Similar activities were shown by **24** which was also found to be active against Candida and Bacillus atrophies. All the compounds, except the ligand, have shown low to weak activities against one or more microbial strains as shown in table 3.23.

Table 3.23: In Vitro antimicrobial activities of H-HHAQ and its metal complexes against different animal and plant pathogens

Compounds	*Bacillus atrophaeus (cm)*	*Bacillus subtilis (cm)*	*Klebsiella pneumoniae (cm)*	*Salmonella typhus (cm)*	*Pseudomonas aeruginosa (cm)*	*Escherichia coli (cm)*	*Staphylococcus aureus (cm)*	*Candida albican (cm)*	*Agrobacterium tumefaciens (cm)*	*Erwinia carotovora (cm)*
H-HHAQ	---	---	---	---	---	---	---	---	---	---
22	2.1	1.7	---	---	1.4	1.6	1.7	2.5	1.7	1.1
21	1.7	1.5	2.8	---	1.4	2.0	2.1	1.8	1.6	---
23	1.2	1.5	1.0	---	1.5	2.5	1.4	2.0	2.4	1.1
24	2.9	2.5	---	---	1.5	2.1`	1.6	2.1	2.5	---
Standard	2.5	2.6	2.9	4.2	3.6	3.8	3.4	1.6	1.5	2.6

Gram positive bacteria: *Bacillus atrophaeus*, *Bacillus subtilis*, *Staphylococcus aureus*, standard used was erythromycin in 6 µM

Gram negative bacteria: *Klebsiella pneumoniae*, *Salmonella typhus*, *Pseudomonas aeruginosa*, *Escherichia coli*, *Agrobacterium tumefaciens*, *Erwinia carotovora*, standard used was ciprofloxacin in 6 µM

Fungal Strain: *Candida albican*, standard used was clothrimazol in 6 µM

3.5.9 Thermodynamics and Thermal studies

Thermal degradation of the ligand H-HHAQ and its divalent metal complexes were evaluated in the temperature range 30-1000 ^{o}C. The thermal pyrolysis in the form of TG curves, shown in figure 1 and the corresponding DTA peaks are shown in figure 2. Based upon the Td temperatures the order of stability may vary viz; 220 ^{o}C, 225 ^{o}C, 230 ^{o}C and 550 ^{o}C for **21, 22, 23** and **24** respectively. For ligand H-HHAQ the Td temperature is 245 ^{o}C. TG and DTA curves are shown in figure 3.19 and 3.20 respectively for H-HHAQ and its metal complexes.

Table 3.24: Kinetic and thermodynamic parameters of H-HHAQ and its metal complexes

Compound	**Ts in K**	**Ea, KJ/mol**	**ΔH, KJ/mol**	**$\Delta G^{\#}$, KJ/mol**	**$\Delta S^{\#}$, $Jmol^{-1}K^{-1}$**	**Order of reaction, n**
H-HHAQ	526.5	8.75	4.37	136.30	-250.56	5
21	501.6	20.30	16.1	138	-243.03	∞
22	775.5	12.00	5.5	202	-253.33	2
23	560	20.8	16.2	154.76	-247.5	5
24	855.7	31.65	24.53	248.74	-262.02	1/2

By comparing the data in table 3.25, it is clear that the ligand and all its metal complexes decompose in two step degradation process. The difference between the ligand and the metal complexes lie in the final step, for the ligand no residue is found whereas the complexes decompose leaving behind metal or the corresponding oxides as residues. From table aaa it is apparent that ligand have 8.75 KJ/mol activation energy and follow

Table 3.25: Thermo analytical results of H-HHAQ and its complexes

Compound	TG Temp. range/ ^{o}C	Stage	Mass loss % Calc.	Mass loss % Found	DTA	Moiety evolved
H-HHAQ	30-400	I	67.3	66.2	(+)5, (-)18,	N_2, CO, $C_{12}H_{10}O_2$
	400-600	II	32.3	33.8	(-)22, (-)25	C_6H_4, C_2H_2, $1/2N_2$, $1/2H_2$
21	30-280	I	18.8	17.0	(-)2, (+)8	$C_{12}H_8$
	280-620	II	69.6	68.1	(+)32, (-)15	2 $C_{12}H_{10}O_2$, 2CO, C_2H_2, $3/2N_2$, H_2
	>620	Res	9.6	11.3	---	CoO
22	30-390	I	39.9	39.2	(-)12, (-)9, (-)18	$C_{12}H_8$, 3N2, C_2H_2, 2CO
	390-640	II	47.9	47.2	(-)38, (+)1, (-)14, (-)29	2 $C_{12}H_{10}O_2$
	>640	Res	10.5	11.4	---	NiO
23	30-450	I	55.6	56.0	(-)5.8, (-)5.6, (-)15.3, (-)18	$C_{12}H_8$, $1/2N_2$, 2CO, $2C_2H_2$, N_2O_4
	450-600	II	48.2	48.2	(-)12.0	2 $C_{12}H_{10}O_2$
	>600	Res	10.1	10.9	---	CuO
24	30-380	I	47.9	47.5	(-)0.5, (+)5.6, (-)5.3	$C_{12}H_8$, $3N_2$, 2CO, $2C_2H_2$
	380-680	II	48.8	49.9	(-)5.0	2 $C_{12}H_{10}O_2$
	>680	Res	6.8	5.1	---	Zn

the 5^{th} order kinetics for its decomposition. The negative entropy value and high Gibb's free energy term represent that decomposition is not favored for the parent compound. H-HHAQ follows the two step degradation, including the formation of free radicals like phenol and benzene. The two phenol free radicals combine together to produce the fused biphenylenediol. Along with bipheneylenediol one mole of carbon monoxide gas and one mole of nitrogen gas are released in the first step. In the second step the benzene free radical produces the cyclohexa-1,3-diene-5-yne as a product along with one mole of acetylene, half mole of dinitrogen and dihydrogen gases. The degradation route is shown below in scheme 3.31.

$C_{21}H_{17}N_3O_3 \rightarrow C_{12}H_{10}O_2 + CO + N_2 + C_8H_7N$ I Stage

$C_8H_7N \rightarrow C_6H_4 + C_2H_2 + 1/2H_2 + 1/2N_2$ II Stage

Scheme 3.31 Thermal degradation of H-HHAQ

Compound **21** follow thermal degradation in two steps, in the first step the two free radicals of bezene are produced which combine together to produce bipheylene. There are two exothermic DTA peaks for the first step of pyrolysis. In the second stage two moles of acetylene, 3/2 moles of nitrogen, and two moles of biphenylenediol are produced. Cobalt oxide remains as residue. There are two exothermic DTA peaks observed for the second step of pyrolysis. It has negative entropy of activation, and high value of Gibb's free energy of activation and reasonable enthalpy of activation. According to Horowitz method **21** follows infinite order of degradation. The degradation route is shown below in scheme 3.32:

$C_{42}H_{32}N_6O_6Co \rightarrow C_{12}H_8 + C_{30}H_{24}CoN_6O_6$ I Stage

$C_{30}H_{24}CoN_6O_6 + O_2 \rightarrow 2C_{12}H_{10}O_2 + 2C_2H_2 + 3/2N_2 + CoO$ II Stage

Scheme 3.32 Thermal degradation of 21

Compound **22** starts decomposition at 220 ^{o}C and ends at 650 ^{o}C producing nickel oxide as residue. It also follows two steps degradation; first step is the same step to compound **21**, with the production of biphenylene. This step of degradation is represented by the production of two intermediate free radicals of benzene moiety. Apart from it two moles each of carbon monoxide and acetylene and three moles of dinitrogen, are also produced. Three DTA peaks are observed for this stage, including one exothermic and two endothermic peaks. The fusion of two benzene free radicals to produce biohenylene is endothermic process. The second stage of degradation is represented by the production of the same phenol free radicals which may combine together producing two moles biphenol as whole in the degradation process. Nickel oxide remains as residue in the whole degradation process of **22**. The second stage is represented by marked exothermic DTA peak having the other two as shoulder counterparts. Activation energy of **22** is lower than **21** and follow second order degradative kinetics. Entropy value is more negative than **21** and also the Gibb's free energy of activation is also high depicting the stable nature of the parent compounds. The degradative route is shown in scheme 3.33:

$C_{42}H_{32}N_6NiO_6 \rightarrow C_{12}H_8 + 3N_2 + 2CO + 2C_2H_2 + C_{24}H_{20}NiO_4$ I Stage

$C_{24}H_{20}NiO_4 + O_2 \rightarrow 2C_{12}H_{10}O_2 + NiO$ II Stage

Scheme 3.33 Thermal degradation of 22

For **23** the oxidative degradation starts 450 ^{o}C with the release of the same biphenylene product after the reaction between the two benzene free radicals with each other. It is accompanied with the release of two moles each of the acetylene and carbon monoxide gases. Apart from it one mole each of nitrogen dioxide and dinitrogen tetra oxide which may further undergoes decomposition adding to the molar quantity of nitrogen dioxide. This stage of pyrolysis depicts four exothermic DTA peaks. The second and final stage of pyrolysis is accompanied by the release of biphenol moiety leaving behind the copper

oxide as residue. This step has got one huge exothermic DTA peak. If table 1 is consulted for the thermodynamic parameters it can be seen that its entropy of activation is negative than **21** and positive than **22**. Same trend can be seen for Gibb's free energy of activation; while the enthalpy change of activation is almost equal to **21**. The activation energy is higher than both **21** and **22** and follow 5^{th} order kinetics. The decomposition of the compound may be seen in scheme 3.34:

$C_{42}H_{32}CuN_6O_6 \rightarrow C_{12}H_8 + 1/2N_2 + 2CO + 2C_2H_2 + NO_2 + 2N_2O_4 + C_{24}H_{20}CuO_4$ I Stage

$C_{24}H_{20}CuO_4 + O_2 \rightarrow 2C_{12}H_{10}O_2 + CuO$ II Stage

Scheme 3.34 Thermal degradation of 23

Decomposition for **24** starts around 230 ^oC and completes at 680 ^oC. The whole degradation of the compound takes place in two steps. In the first step biphenylene is produced by the fusion of benzene free radicals along with the release of three moles of dinitrogen, two moles of acetylene and two moles of carbon monoxide. The whole degradation is comprised of four DTA peaks, all of them are exothermic. It includes three exothermic DTA peaks for the first stage of decomposition and one huge DTA peak for the second stage of decomposition. The second stage of decomposition releases the biphenol moiety, whereas zinc remains as residue in the metallic state. The degradation is shown in the following scheme 3.35:

$C_{42}H_{32}N_6O_6Zn \rightarrow C_{12}H_8 + 3N_2 + 2CO + 2C_2H_2 + + C_{24}H_{20}O_4Zn$ I Stage

$C_{24}H_{20}O_4Zn \rightarrow 2C_{12}H_{10}O_2 + Zn$ II Stage

Scheme 3.35 Thermal degradation of 24

By comparing the data in table 3.26 it becomes clear that the values of activation energy, change in entropy of activation, change in Gibb's free energy of activation, change in enthalpy of activation are high for **24** than any other complex of the same ligand.

Therefore zinc produces the stable complex with H-HHAQ, representing that the degradation is less favoured in this case.

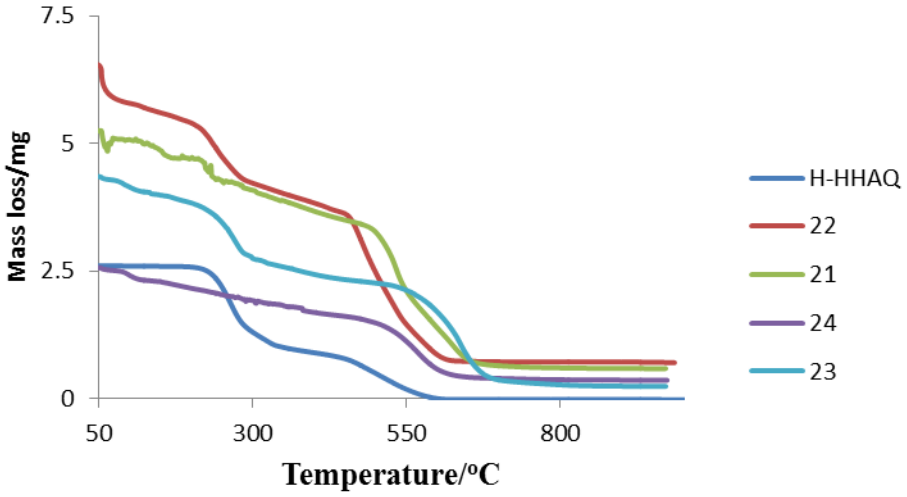

Figure 3.19. Thermogravimetric plots of H-HHAQ and its metal complexes

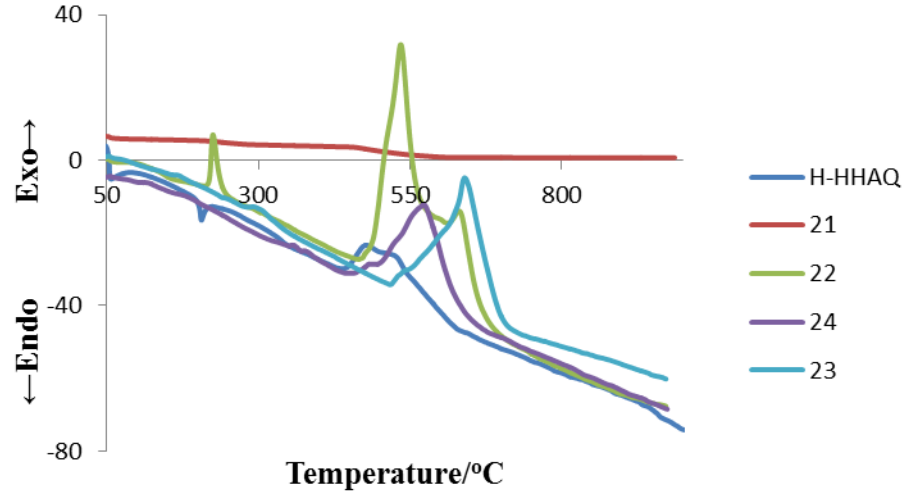

Figure 3.20. Differential thermogravimetric curves for H-HHAQ and its metal complexes

3.5.10 Conclusion

The novel Schiff base ligand H-HHAQ was synthesized from aminobenzhydrazin which is actually a heterocyclic derivative of salicyldehyde. It was complexed with divalent

metal ions like Co(II), Ni(II), Cu(II) and Zn(II) to yield octahedral metal complexes. The ligand and its metal complexes were completely characterized by different analytical and spectroscopic techniques and was assigned composition and structures. Apart from it the ligand was also characterized by single crystal studies and it was found out that the compound is having intermolecular and intramolecular hydrogen bonding responsible for crystal packing of the ligand. All the compounds were studied for their inhibiting activities for acetylcholinesterase, butyrylcholinesterase, urease and α-chymotrypsin enzymes. It was found out that 22 has very strong inhibiting activity for acetylcholinesterase viz; 13±1.22 µM±SEM and butyrylcholinesterase 53±0.03 µM±SEM, 23 is also showing some activity against acetylcholinesterase and butyrylcholinesterase (87±0.138 µM±SEM whereas, 24 is also show weak activity for acetylcholinesterase. Therefore it becomes apparent that the metal based drug for the treatment of Alzheimer disease can be designed. All the compounds tested for their In Vitro antimicrobial activities were found very weak in activities. The thermal degradation of the compounds reveal that the order of decreasing activation energies is $E^*_{Zn}<E^*_{Cu}<E^*_{Ni}<E^*_{Co}$ and decreasing stability is Zn(II) <Cu(II) <Co(II) <Ni(II).

3.6 References

[1] a. H. B. Gray and C.J. Ballhausen, *J. Am. Chem. Soc.*, **1963**, *85* (3), 260.

b. H. B. Gray, *Trans. Met. Chem.*, **1965**, 1, 239.

[2] H. Ünver and Z. Hayvalı, *Spectrochim. Acta* Part A: **2010**, 75, 782.

[3] S.N. Pal and S. Pal, *Inorg. Chem.*, **2001**, 40, 4807.

[4] L. W. Juanita, F. M. Selwyn, L. Anders, H. Mikael, J. Susan, *Inorg. Chim. Acta*, **2008**, 361(7), 2094.

[5] I. B. Ashley, *Neurobiology* of *Aging*, **2002**, 23(6), 1031.

[6] Q. Yu, H. W. Holloway, T. Utsuki, A. Brossi, N. H. Greig, *J. Med. Chem.* **1999**, 42, 1855.

[7] N.H. Greig, K. Sambamurti, Q.-S. Yu, T.A. Perry, H.W. Holloway, F. Haberman, A. Brossi, D.K. Ingram, D.K. Lahiri, Butyrylcholinesterase: its selective inhibition and relevance to alzheimer's disease therapy. in: E. Giacobini (Ed.), Butyrylcholinesterase: Its Function and Inhibitors, first ed. Martin Dunitz, *Taylor and Francis Group Plc, United Kindom*, **2003**, 69.

[8] C. Geula, S. Darvesh, *Drugs Today*, **2004**, 40711.

[9] N.H. Greig, T. Utsuki, Q. Yu, X. Zhu, H.W. Holloway, T. Perry, B. Lee, D.K. Ingram and D.K. Lahiri. *Current Medical* Research and *Opinion*, **2001**, 17, 159.

[10] G. F. Makhaeva, A.Y. Aksinenko, V. B. Sokolov, O. G. Serebryakova, R. J. Richardson, *Bioorg. Med. Chem. Let.*, **2009**, 19(19), 5528.

[11] E. Giacobini. *Pharmacol. Res.*, **2004**, 50, 433.

[12] N.H. Greig, T. Utsuki, D.K. Ingram, Y. Wang, G. Pepeu, C. Scali, Q.S. Yu, J. Mamczarz, H.W. Holloway, T. Giordano, D. Chen, K. Furukawa, K. Sambamurti, A. Brossi and D.K. Lahiri. *Proc. Natl. Acad. Sci.USA.*, **2005**, 102, 17213.

[13] É. Józsa, K. Ősz, C. Kállay, P. de Bona, C. A. Damante, G. Pappalardo, E. Rizzarelli and I. Sóvágó, *Dalton Trans.* **2010**, 39, 7046.

[14] F. Musiani, E. Arnofi, R. Casadio and S. Ciurli, *J. Biol. Inorg. Chem.*, **2011**, 6(3), 300.

[15] Zhang L, Mulrooney SB, Leung AF, Zeng Y, Ko BB, Hausinger RP, Sun H. *Biometals*. **2006**, 19(5), 503.

[16] S.Schindler, Reactivity of Copper(I) Complexes Towards Dioxygen, *Eur.J. Inorg. Chem.* **2000**, 2311.

[17] A.C. van de Vusse, S.G. Stomp-van den Berg, A.H. Kessels and W.E. Weber, *BMC Neurol*, **4 (2004),** 13.

[18] C. K. Özer, H. Arslan, D. V. Derveer and N. Külcü, *Molecules.*, **2009**, *14*, 655.

PART II

CHAPTER 4

FLUOROUS CATALYST RECYCLING UTILISING HIGHLY FLUORINATED ZINC COMPOUNDS: RING OPENING POLYMERISATION OF ε-CAPROLACTONE

4.1 Introduction

Arguably, the major disadvantage of homogeneous catalysis is catalyst recovery. This is particularly important if costly precious metal or synthetically complex ligand architectures are present in the (pre)catalyst. Therefore catalyst recycling or recovery has become an important topic of interest, and there are many methods available in literature [1]. One concept that has gained popularity is in the use of biphasic systems, and the temperature dependent miscibility properties of fluorinated and organic solvents have been taken advantage in the design of fluorophilic catalysts [2]. Typically, a ligand is appended with one or more fluorous 'pony-tails' to impart substantially enhanced solubility in a fluorous solvent, and above specific temperatures the fluorous and organic phases become miscible and the catalysis has the advantages of homogeneous catalysis, in particular selectivity and activity. Upon cooling, the solutions phase separate and the fluorous catalyst partitions into the fluorous phase whilst the products remain in the organic phase. Phosphine ligands with fluorous 'pony-tails' have become popular since the first report by Horva´ th and Rabai [3] and there are now a plethora of aryl phosphine ligands with one or more long chain fluorous group substituted onto the aryl ring with a suitable spacer to modulate the electronic effects [4] of the perfluoroalkyl chain. Perfluoroalkyl diarylphosphines $RfPAr_2$ are also popular modular ligands [5]. One

particularly elegant application of this has been reported by Gladysz and co-workers where a labile fluorinated phosphine ligand on a Grubbs type pre-catalyst has more solubility in a fluorous phase, thus retarding the rate of re-coordination and ultimately increasing the activity of the catalyst which resides exclusively in the organic phase [6]. Fluorous techniques for organic transformations are also on the increase [7]. However the disadvantages of this approach are the environmental impact and bio-accumulation of typical fluorinated solvents [8] and, for potential commercial processes, the cost. This has been mitigated to an extent by the development of thermomorphic catalysts. It has been noted that very heavy fluorinated compounds show appreciable solubility in organic solvents only at high temperatures, and upon cooling these precipitate out of solution allowing for easy catalyst recovery. This has begun to be exploited in a number of organic transformations [9]. Interestingly, the use of fluorous supports apparently aids this precipitation [10], and we have recently shown that noncovalent C–F--F–C interactions need to be considered [11]. Herein, we report on a new concept of catalyst recovery, whereby the quenching reagent added to release the polymer from the metal centre contains a fluorous group, which enables catalyst recovery via solvent extraction. We have chosen the ring opening polymerisation of cyclic lactones for our initial investigations as the initiating species is typically a metal alkoxide [12], whilst quenching the reaction is carried out by the addition of acidified organic alcohols. The mechanism(s) are well known and the presence of the initiating alkoxide as an end group suggests a coordination–insertion type mechanism that is prevalent for metal-alkoxide based catalysts. It occurred to us that quenching the reaction with a fluorinated alcohol would produce the polymer and a ‘‘RfO-M’’ moiety, which would selectively partition into a fluorinated solvent and could be separated from the reaction mixture and polymer. The addition of further aliquots of monomer to the recovered catalyst should be able to re-

initiate polymerisation. Poly(caprolactone) is an important polymer as it is biodegradable and has found applications in various fields such as scaffolds in tissue engineering, long-term drug delivery, microelectronics, adhesives and in packaging [12]. Due to this, a large number of catalysts and catalytic systems, spanning virtually the whole periodic table have been investigated, with zinc, aluminium and magnesium compounds prevalent. However, there are no examples known using fluorinated catalysts. Herein we report our initial investigations into fluorous recycling of catalysts for the ring opening polymerisation of e-caprolactone.

4.2 Experimental

All manipulations were carried out using standard Schlenk and glove box techniques under an atmosphere of high purity argon. The solvents like toluene and THF were refluxed, dried and degassed prior to use. Toluene and THF were distilled over potassium, whilst diethyl ether was distilled over Na/K. e-Caprolactone, BnOH, $CF_3(CF_2)_5CH_2CH_2OH$, 1,3-bis(trifluoromethyl)benzene, perfluoromethylcyclohexane and FC-72 were distilled over CaH_2 immediately before use. $[Zn\{N(SiMe_3)_2\}_2]$, $[Zn(OAr)_2(THF)_2]$ [16] and $CF_3(CF_2)_5CH_2CH_2CO_2H$ [19] were prepared according to the literature methods. ^1H, ^{13}C and ^{19}F NMR spectra were recorded on a Bruker AV400 spectrometer operating at 400.13 (^1H), 376.55 (^{19}F) and 100.65 (^{13}C) MHz, and were referenced to the residual ^1H or ^{13}C resonances of the solvent used or external $CFCl_3$ (^{19}F). Infrared spectra were recorded on a Perkin Elmer Spectrum 100 with an ATR accessory. Mass spectra were measured on a MALDI QTOF Premier MS system. GPC data was recorded on a Varian ProStar with a 350 RI detector using a PLgel 5 mm MIXED-D column and calibrated with EasiCal polystyrene standards. Melting points were determined in sealed glass capillaries under argon and are uncorrected. Fluorinated solvents were acquired from Fluorochem or Acotta (FC-72) and all other reagents from

commercial sources and used as received. Partition coefficients were calculated via 19F NMR spectroscopy following the method of Gladysz [20].

4.2.1. $\{CF_3(CF_2)_5CH_2CH_2CO_2\}_2Zn$ (25)

To a solution of $[Zn\{N(SiMe_3)_2\}_2]$ (0.50 g, 1.30 mmol) in THF (10 cm^3) was added a solution of $CF_3(CF_2)_5CH_2CH_2CO_2H$ (1.10 g, 2.8 mmol) in THF (10 cm^3) and the reaction mixture stirred for 3 h. The solvent was removed in vacuo and the residue washed with hexane (2-10 cm^3) then extracted into FC-72. Filtration and removal of the solvent afforded an off-white powder that was recrystallised from 1,3-bis(trifluoromethyl)benzene (0.79 g, 72%).

^1H NMR ($CDCl_3$/1,3-bis(trifluoromethyl)benzene): 1.34 (m, CH_2CF_2), 1.75 (t, $^3JH–F$ = 18.3 Hz, CH_2CO_2); $^{13}C\{^1H\}$ NMR ($CDCl_3$/1,3-bis(trifluoromethyl)benzene): 18.9 (s, CH_2CO_2); 29.8 (t, $^2J_{C–F}$ = 23 Hz, CF2CH2), 118–119 (m, CF_3 and CF_2), 153.6 (s, CO_2); ^{19}F NMR ($CDCl_3$/1,3-bis(trifluoromethyl)benzene): -117.60 (CH_2CF_2), -124.92 (CF_2), -125.93 (CF_2), -126.33 (CF_2), -129.34 (CF_2), -84.48 (CF_3); n (ATR, cm^{-1}): 2943 (w), 1630 (s), 1549 (m), 1490 (m), 1457 (m), 1343 (w), 1310 (w), 1246 (w), 1133 (m), 1108 (m), 1078 (m), 982 (m), 944 (w), 763 (s), 700 (s); $C_{18}F_{26}H_8O_4Zn$ requires: C 25.51%, H 0.95%, found C 26.97%, H 1.65%.

4.2.2. $\{CF_3(CF_2)_5CH_2CH_2O\}_2Zn(OEt_2)_2$ (26)

To a solution of $[Zn\{N(SiMe_3)_2\}_2]$ (0.50 g, 1.3 mmol) in Et_2O (10 cm^3) was added a solution of $CF_3(CF_2)_5CH_2CH_2OH$ (1.04 g, 2.8 mmol) in Et_2O (10 cm^3) and the reaction mixture refluxed for 3 h. The solvent was removed in vacuo and the residue washed with hexane (2-10 cm^3) then extracted into FC-72. Filtration and removal of the solvent afforded an off-white powder that was recrystallised from 1,3-bis(trifluoromethyl)benzene (0.88 g, 86%).

Mpt = 168–172 ^{o}C (dec); ^{1}H NMR (C_6D_6, 400.13 MHz) 3.74 (m, 4H, OCH_2), 2.20 (m, 4H, CH_2CF_2), 3.34 (q, 8H, $^{3}J_{H–H}$ = 7.3 Hz, Et_2O), 1.19 (t, 12H, $^{3}J_{H–H}$ = 7.2 Hz, Et_2O); $^{13}C\{^{1}H\}$ NMR (C_6D_6, 100.65 MHz), 118–119 (m, CF_3 and CF_2), 56.1 (s, CH_2O), 31.3 (t, 2JC–F = 20 Hz, CF_2CH_2); ^{19}F NMR (C_6D_6, 376.55 MHz): -117.70 (CH_2CF_2), -127.73 (CF_2), -125.71 (CF_2), -126.79 (CF_2), -130.41 (CF_2), -85.68 (CF_3); n (ATR, cm^{-1}): 2917 (w), 1672 (w), 1610 (w), 1583 (w), 1517 (m), 1467 (m), 1414 (m), 1379 (m), 1329 (s), 1211 (w), 1102 (w), 1016 (s), 922 (w), 866 (s), 742 (w), 678 (m); $C_{24}H_{28}F_{26}O_4Zn$ requires: C 30.67%, H 3.00%, found C 31.95%, H 3.10%.

4.2.3. Polymerisation experiments

In a typical experiment 600 equivalents of e-caprolactone was added to a solution of the catalyst (1.5 mmol) in THF (10 cm^3) held at 60 ^{o}C and the reaction stirred for 1 h. To this mixture was added the fluorous quenching agent (3.75 mmol of $RfCO_2H$ or RfOH) in 1,3-bis(trifluoromethyl)benzene (15 cm^3) and the reaction stirred for 15 min. The solution was cooled, filtered to isolate the polymer and the phases separated to recover the catalyst in the fluorous layer. The polymer was washed copiously with MeOH and dried in vacuo before analysis by GPC.

4.3. Results and discussion

Our initial investigations began with the zinc bis-carboxylate complex [$(RfCO_2)_2Zn$] (Rf = $CF_3(CF_2)_5CH_2CH_2$), which is readily prepared by the addition of the perfluorinated acid to [$Zn\{N(SiMe_3)_2\}_2$] (Eq. (1)). Multinuclear NMR and infrared spectroscopy confirm the formulation, particularly the absence of resonances due to the $N(SiMe_3)_2$ groups, indicating that both amides have been replaced. The addition of one equivalent of benzyl alcohol affords the zinc carboxylate alkoxide complex [$RfCO_2ZnOBn$] (Scheme 4.1), which has been characterised by in situ ^{1}H NMR spectroscopy; the benzyl methylene resonates at dH = 5.13 ppm. e-Caprolactone (25 equivalents) was then added to the NMR

tube and the NMR spectrum recorded. Insertion of the monomer into the Zn–OBn bond is observed, with a shift in the benzyl methylene resonance to dH = 5.48 ppm. No evidence of insertion into the zinc–carboxylate bond was observed, which is in line with the observations that acetate groups are poor initiators for the ring opening polymerisation of cyclic lactones [13]. After 1 h polymer is observed to precipitate out of the solution. In order to confirm that the OBn group is the initiator, this was quenched with acidified MeOH and the polymer analysed by MALDI-ToF mass spectrometry and NMR spectroscopy, with the benzylic methylene resonating at dH = 5.08 ppm.

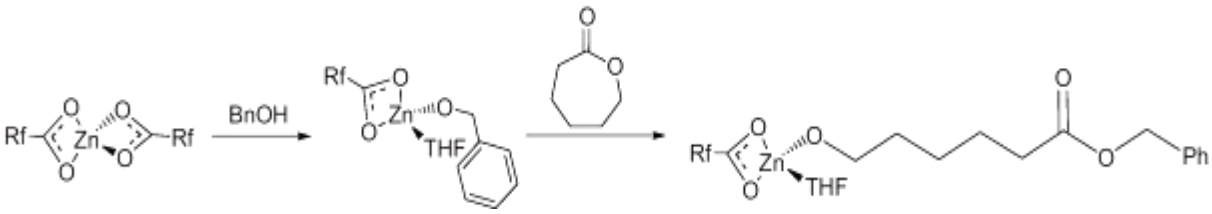

Scheme 4.1 Ring opening polymerisation catalysed by [$(RfCO_2)_2Zn$]

Our hypothesis is that if this catalyst is quenched by the addition of an equivalent of $RfCO_2H$ in a fluorous solvent then the pre-catalyst will be regenerated and preferentially extracted into the fluorous phase. For this to effectively occur the partition coefficient– the preference for partitioning into the fluorous phase over the organic phase – must be high. The measured partition coefficient for the zinc carboxylate is 86.1:14.9 in perfluoromethylcyclohexane: toluene. Therefore it may be predicted that this pre-catalyst would not be efficiently recycled and, when the quenching experiment is conducted, NMR spectroscopy confirms that the pre-catalyst is recovered in the fluorous layer (1,3-bis(trifluoromethyl)benzene) [14], but only in 43% mass balance relative to the first polymerisation. The polymer was isolated and characterised by GPC, which is reported as run 1 in Table 4.1. The calculated and measured number-averaged molecular weights (Mn) are similar which suggests that the polymerisation goes towards completion and the narrow molecular weight distribution suggests that the polymerisation is well controlled

with little transesterification side reactions. Upon addition of BnOH and ecaprolactone to the isolated pre-catalyst, very little polymer is produced which has a lower molecular weight (run 2 in Table 4.1). A further quench and catalyst recovery cycle afforded a negligible amount of an oil that had a Mn of 427 (run 3 in Table 4.1). It is worthy of note that bulk polymerisation of e-caprolactone using [$Zn(OAc)_2$] has been reported with a PDi of 1.10–1.40 [15]. We next turned our attention to zinc aryloxides and alkoxides as these are well known to be superior catalysts for this reaction. We attempted two different strategies to examine catalyst recovery. Firstly, a well-defined non-fluorous zinc phenoxide was used without an initiator and the catalyst quenched using a fluorous alcohol. The hypothesis is that this affords a fluorous zinc species [$(RfO)_2Zn$], that could be extracted using fluorous solvents. Subsequent protonolysis of the Zn–ORf bond with ArOH would regenerate the catalyst (Scheme 4.2).

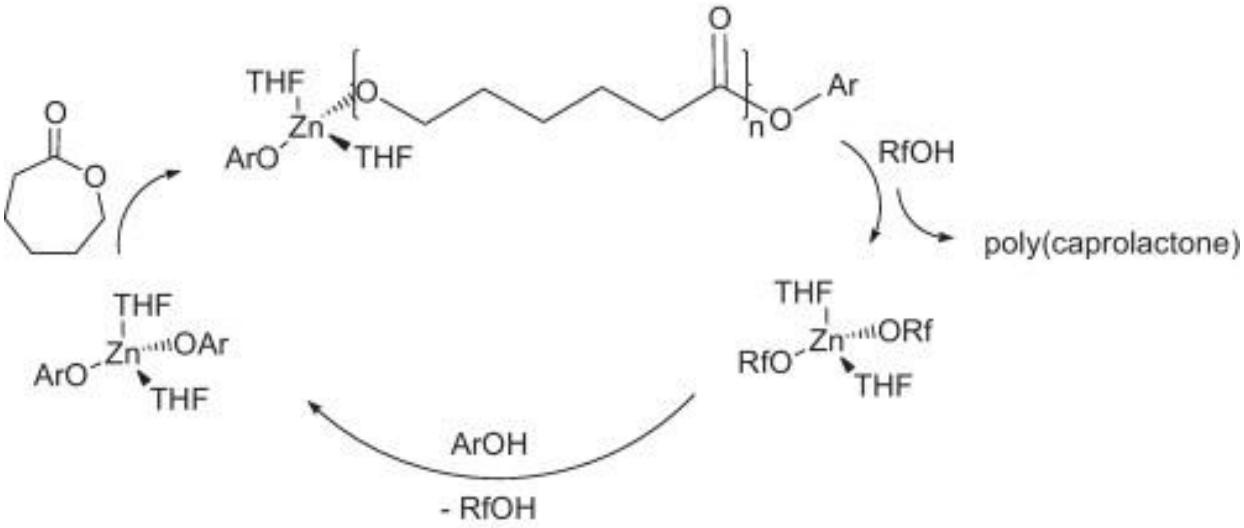

Scheme 4.2 Ring opening polymerisation catalysed by [$(ArO)_2Zn(THF)_2$].

For these experiments we chose the zinc phenoxide complex [$Zn(OAr)_2(THF)_2$] (Ar = 2,6-t- $Bu_2C_6H_3$) as it is known to be a good catalyst for the copolymerisation of epoxides and CO_2 [17]. Addition of ecaprolactone to a THF solution of the catalyst at 60 ^oC afforded a polymer after 1 h. To this solution was added an excess of $CF_3(CF_2)_5CH_2CH_2OH$ in 1,3-bis(trifluoromethyl)benzene to quench the polymerisation.

Separation of the phases and examination of the ^{1}H and ^{19}F NMR spectrum of the residue in the fluorous phase showed that a complex mixture of products had formed, so this approach was not continued. It is worthy of note that this is the first time this compound has been shown to ring open polymerise caprolactone and the polydispersity suggests very good control (run 4 in Table 4.1). The polymer contains an –OAr end group as evidenced from NMR spectroscopy.

Our second approach was to intentionally prepare the intermediate fluorinated alkoxide complex of zinc, and then quench the polymerisation with a fluorous alcohol. Thus we

Table 4.1. Characterisation data for poly(caprolactone) produced by fluorinated (pre)-catalysts (Rf = $CF_3(CF_2)_5CH_2CH_2$).

Run	(Pre)-catalyst	Conditions[a]	*Mn* [b]	Calculated *Mn*	PDi
1	$[(RfCO_2)_2Zn]$	BnOH initiator	2756	3298	1.03
2		1st recycle	1133	3298	1.03
3		2nd recycle	427	3298	1.10
4	$[(ArO)_2Zn(THF)_2]$[c]		2560	3769	1.01
5	$[(RfO)_2Zn(OEt_2)_2]$		5110	8957	1.21
6		1st recycle	2549	8957	1.10
7		2nd recycle	1171	8957	1.15

[a]1:600 catalyst loading, temp = 60 °C; solvent = THF; time = 1 h.

[b]Mark–Houwink correction applied [16].

[c]Ar = 2,6-*t*$Bu_2C_6H_3$

prepared the zinc alkoxide complex $[Zn(OCH_2CH_2(CF_2)_5CF_3)_2(OEt_2)_2]$ by the protonolysis reaction of $[Zn\{N(SiMe_3)_2\}_2]$ with the corresponding alcohol in Et_2O (Eq. (1)). This cleanly produced the expected complex as a colourless oil in good isolated yield after extraction into FC-72 (FC-72 = perfluorohexane) and has been fully characterised. The NMR spectroscopic data show resonances due to the fluorous chains, with the expected coupling patterns [18], and coordinated Et_2O. The absence of resonances at 0.5 ppm in the ^{1}H NMR spectrum confirms that protonolysis of both amide groups has occurred. The partition coefficient for this complex in

perfluoromethylcyclohexane:toluene is 97.3:2.7, which would be predicted to give an improvement in catalyst recycling compared to [$(RfCO_2)_2Zn$]. Upon addition of ε-caprolactone to a THF solution of the catalyst at 60 ^{0}C a polymer precipitated out of solution after 1 h. The polymer shows the expected $CF_3(CF_2)_5CH_2CH_2O$– end group as shown by ^{1}H, $^{13}C\{^1H\}$ and ^{19}F NMR spectroscopy and mass spectrometry. Most diagnostic are the methylene groups of the end group at 54.67 (^{3}JC–F = 4.8 Hz) and 30.01 (^{2}JC–F = 23.5 Hz), and the CF_2 groups that appear as a multiplet between 106 and 116 ppm in the $^{13}C\{^1H\}$ NMR spectrum. The ^{19}F resonances are not shifted relative to the alcohol, as expected. Quenching the polymerization with $CF_3(CF_2)_5CH_2CH_2OH$ and extraction with 1,3-bis(trifluoromethyl) benzene afforded, by NMR spectroscopy, only resonances associated with the fluorous alkoxide and no coordinated THF was observed. Therefore the extractable species is likely to be $[Zn(OCH_2CH_2(CF_2)_5CF_3)_2]_n$, which probably exists as an oligomeric species. This catalyst could be cycled for three times in total (runs 5–7 in Table 4.1), before polymerisation activity stopped and no polymer was produced.

4.4. Conclusions

In conclusion, we have shown that a new method of catalyst recycling using fluorous groups for quenching polymerisations can be utilised in ring opening polymerisation of caprolactone. In our un-optimised systems the catalyst can be recycled three times before deactivation of the catalyst mixture. This catalyst recovery sequence may hold promise for the combination of fluorous separation techniques and conventional catalysis in order to enhance recovery using little of the expensive, environmentally harmful fluorous solvents.

References

[1] M. Benaglia (Ed.), Recoverable and Recyclable Catalysts, John Wiley & Sons, Chichester, UK, **2009**.

[2] (a) J.A. Gladysz, D.P. Curran, I.T. Horva´ th (Eds.), *Handbook of Fluorous Chemistry, Wiley VCH, Weinheim,* **2004**.

(b) A.E.C. Collis, I.T. Horvath, *Catal. Sci. Tech.,* **2011,** 1,912.

(c) L.P. Barthel-Rosa, J.A. Gladysz, *Coord. Chem. Rev*., **1999,** 587, 190.

[3] I.T. Horva´ th, J. Rabai, Science **1994,** 266, 72.

[4] (a) I.T. Horva´ th, G. Kiss, R.A. Cook, J.E. Bond, P.A. Stevens, J. Ra´ bai, E.J. Mozeleski, *J. Am. Chem. Soc.,* **1998**, 120, 3133.

(b) H. Jiao, S. Le Stang, T. Soo´ s, R. Meier, K. Kowski, P. Rademacher, L. Jafarpour, J. B. Hamard, S.P. Nolan, J.A. Gladysz, *J. Am. Chem. Soc.*, **2002,** 124, 1516.

(c) L.J. Alvey, R. Meier, T. Soo´ s, P. Bernatis, J.A. Gladysz, *Eu. J. Inorg. Chem.,* **2000,** 1975.

[5] D. Gudmunsen, E.G. Hope, D.R. Paige, A.M. Stuart, *J. Fluorine Chem.* **2009**, 130, 942, and references therein.

[6] R.C. da Costa, J.A. Gladysz, *Adv. Synth. Catal.*, **2007**, 349 243.

[7] (a) W. Zhang, *Green Chem.*, **2009**, 11, 911.

(b) W. Zhang, *Comb. Chem. High Throughput Screening*, **2007**, 10, 219.

(c) W. Zhang, *Chem. Rev*., **2004**, 104, 2531.

[8] A.B. Lindstrom, M.J. Strynar, E.L. Libelo, *Environ. Sci. Technol.* **2011**, 45, 7954.

[9] (a) M. Wende, R. Meier, J.A. Gladysz, *J. Am. Chem. Soc.*,**2001**, 123, 11490.

(b) M. Wende, J.A. Gladysz, *J. Am. Chem. Soc.*, **2003**, 125, 5861.

(c) K. Ishihara, S. Kondo, H. Yamamoto, *Synlett,* **2001**, 1371.

(d) K. Ishihara, A. Hasegawa, H. Yamamoto, *Synlett* , **2002**, 1299.

(e) K. Mikami, Y. Mikami, H. Matsuzawa, Y. Matsumoto, J. Nishikido, F. Yamamoto, H. Nakajima, *Tetrahedron*, **2002**, 58, 4015.

(f) J. Otera, *Acc. Chem. Res.*, **2004**, 37, 288.

(g) G. Maayan, R.H. Fish, R. Neumann, *Org. Lett.*, **2003**, 5, 3547.

(h) J.A. Gladysz, V. Tesevic, *Topics Organomet. Chem*., **2008**, 23, 67.

(i) D. Mandal, M. Jurisch, C. Consorti, J.A. Gladysz, *Chem. Asian J.* **2008**, 31, 772.

[10] F.O. Seidel, J.A. Gladysz, *Adv. Synth. Catal.*, **2008**, 350, 2443.

[11] R.J. Baker, P.E. Colavita, D. Murphy, J.A. Platts, J.D. Wallis, *J. Phys. Chem. A,* **2012**, 116, 1435.

[12] (a) For recent reviews see: M.J. Stanford, A.P. Dove, *Chem. Soc. Revs.*, **2010**, 39, 486.

(b) M. Labet, W. Thielemans, *Chem. Soc. Rev*., **2009**, 38, 3484.

(c) C.A. Wheaton, P.G. Hayes, B.J. Ireland, *Dalton Trans.*, **2009**, 4832.

(d) N.E. Kamber, W. Jeong, R.M. Waymouth, R.C. Pratt, B.G.G. Lohmeijer, J.L. Hedrick, *Chem. Rev.*, **2007**, 107, 5813.

(e) C.-T. Chen, C.-C. Lin, *Coord. Chem. Rev.*, **2006**, 250, 602.

[13] B.M. Chamberlain, M. Cheng, D.R. Moore, T.M. Ovitt, E.B. Lobkovsky, G.W. Coates, *J. Am. Chem. Soc.*, **2001**, 123, 3229.

[14] It should be noted that 1,3-bis(trifluoromethyl)benzene is an amphiphillic solvent that can dissolve both organic and fluorous compounds. We carefully checked the purity of our extracted species by multinuclear NMR spectroscopy to ensure only the fluorinated compounds were extracted. Poly(caprolactone) shows no solubility in this solvent.

[15] R.R. Gowda, D. Chakraborty, *J. Mol. Catal. A: Chem.*, **2010**, 333, 167.

[16] (a) A. Kowalski, A. Duda, S. Penczek, *Macromolecules*, **1998**, 31, 2114.

(b) A. Duda, Z. Florjanczyk, A. Hofman, S. Slomkowski, S. Penczek, *Macromolecules*, 1990, 23, 1640.

[17] D.J. Darensbourg, M.W. Holtcamp, G.E. Struck, M.S. Zimmer, S.A. Niezgoda, P. Rainey, J.B. Robertson, J.D. Draper, J.H. Reibenspies, *J. Am. Chem. Soc.* **1999**,121, 107.

[18] A.A. Ribeiro Mag, *Magn. Reson. Chem.*, **1997**, 35, 215.

[19] R.J. Baker, T. McCabe, J.E. O'Brien, H.V. Ogilvie, *J. Fluorine Chem.,* **2010**, 131, 621.

[20] C.S. Consorti, F. Hampel, J.A. Gladysz, *Inorg. Chim. Acta*, **2006**, 359, 4874.

STRUCTURE INDEX

S.No	Structure	Identification code
1	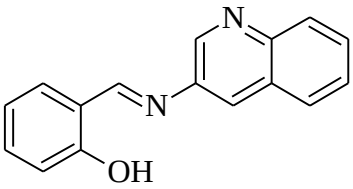	**H-QMP**
2	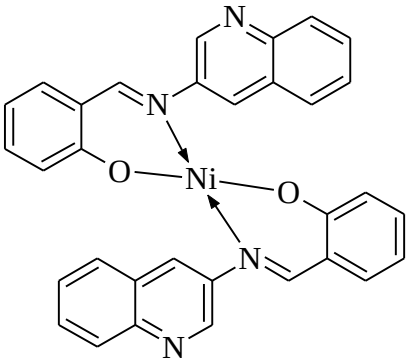	**1**
3	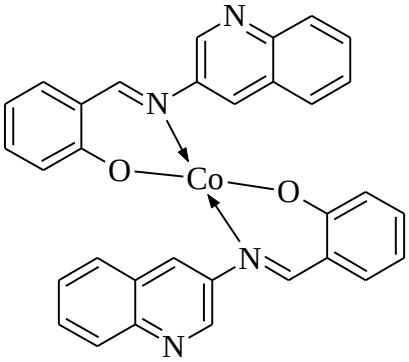	**2**
4	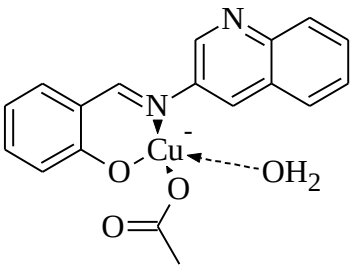	**3**
5	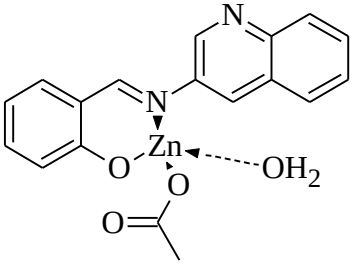	**4**

6	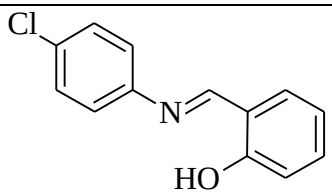	**CIMP**
7	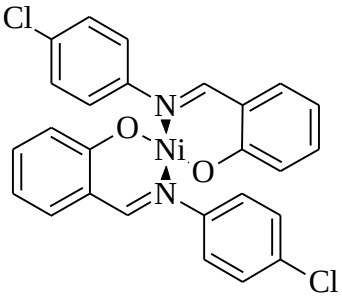	**5**
8	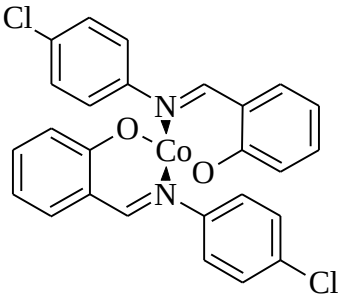	**6**
9	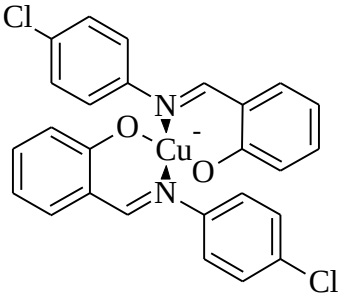	**7**
10	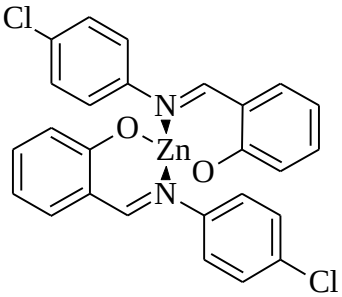	**8**
11	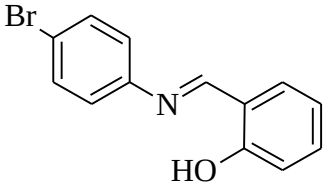	**BIMP**

12	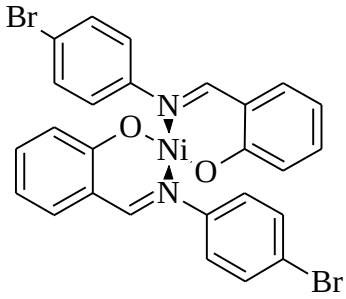	**9**
13	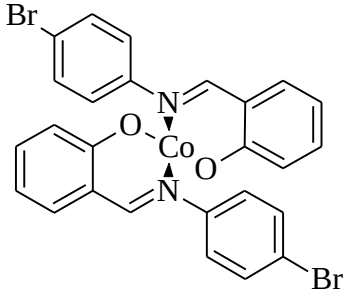	**10**
14	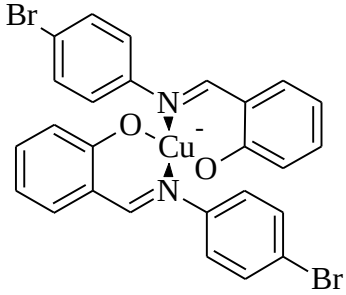	**11**
15	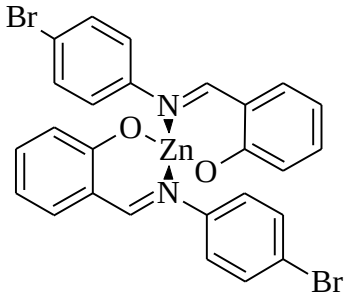	**12**
16	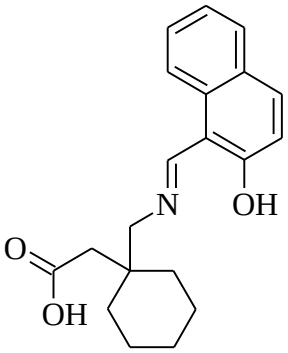	**H-HMAC**

17	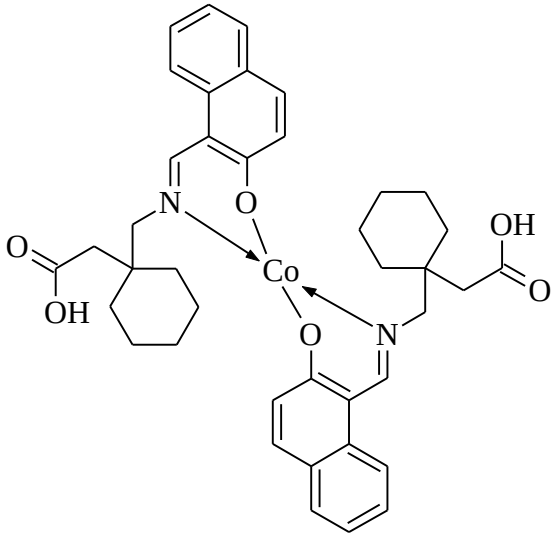	**13**
18	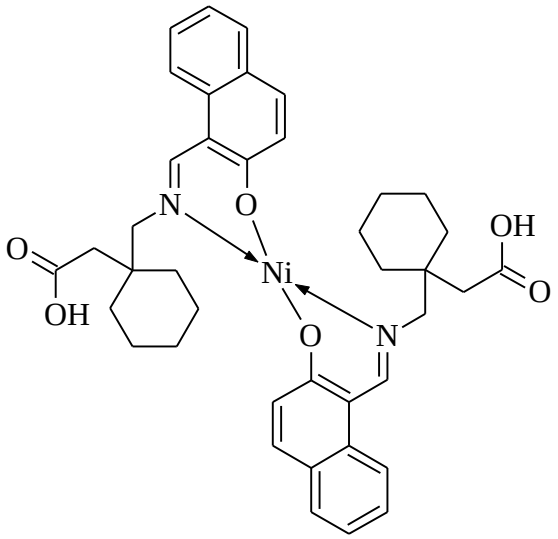	**14**
19	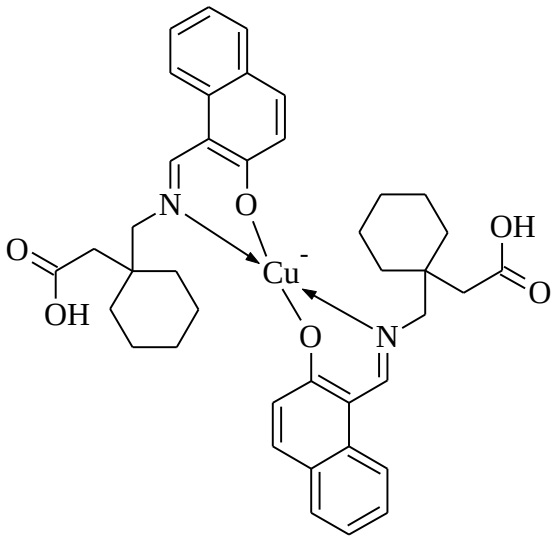	**15**

20	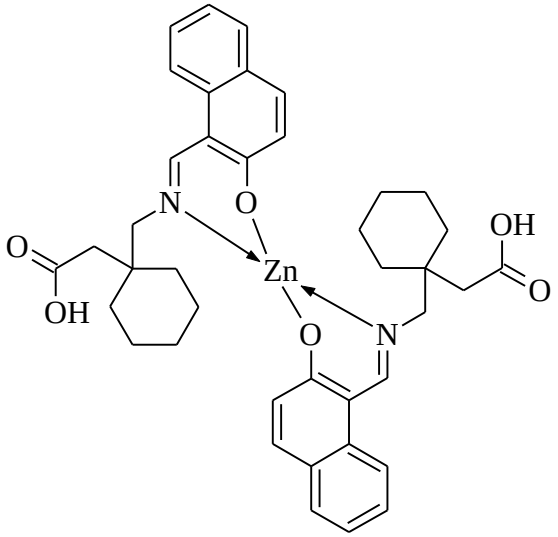	**16**
21	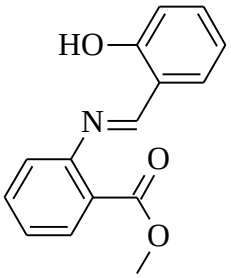	**H-HAB**
22	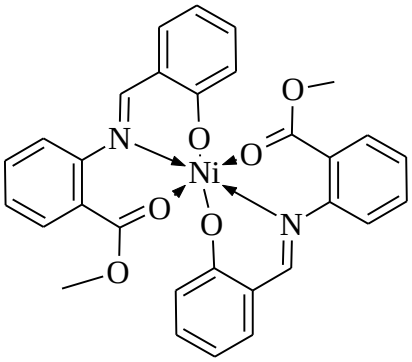	**17**
23	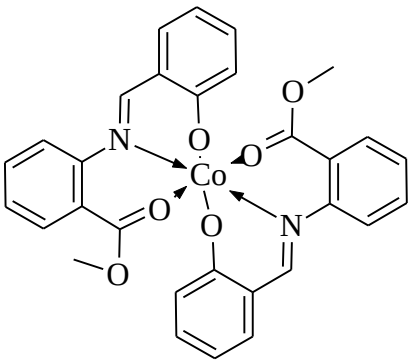	**18**

24	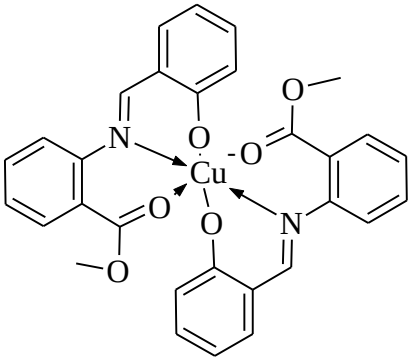	**19**
25	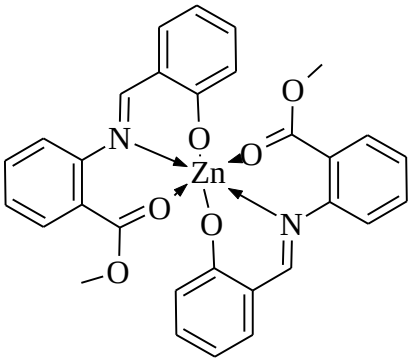	**20**
26	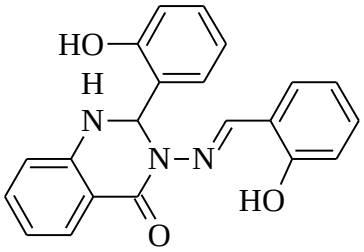	**H-HHAQ**
27	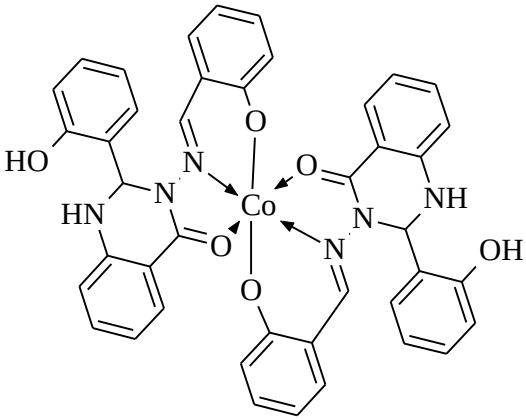	**21**

28	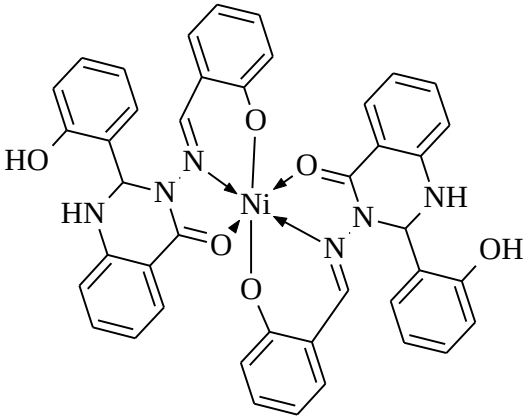	**22**
29	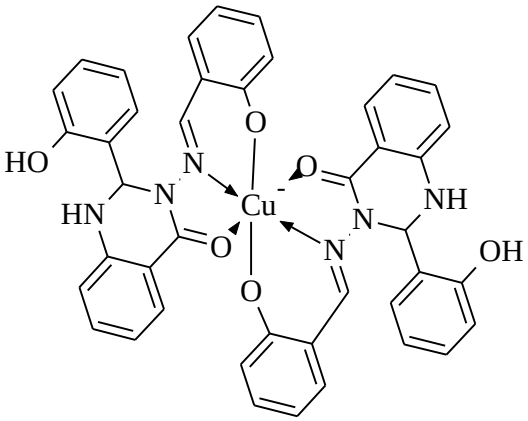	**23**
30	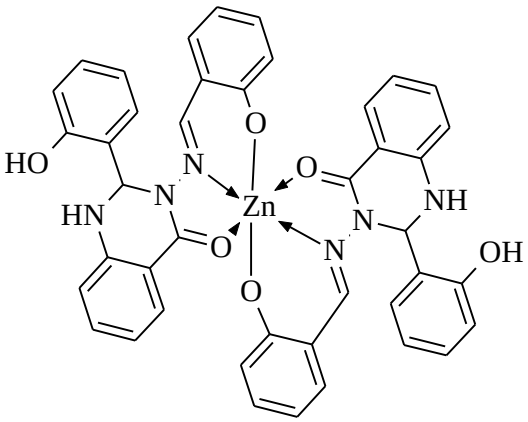	**24**
31	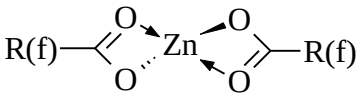	**25**

32	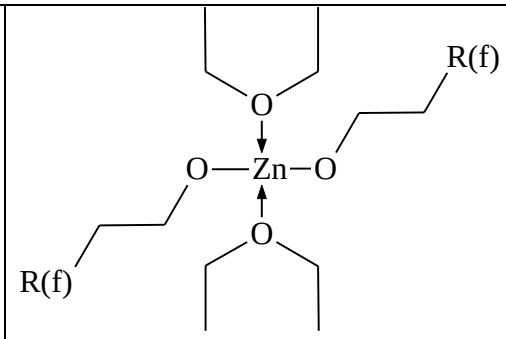	**26**

LIST OF PUBLICATIONS

1. **Muhammad Ikram**, Saeed-Ur-Rehman, Sadia Rehman, Robert J. Baker and Carola Schulzke, Synthesis, characterization and distinct butyrylcholinesterase activities of transition metal complexes of 2-[(*E*)-(quinolin-3-ylimino)methyl]phenol, **Inorganica Chimica acta,** 390 (2012) 210–216.
2. **Mohammed Ikram** and Robert J. Baker, Fluorous catalyst recycling utilising highly fluorinated zinc compounds:Ring opening polymerisation of ε-caprolactone, **Journal of Fluorine Chemistry,** 139 (2012) 58–62.
3. Saeed-Ur-Rehman, **Muhammad Ikram**, Sadia Rehman, Farhat Ullah, Gul Akhtar, Synthesis, Physicochemical, and Biological Studies of Complexes of 2-Aminobenzohydrazine with Co(II), Ni(II), Cu(II), and Zn(II) Chlorides, **Synthesis and Reactivity in Inorganic, Metal-Organic, and Nano-Metal Chemistry,** 40 (2010) 847–854.

LIST OF SUBMITTED MANUSCRIPTS

1. **Muhammad Ikram**, Sadia Rehman, Faridoon, Robert J. Baker, Carola Schulzke, Alexander James Blake, Henry Wong and Saeed-Ur-Rehman, Urease and α-chymotrypsin inhibitory activities of transition metal complexes of new Schiff base ligand: X-ray crystal structure of the Schiff base ligand, Submitted in **Journal of Inorganic Biochemistry**.
2. **Muhammad Ikram**, Sadia Rehman, Robert J. Baker, Saeed-Ur-Rehman, Alexander J.Blake and Tariq Zaman, Synthesis and characterization of transition metal complexes of novel 2-(2-hydroxyphenyl)-3-{[(*E*)-(2-hydroxyphenyl)methylidene]amino}-2,3-dihydroquinazolin-4(1*H*)-one Schiff base

ligand: Crystal structure of the ligand and antimicrobial activities of the compounds, Submitted in **Transition metal chemistry**.

3. **Muhammad Ikram**, Sadia Rehman, Robert J. Baker, Khurshid Ali and Saeed-Ur-Rehman, Kinetic and thermodynamic studies of transition metal complexes of Schiff base ligand by TG-DTA pyrolysis, Submitted in **Journal of Thermal Analysis and Calorimetry**.
4. **Muhammad Ikram**, Sadia Rehman, Ajmal Khan, Robert J. Baker, Saeed-Ur-Rehman and Tariq Zaman, Synthesis, characterization enzyme inhibitory and antimicrobial activities of transition metal complexes of methyl 2-{[(*E*)-(2-hydroxyphenyl)methylidene]amino}benzoate, Submitted in **European Journal of Medicinal Chemistry**.
5. **Muhammad Ikram**, Sadia Rehman, Robert J. Baker, Saeed-Ur-Rehman, Alexander James Blake, and Mughal Qayum, Structural study of metal complexes of neuroleptic drug gabapentin derived Schiff base ligand, Submitted in **Inorganic Chemistry**.